Supported modified hydrotalcites as sorbent for CO_2 capture

Niels Meis

ISBN: 978-90-8891-145-3

The cover picture shows the glacial lake Jökulsárlón in Iceland. The picture was taken in 2008 and shows the result of the anthropogenic global warming. The lake used to be part of the Vatnajökull glacier. However, since the 1930s the glacier is declining and as a result the glacial lake was formed.

Uitgeverij: BOXPress
Printed by: Proefschriftmaken.nl || Printyourthesis.com

Supported modified hydrotalcites as sorbent for CO_2 capture

Gemodificeerde hydrotalcieten op een drager als sorbent voor het afvangen van CO_2

(met een samenvatting in het Nederlands)

Proefschrift

ter verkrijging van de graad van doctor aan de Universiteit Utrecht
op gezag van de rector magnificus, prof.dr. J.C. Stoof, ingevolge het
besluit van het College voor Promoties in het openbaar te verdedigen op
maandag 15 februari 2010 des ochtends te 10.30 uur

door

Niels Nicolaas Andreas Hendrikus Meis

geboren op 30 november 1978 te Vught

Promotor: Prof. Dr. Ir. K.P. de Jong

Co-promotor: Dr. J.H. Bitter

The research described in this thesis was financially supported by CATO (CO_2 Afvang Transport en Opslag), The Netherlands.

" The world is changing; I feel it in the water, I feel it in the earth and I smell it in the air. Much that once was, is lost for none now live who remember it."

'The Lord of the Rings'

Beauty always comes with dark thoughts

'Nightwish'

Contents

Chapter 1

General introduction

General introduction

Climate Change: global warming and the greenhouse effect

The natural greenhouse effect, which was described in the traditional works of Fourier (1824), Tyndall (1861), and Arrhenius (1896), is a process where energy from the sun, in the form of short-wavelength radiation, is partly absorbed by the surface of the Earth. Part of this radiation is re-emitted in the atmosphere as infrared radiation. Greenhouse gases (GHG) like water vapor, carbon dioxide (CO_2), methane (CH_4) and nitrous oxides (N_2O) absorb this radiation released by the Earth's surface. This greenhouse effect allows life as we know it today. Ice cores provide evidence for variation in greenhouse gas concentrations over the past 800,000 years. CO_2 and CH_4 vary between glacial and interglacial periods and concentrations of these gases correlate strongly with temperature. Abundance of these gases in the atmosphere can increase the overall warming of the Earth's surface and this process is called the 'anthropogenic global warming' (AGW) or 'amplified greenhouse effect'.

The concentration of several greenhouse gases have been growing significantly since the industrial revolution in the 18^{th} century, resulting in climate change. The average concentration of CO_2 has increased from 280 ppm to 385 ppm [1] nowadays (2009) and continues to increase because of the enormous human usage of fossil fuels (gas, coal and oil, Figure 1). Worth noticing is that the addition of the first 50 ppm took place in approximately 200 years, while the next 50 ppm addition took place in the following 33 years from around 1973. For each 4 gigatons (Gt) of fossil carbon burned, the atmosphere's CO_2 content rises about 1 ppm and currently the world addition to the atmosphere is about ~8 Gt CO_2 (2008, 9 Gt), which gives rise to 2 ppm annually. Although the precise link between atmospheric greenhouse gases and the climate is still being debated, there remains little doubt that high concentrations of atmospheric CO_2 have strongly affected the Earth's past climates [2].

Next to carbon dioxide, methane is a factor of 21 more effective and nitrous oxide is a factor of 270 more effective in trapping radiation than carbon dioxide. Rare greenhouse gases, such as NF_3 [3] SF_6 [4] and CFC's [5] are also of concern because of their highly efficient radiation trapping compared to carbon dioxide. Although these compounds are more potent as

a radiation absorber than CO_2, carbon dioxide is the largest contributor and the fastest growing emitted component and thus of the highest concern.

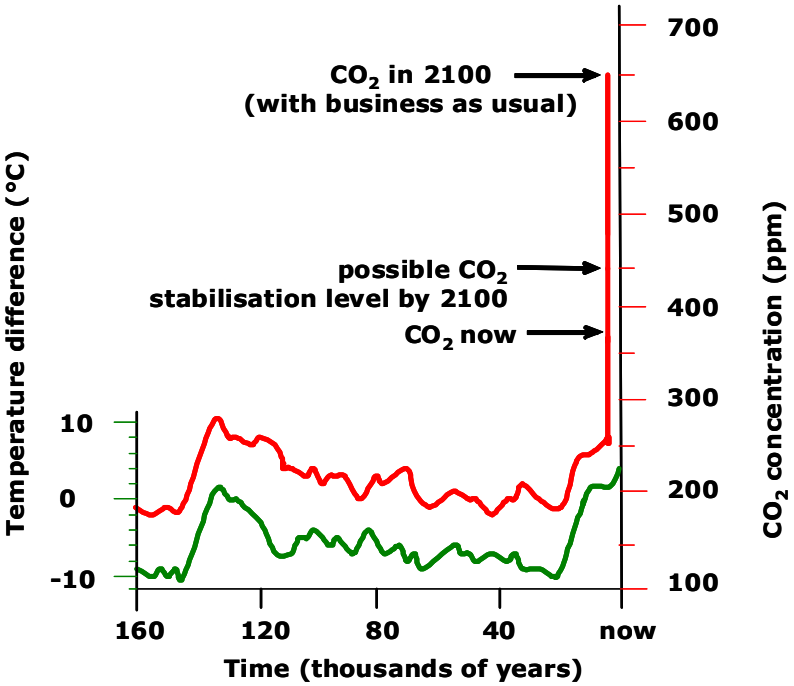

Figure 1. Changes in CO_2 concentration and temperature for the last 160.000 years (from ice cores) and future prediction.

With the rising atmospheric CO_2 concentrations, the Intergovernmental Panel on Climate Change (IPCC) anticipates on a temperature rises of 1.1- 4.0 K and a sea-level rise of 18- 58 cm by 2100 [6]. However, new calculations showed that CO_2 emissions have increased faster than as predicted by the IPCC [7, 8]. Other calculations predict a warming of 2 K between 2000- 2050 with a probability of 75% of exceeding the 2 K when the total emission from 2009 to 2050 does not exceed the 190 Gt [9-11]. Several studies showed that the increase in carbon dioxide and consequently rise in temperature [12, 13] have already caused acidification of oceans [14, 15], shifts in seasons [16, 17], decrease of tropical forests [18], release of methane from permafrost [19], vanishing of arctic summer ice [20] and a decline of glaciers [21-23], which is contributing to sea-level rise. It is believed that passing the

concentration level of 450 ppm will be triggering a feedback process that would lead to rapid and severe climate changes. Therefore, efforts are made to decrease the amount of CO_2 in the atmosphere.

Options to decrease the CO_2 emissions

There is a variety of strategies for reducing fossil fuel usage and it is to be expected that energy demand will have increased with a factor 2- 3 by 2050 (Figure 2). This shows the need to increase the search for alternatives and to decarbonize the energy consumption. Currently, roughly 86% of the world wide energy usage is generated from fossil fuels, 6.5% is produced from nuclear energy and 7.5% comes from renewable sources. The first option to decrease the CO_2 emissions is to reduce the energy intensity by a more efficient use of energy. Examples of energy reduction can be found in transportation (e.g. hybrid or electric cars), buildings (isolation), consumers (use of fluorescent lights or skylights instead of incandescent lights) and industry (more efficient processes, cradle to cradle). Nuclear energy is capable of producing a large fraction of our energy demands, and essentially emits no greenhouse gases. However, the risk of highly radioactive material and nuclear accidents are still main drawbacks for using nuclear energy.

Secondly, the emissions can be decreased by the use of alternatives based on renewable energy that emit little or no CO_2. Examples are wind- [24], solar- [25], water- (hydro- [26], wave- [27], tidal- [28]) and geothermal energy [26], biomass [26, 29] and biofuel [30, 31]. However, these technologies are not sufficient enough to cover all our energy demands at the moment and need improvement.

Thirdly, a short term strategy to decrease the emission of carbon dioxide is CO_2 Capture and Storage (CCS). This is a process whereby CO_2 is captured and concentrated using a sorbent from gases produced by fossil fuel combustion. Subsequently, a pure stream of CO_2 is compressed and transported to a location where it is injected into deep geological formations for permanent storage. Storage of CO_2 can provide an interim solution towards a worldwide economy based on sustainable energy usage (Figure 2).

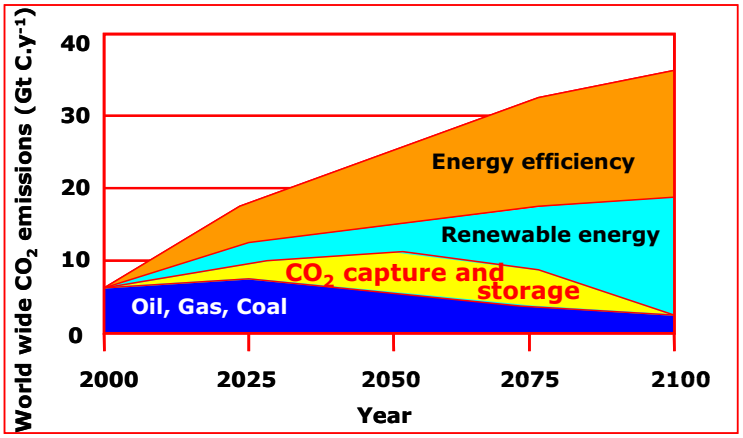

Figure 2. Possible future scenario for CO_2 reduction in time.

Technologies for CO_2 capture

Fossil fueled power plants are the largest CO_2 emitters globally and account for 33- 40% of the total emissions [32, 33]. The main objective for CO_2 capture is to produce a concentrated stream of CO_2 that can be readily transported to a storage site. There are three key routes to capture CO_2 generated at industrial installations, such as power plants, as discussed below.

Oxy-fuel combustion

This technique uses pure oxygen for the combustion of fossil fuels, instead of air. The produced flue gas after reaction consists mainly of steam and concentrated CO_2 gas which only has to be dried and compressed. The advantages are that the flue gas has a much lower volume and a high concentration of CO_2 (>90%). Production of pure oxygen, i.e. separation from the air, in this method is costly, and therefore a drawback in using this process for CO_2 capture.

Post-combustion

Capture and separation of diluted CO_2 from flue gases produced by the combustion of fossil fuels using air is called post-combustion capture. The most common method is chemical

absorption by passing the CO_2 through a sorbent, usually a liquid amine, which binds the CO_2. After loading, the sorbent is heated and/or pressurized and concentrated CO_2 is released. This technique can typically be applied at power plants or industrial plants. At the moment, the energy costs are still 20- 30% higher compared to plants with no CO_2 capture [34]. Promising new technologies which can increase the energy efficiency, include gas membrane separation and solid sorbents.

Pre-combustion

This process consists of two stages where in the first stage fuel is converted to hydrogen and carbon monoxide (syngas), reaction scheme 1 (1). Secondly, carbon monoxide is further converted by the water-gas shift reaction (WGS) with steam to carbon dioxide, and more hydrogen is produced (2). The reaction occurs in two stages, consisting of a high temperature shift (HTS) at ~673 K, usually performed with an iron based catalyst, and a low temperature shift (LTS) at ~523 K, usually performed with a copper based catalyst. Finally, the CO_2 is separated from hydrogen using a sorbent, whereafter the sorbent is heated and/or depressurized and the concentrated CO_2 is released. The total process, when CO_2 capture is considered in the reaction, is named Sorption Enhanced Reaction Process (SERP, Figure 3). The second step of the process, including CO_2 capture, is called Sorption Enhanced Water Gas Shift reaction (SE-WGS). The advantage of pre-combustion is that the produced fuel, hydrogen, is essentially carbon-free and that up to 95% of the CO_2 can be captured.

$$CH_4 + H_2O \leftrightarrow CO + 3H_2 \qquad \Delta H^0 = 206\ KJ.mol^{-1} \qquad (1)$$

$$CO + H_2O \leftrightarrow CO_2 + H_2 \qquad \Delta H^0 = -41\ KJ.mol^{-1} \qquad (2)$$

$$CH_4 + 2\,H_2O \leftrightarrow CO_2 + 4H_2 \qquad (3)$$

Reaction scheme 1. Principal of Sorption Enhanced Reaction Process (SERP).

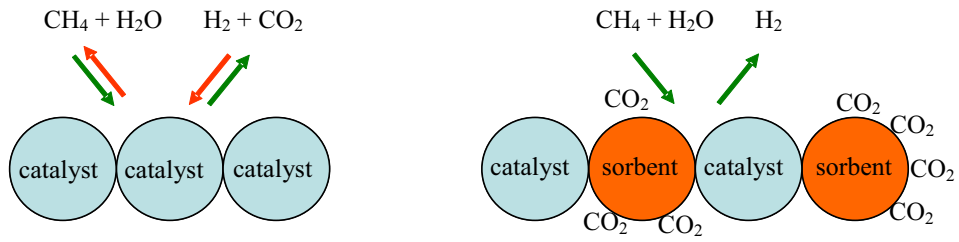

Steam Methane Reforming (SMR) Sorption Enhanced Reforming Process (SERP)

Figure 3. Schematic illustration of the steam methane reforming process without and with CO_2 capture.

The hydrogen economy

Hydrogen is expected to play an important role in future as an energy carrier, via the above described process (SERP). The energy produced during hydrogen combustion is higher than that released by any other fuel on a mass basis (120 $MJ.kg^{-1}$). Currently, the annual production is 0.1 Gt, where 98% comes from the burning of fossil fuels [35]. However, the costs of the production, compared to gasoline, are still too expensive [36] and hydrogen is still at a relatively early stage of development as a consumer fuel. The main advantage of hydrogen as fuel is that no CO_2 or CO is emitted and the only byproduct is water (vapor). The production of hydrogen and electricity from decarbonized fossil fuels with CO_2 capture and storage can be an intermediate towards a hydrogen economy based on renewable hydrogen (Figure 4).

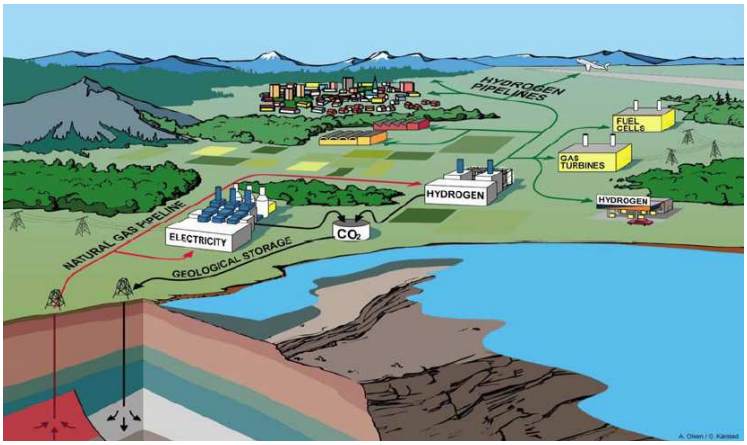

Figure 4. Possible future scenario: Fossil fuels generate electricity and/or hydrogen, the CO_2 is captured, concentrated and permanently stored.

Storage of CO_2

The concentrated CO_2 captured by the above described technologies is stored permanently, after being transported to the location (pipeline, train, truck), underground in deep geological formations (Figure 5). Suitable storage formations can be onshore (on land) and offshore (on sea). These reservoirs typically lie at a depth of 1- 4 km. The three most important storage reservoirs are depleted gas and oil fields, unminable coal beds and aquifers (deep layers containing saline water). Since 1972 CO_2 has been injected in oil fields, for additional oil production. This technique, called Enhanced Oil Recovery (EOR) accounts for almost 50% of the production in the United States. Unminable coal beds typically contain large amounts of methane gas and by injecting CO_2 there can be production of this gas, that is adsorbed onto the surface of the coal, and can make storage economically more viable. Sequestration of CO_2 in aquifers does not produce value-added byproducts as oil or gas, but has the advantage that the estimated carbon storage capacity is exceptionally high (e.g. U.S. ~500 Gt). The concentrated and compressed CO_2 gas (80- 110 bar, ~300 K [37, 38]) is injected underground and there it becomes a dense supercritical fluid of which the volume is considerably reduced, from 1000 m^3 at ground level to 2.7 m^3 at 2 km depth (Figure 6). The IPCC has estimated the global storage capacity at at least 2.000 Gt of CO_2. This would be enough to store 80 years of world wide emissions from fossil use.

CO_2 injections are already utilized in Canada, Australia, Japan and the U.S. A large CO_2 capture and storage project in Norway is the offshore Sleipner project in the North Sea. The relatively high CO_2 concentration (~8%) is separated from the natural gas and injected for permanent storage into a deep saline aquifer. The project has been running since 1996 and about 1 Mt CO_2 is stored annually. Comparable capture and storage trials are found in Weyburn Canada (1.8 $Mt.y^{-1}$), in Salah in Algeria (1 $Mt.y^{-1}$) and in The Netherlands in gas field K12-B located in the North Sea, since 2004 (10- 15 $Kt.y^{-1}$).

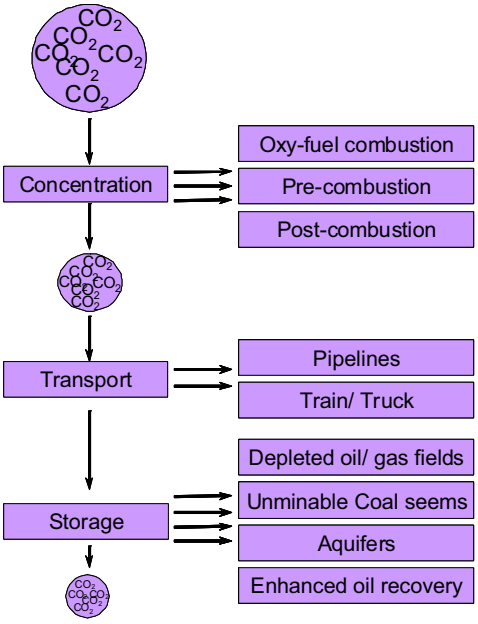

Figure 5. Schematic illustration of concentration, transport & storage of CO_2.

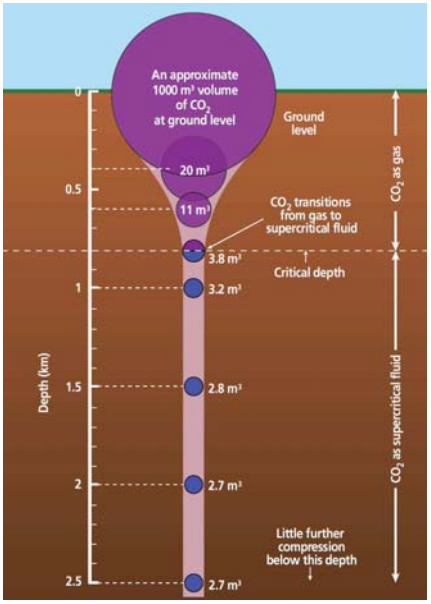

Figure 6. Decrease in volume of CO_2 injected in an underground storage field (80-110 bar, ~300 K at ground level).

CO_2 storage and safety risk

In 1984, at Lake Monoun, Cameroon, 37 people died because of an eruption of a volcano, which resulted in the release of a large amount of carbon dioxide. In 1986 at Lake Nyos, Cameroon, 1700 people died because the magma in this deep lake released at once 1.6 million tonnes of CO_2. This tragic disaster at the crater lake in Nyos is often mentioned

when risks CO_2 storage are discussed. The magma lying underneath the lake leaks carbon dioxide and saturates the water. This 'open' CO_2 lake can therefore not be compared with closed natural reservoirs. Stable natural reservoirs containing CO_2 can be found in North America (Colorado and Arizona-New Mexico), The Netherlands (Werkendam) and several in south-eastern France. Potential risks of CCS include leakage from capture, transport and injection (comparable to the risk in similar existing industrial operations) and slow leaks from storage sites. The risks of CO_2 leakage after injection can be minimized if reservoirs are carefully selected and the best available technologies are used.

CO_2 sorbent materials

Almost al commercial processes today use liquid amines (amine scrubbers). These materials can only be used at low temperature, because of amine degradation at elevated temperatures. Thus, for pre-combustion capture and consequently CO_2 sorption at high temperatures, solid materials have to be used. In recent years, a great deal of interest has been shown in CO_2 capture using a solid sorbent at high temperatures. The ideal solid sorbent for CO_2 capture should be selective towards CO_2, have a high adsorption capacity at high temperatures (>523 K) for pre-combustion and high adsorption capacity at relatively low temperatures (~323 K) for post-combustion, display adequate adsorption and desorption kinetics at operating conditions (facile regeneration), have long term stability upon cyclic use, adequate mechanical strength and low costs of the material. Various sorbents have been investigated for CO_2 capture, such as metal oxides CaO (limestone), CaMgO (dolomite), [39-44] and MgO [45], lithium and sodium zirconates [46-52], activated carbon [53, 54], soda ash [55], and basic alumina [56].

The major disadvantages of these materials are either the poor regeneration properties, slow kinetics, stability at high temperatures, or the low adsorption capacity. Various studies have been reported on the use of hydrotalcite-based sorbents for pre-combustion CO_2 capture at high temperatures [55, 57-62]. Recently, Walspurger and co-workers reported a more detailed study on the mechanism of CO_2 sorption of hydrotalcite [63]. Although these examples showed HT as a potentially good sorbent, the capacity for CO_2 was low. Hydrotalcite supported on Carbon nanofibers (CNF) as support was shown as a promising

alternative solid base catalyst for the synthesis of MIBK [64]. CNF is an attractive support material with favorable physico-chemical properties, i.e. high mechanical strength, high surface area, tunable surface properties and the absence of micropores. These properties might make HT supported on a CNF attractive not only as a base catalyst, but also as a CO_2 sorbent. In this thesis we focus on HT and HT-CNF for CO_2 capture.

Hydrotalcites

The first discovery of hydrotalcite (HT) was in Snarum, Sweden, around 1842. The stoichiometry of hydrotalcites [$Mg_6Al_2(OH)_{16}CO_3.4H_2O$] was first correctly determined by Manasse in 1915 [65]. For a long period of time, the structure was assumed to exist of consecutive layers of brucite [$Mg(OH)_2$], and aluminum hydroxide [$Al(OH)_3$] as proposed by Feitknecht in 1942 [66, 67]. It was not until single crystal X-ray diffraction (XRD) studies on mineral samples were carried out by Allmann and Taylor in the 1960s that the main structural features of LDHs (Figure 7) were understood and the structure of Feitknecht was rebutted [68].

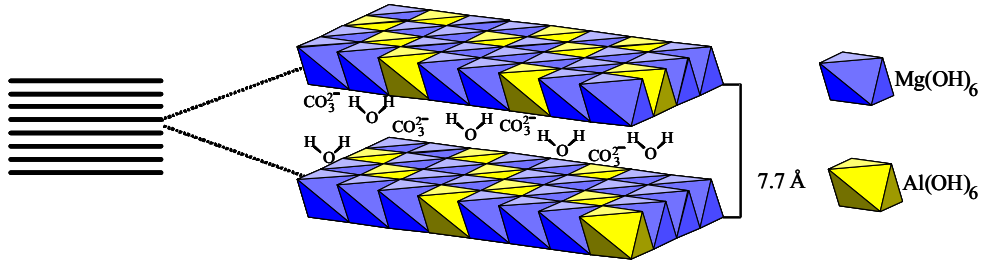

Figure 7. Schematic representation of hydrotalcite.

Hydrotalcite belongs to the class of anionic clay minerals also known as layered double hydroxides. The structure of HT closely resembles that of brucite, $Mg(OH)_2$, where Mg^{2+} is octahedrally coordinated by hydroxyl groups. These octahedra share adjacent edges to form two-dimensional sheets or layers. In HT, part of the Mg^{2+} ions are replaced by Al^{3+} ions. This results in positively charged layers, which are balanced by relatively small charge-compensating anions located in the interlayer region where also hydrating water molecules are accommodated. In the natural mineral hydrotalcite, the structure consists of bivalent Mg^{2+} and trivalent Al^{3+}, where the positive charge is compensated by carbonate anions.

In the preparation of hydrotalcites, the degree of substitution between divalent and trivalent cations can be varied. The range is limited for pure phases to Mg/Al ratios between 2 and 4 [69], although Vaccari [70] and Sels [71] reported larger variation in ratios. Many other hydrotalcites structures are known by combinations of cations incorporated into the brucite layers, such as Mg^{2+}, Cr^{2+}, Mn^{2+}, Fe^{2+}, Co^{2+}, Ni^{2+}, Cu^{2+}, Zn^{2+}, Ru^{2+} and Al^{3+}, Fe^{3+}, Co^{3+}, Ga^{3+}. Additionally, HTs containing V^{4+} and Li^{+} have been reported [72, 73]. More tuning can be possibilities obtained by changing the charge-compensating anions presented in the interlayer of the HT, such as inorganic anions F^-, Cl^-, Br^-, I^- ,CO_3^{2-}, NO_3^-, OH^-, SO_4^{2-} (where carbonate (CO_3^{2-}) has the highest affinity), or organic anions from drug molecules (Diclofenac, Ibuprofen [74], vitamin A and C [75]) and carboxylic acids [76, 77], therephtalaat and benzoate anions [78], citrate [79] and more uncommon molecules such as hexacyano- [80] and boron complexes [81].

Hydrotalcites are traditionally synthesized via co-precipitation of aqueous metal-nitrate (or chloride) solutions at a fixed pH under vigorous stirring. Typically, an aqueous alkaline (NaOH or KOH) solution is used to adjust the pH and an aqueous alkaline-carbonate (Na_2CO_3, K_2CO_3) solution is added as a carbonate source [82, 83]. Normally, a temperature between 333- 353 K is chosen. Higher temperatures usually result in more crystalline material than prepared at lower temperatures >333 K. After ageing for 12- 24 h, the resulting material is filtered, washed and dried at ~393 K. Instead of co-precipitation, hydrotalcites can also be prepared using ammonium hydroxide in stead of alkali carbonates/hydroxides [84-86], the urea method [87, 88], the sol-gel method [89-91] or via microwave heating [92-96].

HT compounds are used in a wide range of areas and are manifold. Various important applications are ion-exchangers [84, 97], sensors [98-100], heat stabilizers in PVC and flame

retardant additives in plastics. Another utilization is the use of HT as base catalysts [64, 101, 102], such as self condensation reaction, cross-aldol condensation of aldehydes and ketonnes, Knoevenagel condensation [103-107], Claisen-Schmidt condensation [108-114], Michael addition [115-117] and transesterification [118-123]. As medical application hydrotalcite is used as antacid [74]. Hydrotalcites can also be used as sorbent for the purification of waste water in order to remove phosphates or heavy metals [124-126]. Current investigation is the use of activated HT as sorbent for CO_2 capture and is of particular interest for the research involved in this thesis.

Activation of hydrotalcites and CO_2 sorption

Since the last decade, HT attracted much interest as a re-usable sorbent for CO_2. However, before HT can adsorb CO_2, the material requires an activation procedure. Upon heat treatment (773 K), HT is converted into a mixed oxide of the type $Mg(Al)O_x$ and this material can be used to adsorb CO_2. Activation procedures of HTs are widely used to obtain a basic catalyst [64, 110, 127-132]. A typical feature of HT materials is the possibility to restore the layered HT structure from the heat-treated HT. The $Mg(Al)O_x$ mixed oxide can be reconstructed via exposure to water at ambient temperatures. This 'memory effect' probably originated from the fact that the cations in the mixed oxide more or less retain their position of the HT precursor. High temperatures (>423 K) during CO_2 sorption prevent the $Mg(Al)O_x$ (activated HT) to reconstruct when exposed to water vapor.

Scope and outline of this thesis

In **Chapter 2** the CO_2 sorption capacity on activated unsupported HT with different platelet sizes and activated HT supported on carbon nanofibers (CNF) for pre-combustion capture is studied. The change in surface area after activation and loading with CO_2 at 523 K was studied with N_2-physisorption. The higher capacity of activated supported HT samples was discussed. The increase in capacity is considered to originate from a higher concentration of defects on the HT-CNF. **Chapter 3** deals with activated alkali carbonate (Na, K) promoted HT and HT-CNF. The presence of alkali carbonate in proximity of activated HTs increased

the CO_2 capacity largely for unsupported HTs and moderately for supported HTs. The location of the alkali carbonate was investigated with XRD, SEM and TEM-EDX. The influence of different loadings of potassium carbonate was investigated with N_2-physisorption. In **Chapter 4** of this thesis the focus is on post-combustion CO_2 capture at low temperature (~373 K). Potassium carbonate supported on carbon nanofibers was investigated for sorption capacity and stability. The novel sorbent was compared with Al_2O_3 and active carbon (AC) loaded with potassium carbonate. Physical properties of these materials were evaluated with XRD, SEM and N_2-physisorption. The potassium carbonate supported CNF revealed superior properties as CO_2 sorbent at low desorption temperatures, having a good stability, the highest capacity and excellent regeneration properties compared to the aluminum and AC sorbents. Finally, in **Chapter 5,** the results from the previous chapters are summarized together with concluding remarks.

References

1. Rahmstorf, S., et al., *Recent climate observations compared to projections.* Science, 2007. **316**(5825): p. 709-709.
2. Montanez, I.P., et al., *CO_2-forced climate and vegetation instability during late paleozoic deglaciation.* Science, 2007. **315**(5808): p. 87-91.
3. *Rare greenhouse gas adds to climate concerns.* Nature, 2008: p. 1163.
4. McMillan, C.A. and G.A. Keoleian, *Not All Primary Aluminum Is Created Equal: Life Cycle Greenhouse Gas Emissions from 1990 to 2005.* Environmental Science & Technology, 2009. **43**(5): p. 1571-1577.
5. Stemmler, K., et al., *Emissions of the Refrigerants HFC-134a, HCFC-22, and CFC-12 from Road Traffic: Results from a Tunnel Study (Gubrist Tunnel, Switzerland).* Environmental Science & Technology, 2004. **38**(7): p. 1998-2004.
6. *Intergovernmental Panel on Climate Change.* IPCC, Climate Change 2007: The Physical Science Basis (Cambrigde Univ. Press, Cambridge, 2007).
7. Canadell, J.G. and M.R. Raupach, *Managing forests for climate change mitigation.* Science, 2008. **320**(5882): p. 1456-1457.
8. Kintisch, E., *Global Warming: Projections of Climate Change Go From Bad to Worse, Scientists Report.* Science, 2009. **323**(5921): p. 1546-1547.

9. Meinshausen, M., et al., *Greenhouse-gas emission targets for limiting global warming to 2 °C.* Nature, 2009. **458**(7242): p. 1158-1162.
10. Allen, M.R., et al., *Warming caused by cumulative carbon emissions towards the trillionth tonne.* Nature, 2009. **458**(7242): p. 1163-1166.
11. Schmidt, G. and D. Archer, *Climate change: Too much of a bad thing.* Nature, 2009. **458**(7242): p. 1117-1118.
12. Wigley, T.M.L., *The climate change commitment.* Science, 2005. **307**(5716): p. 1766-1769.
13. Meehl, G.A., et al., *How Much More Global Warming and Sea Level Rise?* Science, 2005. **307**(5716): p. 1769-1772.
14. Zeebe, R.E., et al., *Oceans - Carbon emissions and acidification.* Science, 2008. **321**(5885): p. 51-52.
15. Ruttimann, J., *Oceanography: Sick seas.* Nature, 2006. **442**(7106): p. 978-980.
16. Thomson, D.J., *Climate change: Shifts in season.* Nature, 2009. **457**(7228): p. 391-392.
17. Kerr, R.A., *Climate change - Global warming coming home to roost in the American West.* Science, 2007. **318**(5858): p. 1859-1859.
18. Bonan, G.B., *Forests and climate change: Forcings, feedbacks, and the climate benefits of forests.* Science, 2008. **320**(5882): p. 1444-1449.
19. Nisbet, E.G. and J. Chappellaz, *Shifting Gear, Quickly.* Science, 2009. **324**(5926): p. 477-478.
20. Kerr, R.A., *GLOBAL WARMING: Arctic Summer Sea Ice Could Vanish Soon But Not Suddenly.* Science, 2009. **323**(5922): p. 1655-.
21. Luthi, D., et al., *High-resolution carbon dioxide concentration record 650,000-800,000 years before present.* Nature, 2008. **453**(7193): p. 379-382.
22. Lunt, D.J., et al., *Late Pliocene Greenland glaciation controlled by a decline in atmospheric CO_2 levels.* Nature, 2008. **454**(7208): p. 1102-U41.
23. Meier, M.F., et al., *Glaciers dominate Eustatic sea-level rise in the 21st century.* Science, 2007. **317**(5841): p. 1064-1067.
24. Bockris, J.O. and T.N. Veziroglu, *Estimates of the price of hydrogen as a medium for wind and solar sources.* International Journal Of Hydrogen Energy, 2007. **32**(12): p. 1605-1610.
25. Armor, J.N., *Addressing the CO_2 dilemma.* Catalysis Letters, 2007. **114**(3-4): p. 115-121.
26. Moriarty, P. and D. Honnery, *Intermittent renewable energy: The only future source of hydrogen?* International Journal Of Hydrogen Energy, 2007. **32**(12): p. 1616-1624.

27. Callaway, E., *To catch a wave.* Nature, 2007. **450**(7167): p. 156-159.
28. Nicholls-Lee, R.F. and S.R. Turnock, *Tidal energy extraction: renewable, sustainable and predictable.* Science Progress, 2008. **91**: p. 81-111.
29. Balat, M. and M. Balat, *Political, economic and environmental impacts of biomass-based hydrogen.* International Journal of Hydrogen Energy, 2009. **34**(9): p. 3589-3603.
30. Marris, E., *Drink the best and drive the rest.* Nature, 2006. **444**(7120): p. 670-672.
31. *Biofuelling the future.* Nature, 2006. **444**(7120): p. 669-669.
32. Wang, M.H., C.G. Lee, and C.K. Ryu, *CO2 sorption and desorption efficiency of Ca_2SiO_4.* International Journal of Hydrogen Energy, 2008. **33**(21): p. 6368-6372.
33. Figueroa, J.D., et al., *Advances in CO_2 capture technology--The U.S. Department of Energy's Carbon Sequestration Program.* International Journal of Greenhouse Gas Control, 2008. **2**(1): p. 9-20.
34. Change, I.P.o.C., *Carbon Dioxide Capture and Storage: Special Report of the Intergovernmental Panel on Climate Change* Cambridge University Press, 2005.
35. Marban, G. and T. Vales-Solis, *Towards the hydrogen economy?* International Journal Of Hydrogen Energy, 2007. **32**(12): p. 1625-1637.
36. Lattin, W.C. and V.P. Utgikar, *Transition to hydrogen economy in the United States: A 2006 status report.* International Journal Of Hydrogen Energy, 2007. **32**(15): p. 3230-3237.
37. Baklid, A.K., R.; Owren, G, *Sleipner Vest CO_2 disposal, CO_2 injection into a shallow underground aquifer.* Presented paper on the 1996 SPE Annual technical Conference and Exhibition, 1996. Denver, Colorado, USA, SPE paper 36600, 1-9.
38. Abu-Zahra, M.R.M., et al., *New process concepts for CO2 post-combustion capture process integrated with co-production of hydrogen.* International Journal of Hydrogen Energy, 2009. **34**(9): p. 3992-4004.
39. Readman, J.E. and R. Blom, *The use of in situ powder X-ray diffraction in the investigation of dolomite as a potential reversible high-temperature CO_2 sorbent.* Physical Chemistry Chemical Physics, 2005. **7**(6): p. 1214-1219.
40. Martavaltzi, C.S. and A.A. Lemonidou, *Development of new CaO based sorbent materials for CO_2 removal at high temperature.* Microporous and Mesoporous Materials, 2008. **110**(1): p. 119.
41. P.D. Cobden, G.D.E., S. Booneveld, J.W. Dijkstra, D. Jansen and and R.W.v.d. Brink, *Sorption-enhanced steam-methane reforming: CaO-$CaCO_3$ Capture technology.* energy procedia, 2008. **00**(0000): p. 1-7.

42. Manovic, V. and E.J. Anthony, *Sequential SO_2/CO_2 capture enhanced by steam reactivation of a CaO-based sorbent.* Fuel, 2008. **87**(8-9): p. 1564-1573.
43. Gallucci, K., S. Stendardo, and P.U. Foscolo, *CO_2 capture by means of dolomite in hydrogen production from syn gas.* International Journal of Hydrogen Energy, 2008. **33**(12): p. 3049-3055.
44. Alvarez, D. and J.C. Abanades, *Determination of the Critical Product Layer Thickness in the Reaction of CaO with CO_2.* Industrial & Engineering Chemistry Research, 2005. **44**(15): p. 5608.
45. Lee, S.C., et al., *Development of regenerable MgO-based sorbent promoted with K_2CO_3 for CO_2 capture at low temperatures.* Environmental Science & Technology, 2008. **42**(8): p. 2736-2741.
46. Ida, J. and Y.S. Lin, *Mechanism of high-temperature CO_2 sorption on lithium zirconate.* Environmental Science & Technology, 2003. **37**(9): p. 1999-2004.
47. Ida, J., R.T. Xiong, and Y.S. Lin, *Synthesis and CO_2 sorption properties of pure and modified lithium zirconate.* Separation And Purification Technology, 2004. **36**(1): p. 41-51.
48. Xiong, R.T., J. Ida, and Y.S. Lin, *Kinetics of carbon dioxide sorption on potassium-doped lithium zirconate.* Chemical Engineering Science, 2003. **58**(19): p. 4377-4385.
49. Ochoa-Fernandez, E., et al., *Nanocrystalline lithium zirconate with improved kinetics for high-temperature CO_2 capture.* Chemistry Of Materials, 2006. **18**(6): p. 1383-1385.
50. Nair, B.N., et al., *Processing of lithium zirconate for applications in carbon dioxide separation: Structure and properties of the powders.* Journal Of The American Ceramic Society, 2004. **87**(1): p. 68-74.
51. Zhao, T.J., et al., *Preparation and high-temperature CO_2 capture properties of nanocrystalline Na_2ZrO_3.* Chemistry Of Materials, 2007. **19**(13): p. 3294-3301.
52. Alcerreca-Corte, I., E. Fregoso-Israel, and H. Pfeiffer, *CO_2 absorption on Na_2ZrO_3: A kinetic analysis of the chemisorption and diffusion processes.* Journal Of Physical Chemistry C, 2008. **112**(16): p. 6520-6525.
53. Yong, Z., V. Mata, and A.E. Rodrigues, *Adsorption of carbon dioxide at high temperature - a review.* Separation And Purification Technology, 2002. **26**(2-3): p. 195-205.
54. Yong, Z., V.G. Mata, and A.E. Rodrigues, *Adsorption of carbon dioxide on chemically modified high surface area carbon-based adsorbents at high temperature.* Adsorption-Journal Of The International Adsorption Society, 2001. **7**(1): p. 41-50.

55. Ficicilar, B. and T. Dogu, *Breakthrough analysis for CO_2 removal by activated hydrotalcite and soda ash.* Catalysis Today, 2006. **115**(1-4): p. 274-278.
56. Yong, Z., V. Mata, and A.E. Rodriguez, *Adsorption of carbon dioxide onto hydrotalcite-like compounds (HTlcs) at high temperatures.* Industrial & Engineering Chemistry Research, 2001. **40**(1): p. 204-209.
57. Beaver, M.G., H.S. Caram, and S. Sircar, *Selection of CO_2 chemisorbent for fuel-cell grade H_2 production by sorption-enhanced water gas shift reaction.* International Journal of Hydrogen Energy, 2009. **34**(7): p. 2972-2978.
58. Lee, K.B., et al., *Production of fuel-cell grade hydrogen by thermal swing sorption enhanced reaction concept.* International Journal of Hydrogen Energy, 2008. **33**(2): p. 781-790.
59. Oliveira, E.L.G., C.A. Grande, and A.E. Rodrigues, *CO_2 sorption on hydrotalcite and alkali-modified (K and Cs) hydrotalcites at high temperatures.* Separation and Purification Technology, 2008. **62**(1): p. 137-147.
60. Reddy, M.K.R., et al., *Influence of water on high-temperature CO_2 capture using layered double hydroxide derivatives.* Industrial & Engineering Chemistry Research, 2008. **47**(8): p. 2630-2635.
61. Lee, K.B., et al., *Chemisorption of carbon dioxide on potassium-carbonate-promoted hydrotalcite.* Journal Of Colloid And Interface Science, 2007. **308**(1): p. 30-39.
62. Ding, Y. and E. Alpay, *High temperature recovery of CO_2 from flue cases using hydrotalcite adsorbent.* Process Safety And Environmental Protection, 2001. **79**(B1): p. 45-51.
63. Stéphane Walspurger, et al., *The Crucial Role of the K^+-Aluminium Oxide Interaction in K^+-Promoted Alumina- and Hydrotalcite-Based Materials for CO_2 Sorption at High Temperatures.* ChemSusChem, 2008. **1**(7): p. 643-650.
64. Winter, F., et al., *Hydrotalcites supported on carbon nanofibers as solid base catalysts for the synthesis of MlBK.* Journal Of Catalysis, 2005. **236**(1): p. 91-100.
65. Manasse, E., Atti. Soc. Toscana Sc. Nat. Proc. Verb., 1915. **24**: p. 92.
66. Feitknecht, W., Gerber, M., *Zur Kenntnis der Doppelhydroxyde und basischen Doppelsalze II. Über Mischfällungen aus Calcium-Aluminiumsalzlösungen.* Helvetica Chimica Acta, 1942. **25**(1): p. 106-131.
67. Feitknecht, W., *Über die Bildung von Doppelhydroxyden zwischen zwei- und dreiwertigen Metallen.* Helvetica Chimica Acta, 1942. **25**(3): p. 555-569.
68. Almann, R., *The Crystal Structure of Pyroaurite.* Acta Crystallographica Section B, 1968. **B24**(7): p. 972-977.

69. Cavani, F., F. Trifiro, and A. Vaccari, *Hydrotalcite-type anionic clays: Preparation, properties and applications.* Catalysis Today, 1991. **11**(2): p. 173.
70. Vaccari, A., *Preparation and catalytic properties of cationic and anionic clays.* Catalysis Today, 1998. **41**(1-3): p. 53-71.
71. Sels, B.F., D.E. De Vos, and P.A. Jacobs, *Hydrotalcite-like anionic clays in catalytic organic reactions.* Catalysis Reviews, 2001. **43**(4): p. 443 - 488.
72. Velu, S., et al., *New hydrotalcite-like anionic clays containing Zr4+ in the layers.* Chemical Communications, 1997(21): p. 2107-2108.
73. Hernandez-Moreno, M.J., et al., *IR characteristics of hydrotalcite-like compounds.* Physics and Chemistry of Minerals, 1985. **12**(1): p. 34-38.
74. Mohanambe, L. and S. Vasudevan, *Anionic clays containing anti-inflammatory drug molecules: Comparison of molecular dynamics simulation and measurements.* Journal Of Physical Chemistry B, 2005. **109**(32): p. 15651-15658.
75. Hwang, S.H., Y.S. Han, and J.H. Choy, *Intercalation of functional organic molecules with pharmaceutical, cosmeceutical and nutraceutical functions into layered double hydroxides and zinc basic salts.* Bulletin Of The Korean Chemical Society, 2001. **22**(9): p. 1019-1022.
76. Carlino, S., *The intercalation of carboxylic acids into layered double hydroxides: A critical evaluation and review of the different methods.* Solid State Ionics, 1997. **98**(1-2): p. 73-84.
77. Dutta, P.K. and D.S. Robins, *Pyrene Sorption In Organic Layered Double-Metal Hydroxides.* Langmuir, 1994. **10**(6): p. 1851-1856.
78. Kooli, F., et al., *Synthesis and properties of terephthalate and benzoate intercalates of Mg-Al layered double hydroxides possessing varying layer charge.* Chemistry Of Materials, 1996. **8**(8): p. 1969-1977.
79. Kumar, P.P., A.G. Kalinichev, and R.J. Kirkpatrick, *Hydration, swelling, interlayer structure, and hydrogen bonding in organolayered double hydroxides: Insights from molecular dynamics simulation of citrate-intercalated hydrotalcite.* Journal Of Physical Chemistry B, 2006. **110**(9): p. 3841-3844.
80. Carpani, I., et al., *Intercalation of Iron(III) hexacyano complex in a Ni,Al hydrotalcite-like compound.* Journal Of Physical Chemistry B, 2006. **110**(14): p. 7265-7269.
81. Wang, Z.L., et al., *Intercalation and photophysical properties of the tetra-(8-hydroxyquinolinato) boron complex and 3,3 ', 4,4 '-benzophenone tetracarboxylic anion into Mg-Al layered double hydroxides.* Inorganic Chemistry, 2006. **45**(11): p. 4364-4371.

82. Di Serio, M., et al., *Heterogeneous Catalysts for Biodiesel Production.* Energy & Fuels, 2008. **22**(1): p. 207-217.
83. Sharma, S.K., P.A. Parikh, and R.V. Jasra, *Solvent free aldol condensation of propanal to 2-methylpentenal using solid base catalysts.* Journal of Molecular Catalysis A: Chemical, 2007. **278**(1-2): p. 135-144.
84. Bontchev, R.P., et al., *Synthesis, characterization, and ion exchange properties of hydrotalcite* $Mg_6Al_2(OH)_{16}(A)_x(A')_{2-x}\cdot 4H_2O$ (A, A' = Cl^-, Br^-, I^-, and NO_3^-, $2 \geq x \geq 0$) *derivatives.* Chemistry Of Materials, 2003. **15**(19): p. 3669-3675.
85. Cantrell, D.G., et al., *Structure-reactivity correlations in MgAl hydrotalcite catalysts for biodiesel synthesis.* Applied Catalysis A-General, 2005. **287**(2): p. 183-190.
86. Kiraly, Z., et al., *Preparation of Ultrafine Palladium Particles on Cationic and Anionic Clays, Mediated by Oppositely Charged Surfactants:Catalytic Probes in Hydrogenations.* Langmuir, 2001. **17**(17): p. 5381-5387.
87. Ogawa, M. and H. Kaiho, *Homogeneous precipitation of uniform hydrotalcite particles.* Langmuir, 2002. **18**(11): p. 4240-4242.
88. Costantino, U., et al., *New synthetic routes to hydrotalcite-like compounds - Characterisation and properties of the obtained materials.* European Journal Of Inorganic Chemistry, 1998(10): p. 1439-1446.
89. Bolognini, M., et al., *Mg/Al mixed oxides prepared by coprecipitation and sol-gel routes: a comparison of their physico-chemical features and performances in m-cresol methylation.* Microporous And Mesoporous Materials, 2003. **66**(1): p. 77-89.
90. Lopez, T., et al., *Synthesis and characterization of sol-gel hydrotalcites. Structure and texture.* Langmuir, 1996. **12**(1): p. 189-192.
91. Tichit, D., et al., *Synthesis and characterization of Zn/Al and Pt/Zn/Al layered double hydroxides obtained by the sol-gel method.* Microporous and Mesoporous Materials, 2005. **80**(1-3): p. 213-220.
92. Benito, P., et al., *Influence of microwave radiation on the textural properties of layered double hydroxides.* Microporous And Mesoporous Materials, 2006. **94**(1-3): p. 148-158.
93. Bergada, O., et al., *Microwave effect during aging on the porosity and basic properties of hydrotalcites.* Microporous And Mesoporous Materials, 2007. **101**(3): p. 363-373.
94. Rivera, J.A., G. Fetter, and P. Bosch, *Microwave power effect on hydrotalcite synthesis.* Microporous And Mesoporous Materials, 2006. **89**(1-3): p. 306-314.
95. G. Fetter, F.H., ndez, A.M. Maubert, V.H. Lara, P. Bosch, *Microwave Irradiation Effect on Hydrotalcite Synthesis.* Journal of porous materials, 1997. **4**(1): p. 27-30.

96. Kannan, S. and R.V. Jasra, *Microwave assisted rapid crystallization of Mg-M(III) hydrotalcite where M(III) = Al, Fe or Cr.* Journal Of Materials Chemistry, 2000. **10**(10): p. 2311-2314.
97. Costantino, U., et al., *Anion exchange of methyl orange into Zn-Al synthetic hydrotalcite and photophysical characterization of the intercalates obtained.* Langmuir, 1999. **15**(13): p. 4454-4460.
98. Liu, J.P., et al., *Facile and large-scale production of ZnO/Zn-Al layered double hydroxide hierarchical heterostructures.* Journal Of Physical Chemistry B, 2006. **110**(43): p. 21865-21872.
99. Scavetta, E., et al., *[Ni/Al---Cl]-based hydrotalcite electrodes as amperometric sensors: preparation and electrochemical study.* Electrochimica Acta, 2001. **46**(17): p. 2681-2692.
100. Kim, T.W., M. Sahimi, and T.T. Tsotsis, *Preparation of Hydrotalcite Thin Films Using an Electrophoretic Technique.* Industrial & Engineering Chemistry Research, 2008. **47**(23): p. 9127-9132.
101. Winter, F., et al., *A hydrotalcite-based catalyst system for the single-stage liquid-phase synthesis of MIBK.* Applied Catalysis A-General, 2006. **307**(2): p. 231-238.
102. Winter, F., A.J. van Dillen, and K.P. de Jong, *Supported hydrotalcites as highly active solid base catalysts.* Chemical Communications, 2005(31): p. 3977-3979.
103. Li, F., et al., *Structure and basicity of mesoporous materials from Mg/Al/In layered double hydroxides prepared by separate nucleation and aging steps method.* Journal of Porous Materials, 2005. **12**(1): p. 55-63.
104. Climent, M.J., et al., *Increasing the basicity and catalytic activity of hydrotalcites by different synthesis procedures.* Journal Of Catalysis, 2004. **225**(2): p. 316-326.
105. McCluskey, A., et al., *Green chemistry approaches to the Knoevenagel condensation: comparison of ethanol, water and solvent free (dry grind) approaches.* Tetrahedron Letters, 2002. **43**(17): p. 3117-3120.
106. Angelescu, E., et al., *Solid base catalysts obtained from hydrotalcite precursors, for Knoevenagel synthesis of cinamic acid and coumarin derivatives.* Applied Catalysis A-General, 2006. **308**: p. 13-18.
107. Vidruk, R., et al., *Grain boundary control in nanocrystalline MgO as a novel means for significantly enhancing surface basicity and catalytic activity.* Journal of Catalysis, 2009. **263**(1): p. 196-204.
108. Abello, S., et al., *Aldol condensations over reconstructed Mg-Al hydrotalcites: Structure-activity relationships related to the rehydration method.* Chemistry-A European Journal, 2005. **11**(2): p. 728-739.

109. Abello, S., et al., *Nanoplatelet-based reconstructed hydrotalcites: towards more efficient solid base catalysts in aldol condensations.* Chemical Communications, 2005(11): p. 1453-1455.
110. Roelofs, J., et al., *On the structure of activated hydrotalcites as solid base catalysts for liquid-phase aldol condensation.* Journal Of Catalysis, 2001. **203**(1): p. 184-191.
111. Tichit, D., et al., *Comparison of the structural and acid-base properties of Ga- and Al-containing layered double hydroxides obtained by microwave irradiation and conventional ageing of synthesis gels.* Journal Of Materials Chemistry, 2002. **12**(12): p. 3832-3838.
112. Abello, S., et al., *Study of alkaline-doping agents on the performance of reconstructed Mg-Al hydrotalcites in aldol condensations.* Applied Catalysis A-General, 2005. **281**(1-2): p. 191-198.
113. Abello, S., et al., *Accelerated study of the citral-acetone condensation kinetics over activated Mg-Al hydrotalcite.* Applied Catalysis A-General, 2007. **325**(1): p. 121-129.
114. Dubey, A., B.G. Mishra, and D. Sachdev, *Catalytic applications of ordered mesoporous magnesium oxide synthesized by mesoporous carbon.* Applied Catalysis A-General, 2008. **338**(1-2): p. 20-26.
115. Prescott, H.A., et al., *Application of calcined Mg-Al hydrotalcites for Michael additions: an investigation of catalytic activity-and acid-base properties.* Journal Of Catalysis, 2005. **234**(1): p. 119-130.
116. Veldurthy, B., J.M. Clacens, and F. Figueras, *Magnesium-lanthanum mixed metal oxide: A strong solid base for the Michael addition reaction.* Advanced Synthesis & Catalysis, 2005. **347**(6): p. 767-771.
117. Vijaikumar, S., A. Dhakshinamoorthy, and K. Pitchumani, *L-proline anchored hydrotalcite clays: An efficient catalyst for asymmetric Michael addition.* Applied Catalysis A-General, 2008. **340**(1): p. 25-32.
118. Xie, W.L., H. Peng, and L.G. Chen, *Calcined Mg-Al hydrotalcites as solid base catalysts for methanolysis of soybean oil.* Journal Of Molecular Catalysis A-Chemical, 2006. **246**(1-2): p. 24-32.
119. Shumaker, J.L., et al., *Biodiesel production from soybean oil using calcined Li-Al layered double hydroxide catalysts.* Catalysis Letters, 2007. **115**(1-2): p. 56-61.
120. Bulbule, V.J., et al., *Transesterification of alpha-haloesters and beta-ketoesters over Mg-Al-hydrotalcites (HT)-like anionic clays.* Journal Of Molecular Catalysis A-Chemical, 2007. **276**(1-2): p. 158-161.

121. Macala, G.S., et al., *Transesterification catalysts from iron doped hydrotalcite-like precursors: Solid bases for biodiesel production.* Catalysis Letters, 2008. **122**(3-4): p. 205-209.
122. Liu, Y., et al., *Transesterification of poultry fat with methanol using Mg-A1 hydrotalcite derived catalysts.* Applied Catalysis a-General, 2007. **331**: p. 138-148.
123. Shumaker, J.L., et al., *Biodiesel synthesis using calcined layered double hydroxide catalysts.* Applied Catalysis B-Environmental, 2008. **82**(1-2): p. 120-130.
124. Lazaridis, N.K., T.A. Pandi, and K.A. Matis, *Chromium(VI) removal from aqueous solutions by Mg-Al-CO_3 hydrotalcite: Sorption-desorption kinetic and equilibrium studies.* Industrial & Engineering Chemistry Research, 2004. **43**(9): p. 2209-2215.
125. Álvarez-Ayuso, E. and H.W. Nugteren, *Purification of chromium(VI) finishing wastewaters using calcined and uncalcined Mg-Al-CO_3-hydrotalcite.* Water Research, 2005. **39**(12): p. 2535-2542.
126. Lazaridis, N.K., *Sorption removal of anions and cations in single batch systems by uncalcined and calcined Mg-Al-CO_3 hydrotalcite.* Water Air And Soil Pollution, 2003. **146**(1-4): p. 127-139.
127. Kustrowski, P., et al., *Influence of thermal treatment conditions on the activity of hydrotalcite-derived Mg-Al oxides in the aldol condensation of acetone.* Microporous And Mesoporous Materials, 2005. **78**(1): p. 11-22.
128. Kustrowski, P., et al., *Aldol condensation of citral and acetone over mesoporous catalysts obtained by thermal and chemical activation of magnesium-aluminum hydrotalcite-like precursors.* Applied Catalysis A-General, 2006. **302**(2): p. 317-324.
129. Tichit, D., et al., *Textural Properties And Catalytic Activity Of Hydrotalcites.* Journal Of Catalysis, 1995. **151**(1): p. 50-59.
130. Abello, S. and J. Perez-Ramirez, *Steam activation of Mg-Al hydrotalcite. Influence on the properties of the derived mixed oxides.* Microporous And Mesoporous Materials, 2006. **96**(1-3): p. 102-108.
131. Winter, F., et al., *On the nature and accessibility of the Bronsted-base sites in activated hydrotalcite catalysts.* Journal Of Physical Chemistry B, 2006. **110**(18): p. 9211-9218.
132. Abello, S., D. Vijaya-Shanker, and J. Perez-Ramirez, *Stability, reutilization, and scalability of activated hydrotalcites in aldol condensation.* Applied Catalysis A-General, 2008. **342**(1-2): p. 119-125.

Chapter 2

Support and size effects of activated hydrotalcites for pre-combustion CO_2 capture

Abstract

A series of Mg-Al hydrotalcites (HT) with lateral platelet sizes ranging from 40 nm to 2 μm were hydrothermally prepared. Small HT platelets (~20 nm) were obtained by deposition onto a carbon nanofiber (CNF) support. The CO_2 sorption capacity at 523 K for the activated unsupported HT was low (~0.1 $mmol.g^{-1}$), regardless of the platelet size of the HT precursor. In addition, no relation was found between CO_2 sorption properties of activated HTs and their specific surface area. The sorption capacity of the activated CNF-supported HTs was increased, depending on the HT loading, by an order of magnitude (1.3- 2.5 $mmol.g^{-1}_{HT}$) compared to the activated unsupported HT. We propose that the CO_2-sorption capacity of HT is determined by the amount of low-coordination oxygen sites in the $Mg(Al)O_x$ nanoparticles, which is highest on supported HT.

Introduction

Carbon Capture and Storage (CCS) is an option to decrease the vast amounts of CO_2 (28 Gton in 2005 [1]) released into the atmosphere due to fossil fuel utilization [2]. CO_2 capture can be divided in two classes, i.e. end of pipe capture for example at power plants; this is the so-called post-combustion capture. Alternatively, CO_2 affiliated with the production of hydrogen, for example via the water-gas shift reaction (WGSR: $CO + H_2O \leftrightarrow CO_2 + H_2$) can be captured, preventing the release of CO_2, and driving the equilibrium of the reaction to the hydrogen side; this is one of the options for pre-combustion. For post-combustion, the commercially used amines are corrosive, thus special reactor materials are needed [3]. Alternatives based on solid sorbents involve modified SBA15- [4-6] and MCM41-amines [4, 5], MOFs [7-10] and ZIFs [11, 12]. For pre-combustion capture high temperatures (>250 °C) are required. Most of the studied materials, *e.g.* lithium zirconates [13-16], sodium zirconates [17, 18], CaO [19-21], basic alumina [22] and carbon based adsorbents [23-25], do not meet the required properties with respect to sorption capacities, kinetics and mechanical strength.

Optimal sorbents for pre-combustion use should display properties such as selectivity towards CO_2, a high adsorption capacity at high temperatures (>523 K), adequate adsorption and desorption kinetics at operating conditions (facile regeneration), long term stability upon cyclic use, adequate mechanical strength and low costs. A number of solid basic oxides, especially hydrotalcites, are promising as re-usable sorbent [26-29]. Hydrotalcites (HT) belong to the class of anionic clay minerals also known as layered double hydroxides. The structure of HT closely resembles that of brucite, $Mg(OH)_2$, where Mg^{2+} is octahedrally coordinated by hydroxyl groups. These octahedra share adjacent edges to form sheets or layers. In HT, part of the Mg^{2+} ions are replaced by Al^{3+} ions. This results in positively charged layers, which are balanced by charge-compensating anions (*e.g.* Cl^-, Br^-, CO_3^{2-}, I^-, NO_3^-, OH^-, SO_4^{2-}, …) located in the interlayer region where also hydrating water molecules are accommodated. HTs has received considerable attention in recent years because of their wide range of applications, such as base catalysts [30-34], ion exchangers [35, 36], polymer stabilizers and drug targets [37]. The edges, thus the lateral dimensions of the HT, have a significant influence on their catalytic behaviour [30, 32, 38].

Previous work from our group [30] showed an increase in activity in base catalysis with decreasing platelets size for activated HTs (self condensation of acetone). It was concluded that only the basic sites at the edges of the hydrotalcites platelets were involved in this low temperature reaction (273 K). In this work we report on a structure-activity relationship of the Mg-Al hydrotalcites platelet size before activation and the textural properties of the activated materials with their CO_2 capture properties. The samples were characterized using XRD, SEM, TEM and nitrogen physisorption.

2. Experimental

2.1 Preparation of unsupported hydrotalcites

To an aqueous solution (150 mL) containing 0.7 mol NaOH and 0.09 mol Na_2CO_3 an aqueous solution (70 mL) of 0.1 mol $Mg(NO_3)_2 \cdot 6H_2O$ and 0.05 mol $Al(NO_3)_3 \cdot 9H_2O$ was added drop wise. The resulting white suspension was aged at 298 K for 24 h under vigorous stirring. Subsequently, the suspension was filtered and washed extensively with demineralized water. The sample, further denoted as HT_{298}, was dried for 24 h at 393 K. To increase the crystallite size of the HT, the ageing was also performed at 313, 333 and 353 K. These as-synthesized samples will further be denoted as $HT_{313,}$ HT_{333} and HT_{353}. Ageing at higher temperatures, i.e. 373, 393, 413 and 433 K was performed in an autoclave. The synthesis mixture of NaOH, Na_2CO_3, $Mg(NO_3)_2 \cdot 6H_2O$ and $Al(NO_3)_3 \cdot 9H_2O$ as described above was first stirred for 1 h at room temperature. Next, the precipitate was poured into a Teflon holder and placed into a stainless steel rotating autoclave followed by ageing for 16 h at the desired temperature. Subsequently, the suspension was filtered and washed extensively with demineralized water and dried for 24 h at 393 K. The as-synthesized samples are further denoted as HT_{373}, HT_{393}, HT_{413} and HT_{433}.

Preparation of hydrotalcites using the 'urea procedure' [39]

An aqueous solution (150 mL) of 0.1 mol $Mg(NO_3)_2 \cdot 6H_2O$, 0.05 mol $Al(NO_3)_3 \cdot 9H_2O$ and 0.75 mol urea was vigorously stirred and heated at 363 K and kept at this temperature for 24h. The pH increased from 3.0 to ~9.0 at the end of the reaction. The

resulting white suspension was filtered, washed extensively with demineralized water and dried at 393 K for 24 h. This as-synthesized sample is further denoted as HT_{urea}.

2.2 Preparation of supported hydrotalcites

Carbon nanofibers

A silica-supported nickel catalyst with a metal loading of 20 wt% was prepared by deposition precipitation using the hydrolysis of urea at 363 K [40]. Silica (8.5 g), nickel nitrate (10.6 g) and urea (7.9 g) were suspended in 1L of demineralized water and vigorously stirred. The reaction mixture was heated at 363 K and kept at this temperature for 16 h. The resulting green suspension was filtered, washed extensively with demineralized water and dried at 393 K for 24 h. A sieve fraction of 425- 850 μm of the catalyst precursor was calcined in static air at 873 K (5 $K.min^{-1}$) for 3 h. Next, the Ni catalyst precursor (5.0 gram) was reduced *in situ* at 973 K in a fixed bed reactor for 2 h in a 30% H_2/N_2 flow (800 $mL.min^{-1}$). After lowering the temperature to 823 K, synthesis gas (33% CO/13% H_2), balanced with N_2 was passed through the reactor for 24 h at a pressure of 2 bar in a total flow of 800 $mL.min^{-1}$. Removal of the growth catalyst and oxidation of CNF was performed as reported in literature [41, 42] using subsequent treatments in aqueous 1 M KOH and concentrated HNO_3.

CNF supported hydrotalcites

To prepare supported Mg-Al hydrotalcites (Mg/Al=2, (at/at)), 5.0 g CNF were impregnated in a 250 mL round-bottom flask with a solution containing 3.3 mL of $Mg(NO_3)_2$ (1.4 M) and $Al(NO_3)_3$ (0.7 M). After drying for 1 hour at 393 K, a solution of 3.0 mL NaOH (8.3 M) and Na_2CO_3 (0.56 M) was added. Ageing was performed in a water-saturated atmosphere, under a nitrogen flow (7 $mL.min.^{-1}$) for 16 h at 333 K, followed by extensive washing with demineralized water and drying at 393 K for 24 h. This as-synthesized sample is denoted as HT_{10}-CNF, with the number 10 referring to the weight loading (%) of HT deposited on CNF. The reported nominal weight loadings are close to the actual loadings as reported earlier [32].

A second sample was prepared as described above with a solution containing 3.3 mL of $Mg(NO_3)_2$ (0.7 M) and $Al(NO_3)_3$ (0.35 M). This as-synthesized sample is denoted as HT_5-

CNF. The third sample was prepared as described above. After that, the synthesis procedure was repeated once. This as-synthesized sample is denoted as HT_{18}-CNF. General supported samples will be referred to 'HT-CNF'.

2.3 Characterization

Powder X-ray diffraction (XRD) patterns were measured using a Bruker-AXS D8 advance powder diffraction apparatus equipped with an automatic divergence slit (filtered Co-K_α radiation λ = 1.79026 Å). N_2-physisorption measurements were performed using a Micromeritics Tristar 3000 analyzer after drying the samples at 393 K in vacuum for at least 20 h prior to the measurements, pore volume at P/P_0 = 0.995. CO_2 loaded samples ($HT_{act\text{-}CO2}$) for nitrogen physisorption were cooled to RT after the adsorption step (vide infra). SEM micrographs were obtained using a Philips XL30FEG electron microscope equipped with an EDX detector for elemental analysis. TEM micrographs were obtained with a FEI Technai 20 FEG TEM operating at 200kV equipped with an EDX detector. TEM samples were dispersed on a holey carbon film supported on a copper grid. A Branson Sonifier 450 W was used for ultrasonic treatment for 1 h at 323 K.

2.4 CO_2 sorption measurements

CO_2 sorption measurements were performed in a quartz plug-flow reactor with an inner diameter of 12 mm. The gas flows (N_2, CO_2) were passed down-flow through the reactor and controlled via mass flow controllers (Brooks 5850s). The total pressure in the setup was maintained at 1.10 bar, using a backpressure controller (Brooks 5866). A tubular oven was placed around the reactor to control the process temperature. The reactor was loaded with 2.0 g of sample (bed height 35 mm) using a sieve fraction with particle sizes of 212- 500 µm. For HT-CNF the reactor was loaded with 5 g of sample (bed height 85 mm), which contained 0.25, 0.5 or 1.0 g of HT. All samples were activated by heating in N_2 (30 $mL.min^{-1}$) at 773 K (5 $K.min^{-1}$) for 1 h to remove CO_2 and water from the starting material (HT_{act}, activation step). The activated samples are denoted as $HT_{T\text{-}act}$ and HT_{act}-CNF, where T is the synthesis temperature in K and 'act' refers to the activation step. After activation, all samples were subjected to at least two identical adsorption (523 K) and desorption (773 K) cycles to assess reproducibility.

Conditions for the adsorption and desorption steps are given in Table 1. The total flow throughout all experiments was 30 mL.min^{-1}. N_2 was humidified with CO_2 free water using a saturator set at 331 K. All adsorption experiments were performed for 30 minutes in 5% CO_2. After adsorption, the system was flushed with N_2. Desorption was performed by heat treatment in dry nitrogen (30 mL.min^{-1}) at 773 K (5 K.min^{-1}) for 1 h. To prevent gasification of the CNF support material at higher temperatures in steam, dry nitrogen was used during desorption in all measurements to obtain comparable results between $HT_{T\text{-}act}$ and HT_{act}-CNF. Blank measurements were performed either with a non adsorbing material (SiC) or CNF, with the same particle size range and bed volume as the HT containing material. There was no CO_2 adsorption by supports. The effluent gas was analyzed by on-line FT-IR using a Midac corporation 2000 M series. For each spectrum, 8 scans were accumulated with a resolution of 4 cm^{-1}; spectra were recorded every 13 seconds. The IR-cell, made of stainless steel, had a path length of 2 mm and contained CaF_2 windows. The sample compartment was continuously purged with a stream of dry N_2 to prevent interference of CO_2 present in the atmosphere. A background spectrum using an empty cell was acquired prior to a sorption measurement. The integrated area from 2280- 2390 cm^{-1} was used to quantify the amount of CO_2 in the gas phase. A CO_2 concentration above 100 ppm is defined as breakthrough. From the breakthrough time and the flow and concentration, the amount of CO_2 was calculated.

Table 1. Experimental conditions for sorption measurements with 2g $HT_{T\text{-}act}$ or 5g HT_{act}-CNF.

	Flow (mL.min^{-1})	**Composition**	**Temp. (K)**
Activation	30	100% N_2	323 → 773 (5 K.min^{-1}, 1h)
Adsorption	30	83% N_2/ 12% H_2O/ 5% CO_2	523 (max. 30 min)
Desorption	30	100% N_2	523 → 773 (5 K.min^{-1}, 1h)

3. Results and discussion

3.1 Characterization of materials

To establish the crystallographic ordering and purity of the as-synthesized HT samples, the samples were analyzed by XRD. Figure 1 shows selected XRD patterns of unsupported as-synthesized HTs (HT_{298}, HT_{333}, HT_{373}, HT_{433} and HT_{urea}). The signals at $2\theta \approx 13.5°$, 27.6°, 40.0°, corresponding to the (003), (006) and (009/ 012) crystal planes, indicate well-formed crystalline layered structures. In addition, at high synthesis temperatures, signals were detected close to the 003 and 006 (11.3° and 24.6°), which can be ascribed to diffractions caused by Kβ radiation. For all samples, except for HT_{urea}, the signals were representative for HTs with interlayer carbonate. In contrast, HT_{urea} showed signals at 62.9°, 67.1°, which were characteristic for a sample with hydroxylic ions (OH^-) in the interlayer [43]. Since the decomposition of urea takes place at relatively low pH (pH~6), the (bi-)carbonate concentration in the solution will be low and hydroxyl ions (OH^-) in the interlayer are favored. To summarize, only crystalline hydrotalcites were detected by XRD, indicating the high purity of all samples.

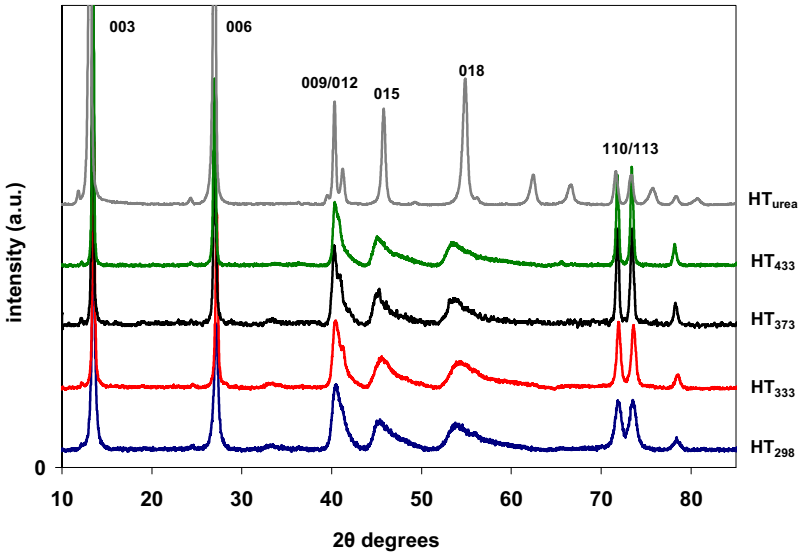

Figure 1. Selected XRD profiles of as-synthesized HT_{298}, HT_{333},HT_{373}, HT_{433} and HT_{urea}.

The selected XRD pattern of the supported hydrotalcite (HT_{10}-CNF) is compared to that of HT_{333} and to pure CNF in Figure 2. In the supported sample, diffraction lines due to the presence of HT, as indicated by the arrows, can be distinguished next to the strong lines of the CNF support. From this figure it is clear that the diffraction lines of hydrotalcite- in the supported sample are broader than those of unsupported HT, which implies that the HT crystallites on the supported sample (HT_{10}-CNF) are smaller and/ or less ordered [44]. In addition, the intensity of the signals for supported HT is much smaller compared to that of the unsupported HT sample, after identical counting times, as a result of the small HT platelets [31] and/or lower amount of HT present.

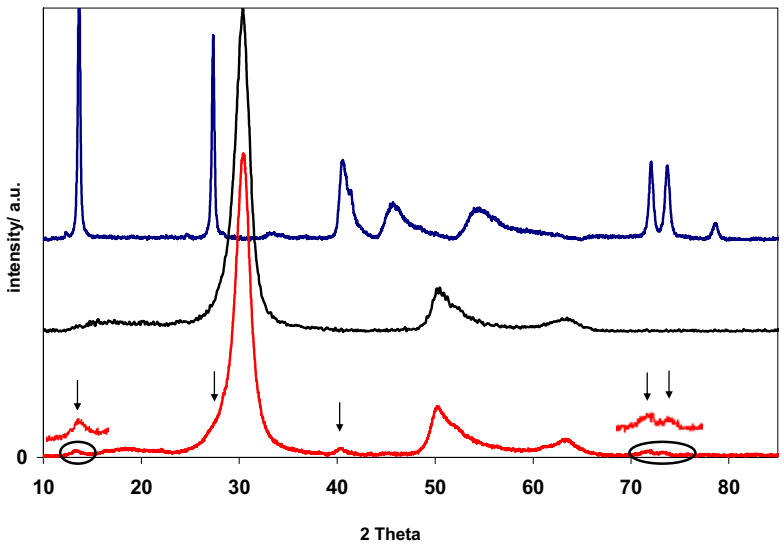

Figure 2. XRD profiles of as-synthesized HT_{333}, CNF, HT_{10}-CNF; arrows indicate HT peaks.

The particle size and morphology of unsupported HT samples were analyzed by SEM while the supported HTs were analyzed by TEM. Figure 3 shows SEM micrographs of selected hydrotalcites (HT_{313}, HT_{373}, HT_{473} and HT_{urea}). Samples prepared using $NaOH/Na_2CO_3$ as a base (Figure 3A-C) showed regular hexagonally shaped HT platelets. The micrographs highlight the difference in lateral platelet size due to the ageing temperature with

an increase in size with increasing temperature. When using urea as the precipitant, very large HT platelets (2 μm, (Fig. 3D)) were obtained in line with literature [39, 45]).

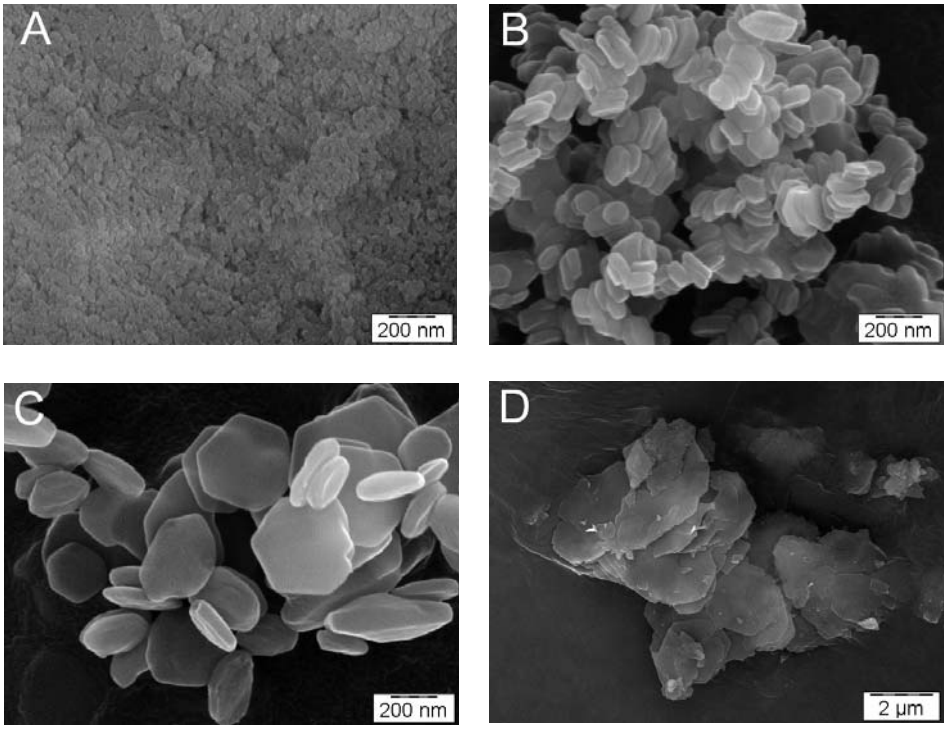

Figure 3. SEM micrographs of A) HT_{313}; B) HT_{373}; C) HT_{433}; D) HT_{urea}.

Figure 4 shows selected bright- and dark-field TEM micrographs of HT_{10}-CNF. In bright field mode, HTs are difficult to distinguish from carbon, because of similarity in density. In dark field mode, i.e. diffraction contrast imaging, the small HT crystallites were more easy to observe (Fig. 4). The dark field micrographs revealed more HTs than could be detected in bright field mode. For clarity the arrows in Fig. 4A indicate some of the HT platelets.

An overview of the average lateral platelet sizes as function of the ageing temperature, based on SEM and TEM by determining the platelets size of 30 individual HT platelets, is shown in Figure 5. Clearly, unsupported as-synthesized HTs samples showed an increase in

lateral platelet size with increasing synthesis temperature. The average crystalline platelets increased from 35 nm (HT_{298}) to 300 nm (HT_{433}). HT_{urea} had the largest lateral platelet size (2 µm), whereas, supported hydrotalcites displayed the smallest crystalline platelets (~20 nm). In conclusion, the HT platelets were tuned from 20 nm to 2 µm and all HT precursor samples showed good crystallinity.

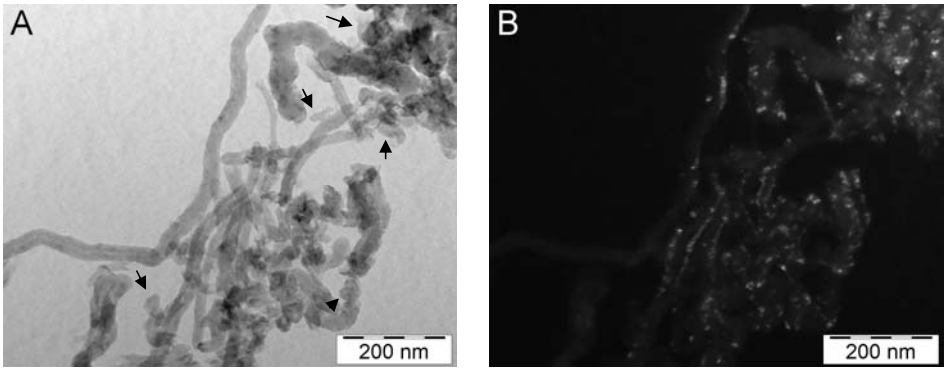

Figure 4. TEM micrographs of HT_{10}-CNF in A) bright field, arrows indicate the HT platelets; B) dark field, small HT crystallites are visible.

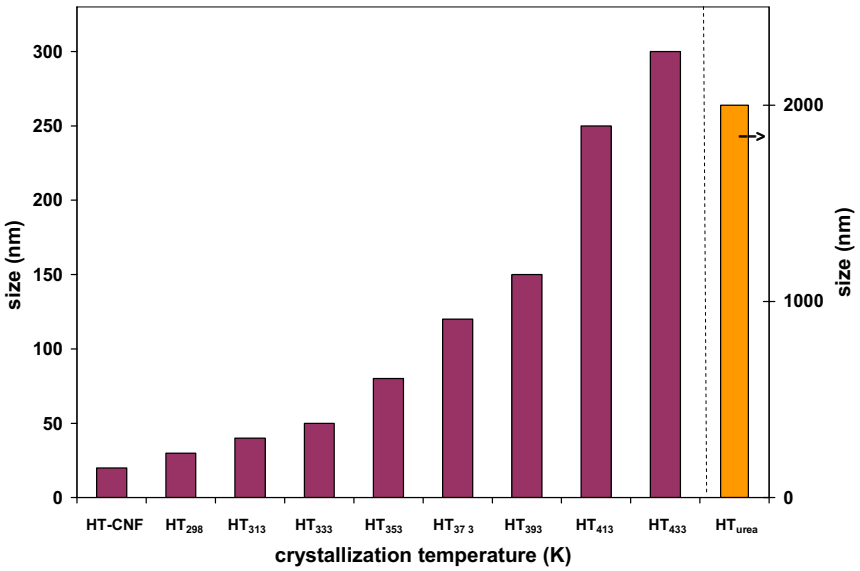

Figure 5. Average platelet size effect on crystallization temperature of as-synthesized HTs.

3.2 CO_2 adsorption and desorption kinetics

Prior to sorption measurements, all samples were activated at 773 K in N_2. Representative breakthrough curves for CO_2 adsorption at 523 K on these activated HT are shown in Figure 6. Please note, after activation the hydrotalcite material still retains its mesoscopic shape, i.e. the platelets are still present, but XRD revealed broad $Mg(Al)O_x$ diffractions. The activated samples are denoted as HT_{act} and HT_{act}-CNF, where 'act' denotes the activated material ($Mg(Al)O_x$) after heat treatment. All activated unsupported HTs showed, within experimental error, the same breakthrough times, which corresponded to a CO_2 capacity of approximately 0.1 $mmol.g^{-1}$, irrespective of the original platelet size.

For the supported activated HTs, the breakthrough times were significantly longer (Fig. 6a). Even though these samples contained only 5, 10 and 18 wt% HT, breakthrough times were 10.1 min for $HT_{5\text{-act}}$-CNF, 9.5 min for $HT_{10\text{-act}}$-CNF (shown) and 13.0 min for $HT_{18\text{-act}}$-CNF, which corresponds to capacities of 2.5, 1.3 and 1.7 $mmol.g^{-1}_{HT}$, i.e. an order of magnitude higher compared to activated unsupported HTs. A selected number of desorption profiles is shown in Figure 7. Under these dry conditions all activated unsupported HTs show similar desorption characteristics.

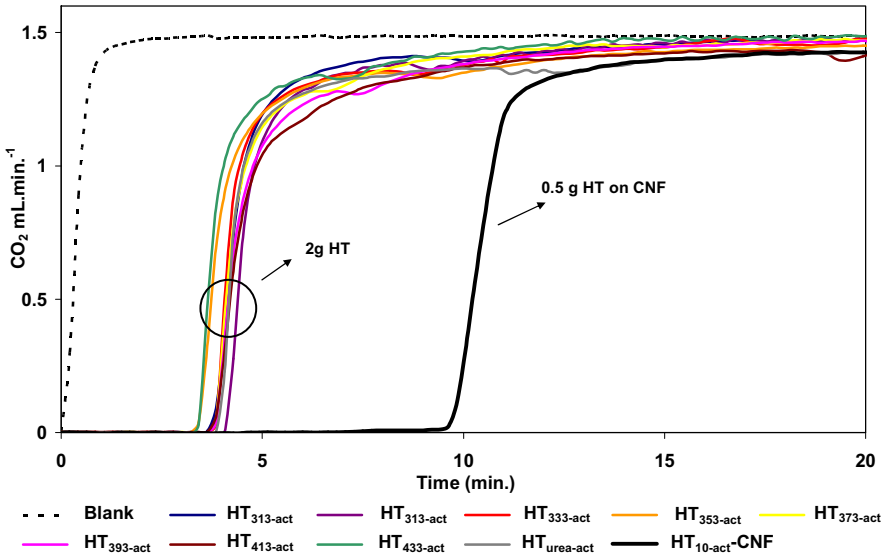

Figure 6. Representative breakthrough curves of activated HTs (2g) and activated HT_{10}-CNF (5g), flow 25 $mL.min^{-1}$ N_2, 3.5 $mL.min^{-1}$ H_2O, 1.5 $mL.min^{-1}$ CO_2 at 523 K.

Desorption of the activated supported sample started at a higher temperature compared to the activated unsupported HT and the first desorption maximum of HT_{10}-CNF occurs at 580 K. These details point to stronger bonding of adsorbed CO_2. The high temperature desorption peak (773 K) is more pronounced with HT-CNF, which is more likely related to absorption. Please note that the presence of steam during desorption will most likely negatively affect the cycle stability of the CNF-supported materials.

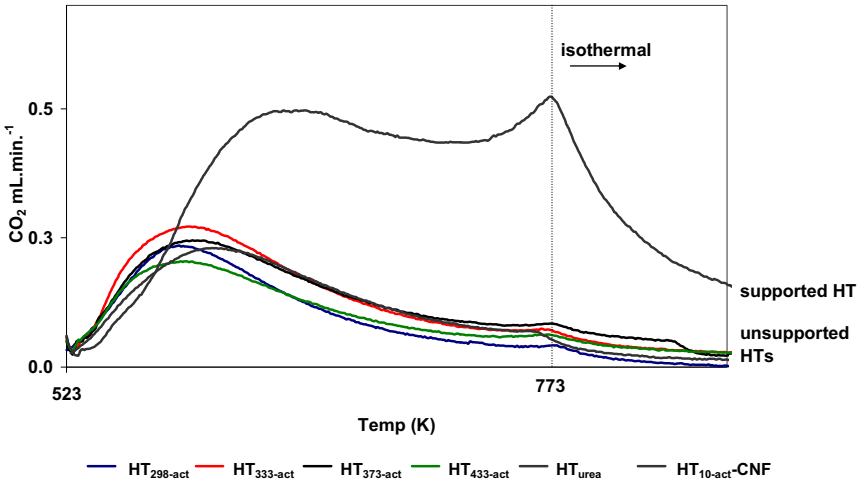

Figure 7. Selected representative desorption profiles of activated HTs and activated HT_{10}-CNF, flow 30 mL.min^{-1} N_2, 523- 773 K 1 h.

Figure 8 summarizes the adsorption capacity at 532 K of all samples as a function of their original HT-platelet size. Unsupported hydrotalcites (platelet size between 30 nm and 2 µm) evidently all have an invariant adsorption capacity (~0.1 mmol.g^{-1}). Lemonidou *et al* [20] also reported that the CO_2 capacity did not depend on size for CaO based materials. However, their materials had sizes in a range of 1-10 µm, while our precursor samples had sizes from 35 nm to 2 µm. Surprisingly, the supported HT samples with a platelet size of ~20 nm had much higher capacities, depending on the HT loading, 1.3- 2.5 mmol.g$^{-1}_{HT}$. Figure 9 shows the CO_2 sorption capacity of $HT_{333\text{-act}}$ and $HT_{10\text{-act}}$-CNF as function of the number of adsorption-desorption cycles. Clearly, the materials showed stable behavior.

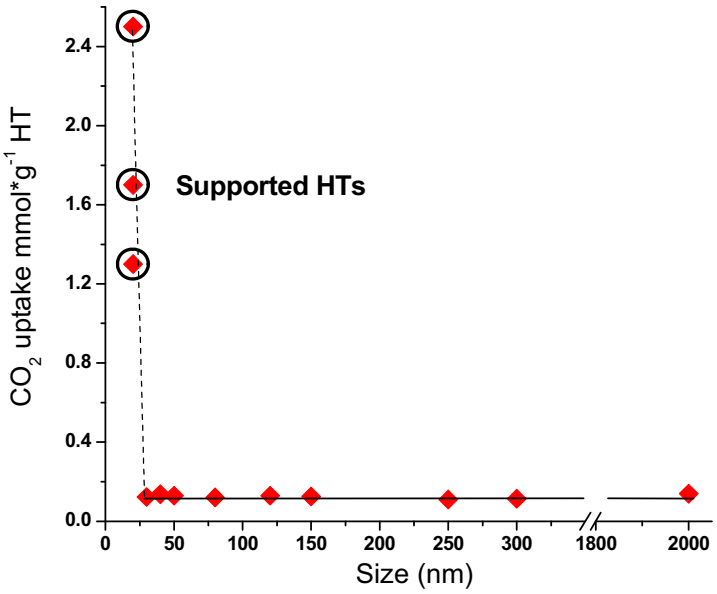

Figure 8. CO_2 capacities at 523 K of all activated (supported) HTs and their laterals sizes. The supported samples have a 10- 25 fold higher capacity than unsupported samples.

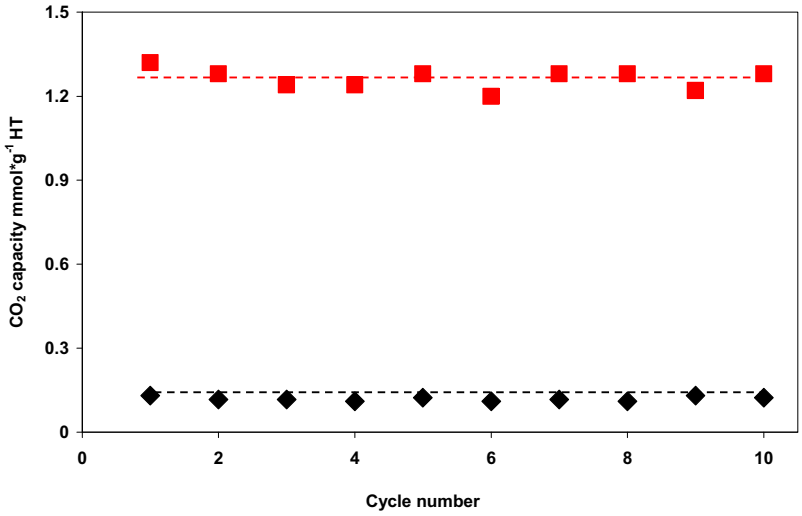

Figure 9. CO_2 capacity as function of adsorption-desorption cycles for 2 selected samples; unsupported $HT_{333\text{-}act}$ (◆) and $HT_{10\text{-}act}$-CNF (■).

Since no relation could be found between platelet size and capacity, the CO_2 capture properties of the HTs with relation to their textural properties, especially after activation were investigated (Table 2). In Table 2 some physico-chemical properties of the unsupported HTs are given. Micropores were not, or hardly, present in the samples. The surface area of the as-synthesized HTs (HT_{as}) varied from 15- 100 $m^2.g^{-1}$ and decreased with increasing platelet size, i.e. with increasing ageing temperature, which is in good agreement with literature [46].

Activation (= heat treatment in N_2 at 773 K, see *2.3*) of the HTs (HT_{act}) resulted in an increase in surface area and pore volume. To investigate how the textural properties of activated HTs changed after CO_2 loading, nitrogen physisorption experiments were also performed on the CO_2 loaded samples (Table 2, $HT_{act\text{-}CO2}$, see *2.4*). All loaded samples showed a decrease in pore volume compared to the activated HT, with the exception of $HT_{373\text{-}act\text{-}CO2}$. After CO_2 loading, the surface areas of samples HT_{298}, HT_{333}, HT_{373} and HT_{433} were in a similar range (117- 129 $m^2.g^{-1}$), whereas surface areas of the other loaded samples (HT_{313}, HT_{353}, HT_{393}, HT_{413} and HT_{urea}) varied significantly. Moreover, after loading with CO_2, the surface area of five samples decreased (HT_{298}, HT_{353}, HT_{393}, HT_{433}, and HT_{urea}), while with the other four samples an increase in surface area (HT_{313}, HT_{333}, HT_{373} and HT_{413}) was found. Thus, both the activated HTs and the CO_2 loaded samples showed non-systematic variations of surface areas and pore volumes.

These results indicate that there is no relation between CO_2 capacity and textural properties, which is in agreement with Kim and co-workers [47]. The pore volume and surface area of the CNF supported HTs were significantly lower than CNF, which indicates a partial filling of the pores with HT (Table 2, bottom). The surface areas and pore volume of activated supported HTs were slightly higher than their precursors.

Table 2. Physico-chemical properties of the various hydrotalcites, HT_{as}, HT_{act} and $HT_{act\text{-}CO2}$.

Sample	HT_{as}		HT_{act}		$HT_{act\text{-}CO2}$	
	S_{BET} ($m^2.g^{-1}$)	V_{tot} ($cm^3.g^{-1}$)	S_{BET} ($m^2.g^{-1}$)	V_{tot} ($cm^3.g^{-1}$)	S_{BET} ($m^2.g^{-1}$)	V_{tot} ($cm^3.g^{-1}$)
HT_{298}	100	0.6	262	0.86	126	0.27
HT_{313}	93	0.67	125	0.74	216	0.57
HT_{333}	53	0.35	68	0.46	117	0.41
HT_{353}	47	0.4	83	0.45	50	0.44
HT_{373}	24	0.11	68	0.16	127	0.44
HT_{393}	21	0.09	209	0.22	23	0.14
HT_{413}	19	0.07	157	0.17	172	0.18
HT_{433}	15	0.07	183	0.17	139	0.2
HT_{urea}	32	0.1	245	0.26	72	0.2
$HT_{333\text{-}us}$					211	0.77
CNF	155	0.34				
HT_5-CNF	107	0.29	124	0.31	-	-
HT_{10}-CNF	97	0.19	114	0.22	110	0.23
HT_{18}-CNF	98	0.18	105	0.20	-	-

As discussed above, the CO_2 sorption capacity of activated unsupported HTs is invariant with the surface area. Therefore, the coverage of CO_2 per nm^2 must increase with decreasing surface area (see Fig. 10). Now, a possible explanation for this observation is made. For MgO, which has a structure similar to the activated HTs, the sites for CO_2 adsorption are expected to associate with low coordinated O^{2-}-Mg^{2+} sites [48-58]. In other words, the 'C' of CO_2 adsorbs on low coordinated oxygen (oxygen surrounded by less than 5 atoms). We propose that the active sites for CO_2 adsorption on activated HTs are also associated with O^{2-}-Mg^{2+} sites ($MgO + CO_2 \leftrightarrow MgCO_3$). During CO_2 sorption the acidic CO_2 reacts with basic O^{2-} sites depending on their coordination. Oxygen atoms located at edges and corners of the crystal planes have stronger basicity than oxygen atoms in basel planes. Therefore, the energy level of surface oxygen increases with decreasing coordination number.

The interactions are assumed mainly to be of the HOMO-LUMO type [53]. Consequently, the HOMO-LUMO energy gap between O^{2-} and CO_2 is reduced on corners and edges (under coordination of oxygen) and thus charge transfer from O^{2-} to CO_2 will occur. Therefore, the interaction from an edge or corner O^{2-} anion with a CO_2 molecule may lead to surface carbonate species [59, 60]. Pettersson *et al* [59, 60] calculated for MgO surfaces the energetically favorable interactions with CO_2. They concluded that on a regular unperturbed MgO(100) surface no CO_2 adsorption occurs. However, 3- and 4 coordinated O^{2-} edges and corners (O_{3c}, O_{4c}) showed a reduction in the (HOMO-LUMO) energy gap. Consequently, adsorption with CO_2 on an edge or corner is more likely to occur (Figure 11), which illustrates our proposal.

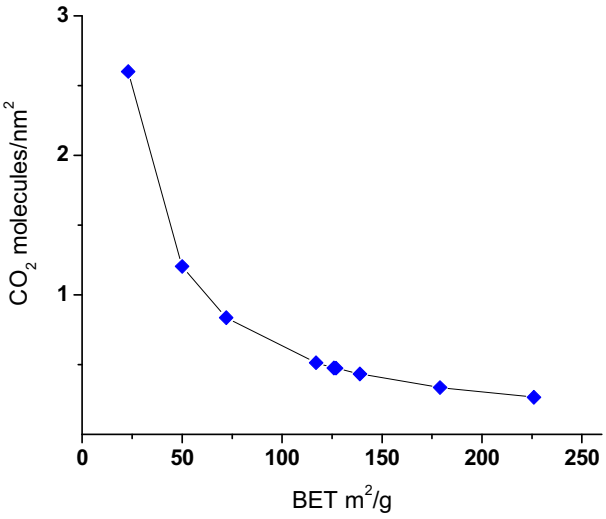

Figure 10. Effect of surface area on activated unsupported HTs: coverage of CO_2 increases with decreasing surface area.

As a result of these findings, we propose that the amount of low-coordinated oxygen in our activated unsupported samples, are identical on a weight-basis for all samples. After activation, the samples lose their original crystalline platelet structure and are all '$Mg(Al)O_x$' like, although the platelets shape of the HTs, as visualized by SEM, remain. Apparently, larger $Mg(Al)O_x$ particles contain more surface defects per unit surface area and,

consequently, higher coverage of CO_2 (Fig. 11). We propose that the high increase of CO_2 capacities of the activated supported HTs, are based on more defects on the small $Mg(Al)O_x$ crystals. The individual crystals are anchored on the CNF, thus have less flexibility, which might contribute to more defects and low-coordinated oxygen. In other words, more adsorption sites are formed in the activated supported HT ($Mg(Al)O_x$) upon heat treatment, as result of the limited mobility. Apparently, for unsupported materials the total number of adsorption sites in the reactor is similar for all samples, since the adsorption capacity is the same for all samples (Figure 6a). We speculate that the number of defects per surface area is larger for larger particles, i.e. those formed from larger HT platelets as for the smaller particles probably as a result of a more difficult annealing, i.e. lower mobility of ions, in larger particles during activation.

Additional evidence for the role of low coordination sites comes from the use of an unsupported ultra sonic treated HT sample (data not shown). Sonication is expected to create defects on the surface/ edges of the HT [61, 62]. Indeed, the capacity of a sonicated sample increased to 0.2 $mmol.g^{-1}$ as compared to the 0.1 $mmol.g^{-1}$ for a regular sample. Unfortunately, after the first cycle, the capacity of the sonicated sample dropped to the original value as the regular HTs.

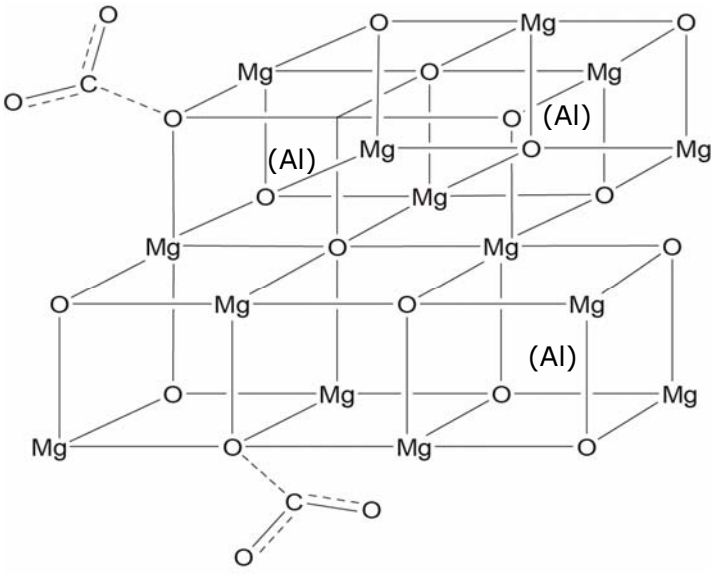

Figure 11. Corners and edges are important for CO_2 adsorption.

Conclusions

In this chapter we have presented a study of CO_2 sorption measurements at 523 K on Mg-Al hydrotalcites with lateral platelet sizes of 20 nm to 2 µm. Unsupported hydrotalcites showed an invariant and low capacity as function of platelet size. An increase by a factor 10-25 in HT-weight based capacities was accomplished by supporting the HT on CNF. Nitrogen physisorption measurements showed no dependence of CO_2 capacity and specific surface area for the unsupported HT. Currently, we tentatively relate the higher capacity of the activated supported samples to a higher density of low coordination oxygen (edges and corners) in the $Mg(Al)O_x$ phase crystal interacting with the CNF surface.

Acknowledgements

This research has been carried out by Inorganic Chemistry and Catalysis, Debye Institute for Nanomaterials Science, Department of Chemistry in the CATO-project (Carbon Capture, Transport and Storage). Marjan Versluijs-Helder, Cor van der Spek, and Ad Mens are thanked for SEM, TEM, and N_2-physisorption measurements. Valuable input from Ruud van den Brink, Paul Cobden, Daan Jansen and Rick Reijers (ECN, Petten the Netherlands) is acknowledged.

References

1. *Intergovernmental Panel on Climate Change.* IPCC, Climate Change 2007: The Physical Science Basis (Cambrigde Univ. Press, Cambridge, 2007).
2. http://CO_2-cato.nl/.
3. Fauth, D.J., et al., *Eutectic salt promoted lithium zirconate: Novel high temperature sorbent for CO_2 capture.* Fuel Processing Technology, 2005. **86**(14-15): p. 1503-1521.

4. Hicks, J.C., et al., *Designing adsorbents for CO_2 capture from flue gas-hyperbranched aminosilicas capable,of capturing CO_2 reversibly.* Journal Of The American Chemical Society, 2008. **130**(10): p. 2902-2903.
5. Yue, M.B., et al., *Efficient CO_2 capturer derived from as-synthesized MCM-41 modified with amine.* Chemistry-a European Journal, 2008. **14**(11): p. 3442-3451.
6. Wang, X., et al., *Infrared Study of CO_2 Sorption over "Molecular Basket" Sorbent Consisting of Polyethylenimine-Modified Mesoporous Molecular Sieve.* The Journal of Physical Chemistry C, 2009. **113**(17): p. 7260-7268.
7. Babarao, R. and J.W. Jiang, *Molecular screening of metal-organic frameworks for CO_2 storage.* Langmuir, 2008. **24**(12): p. 6270-6278.
8. Llewellyn, P.L., et al., *High uptakes of CO_2 and CH_4 in mesoporous metal-organic frameworks MIL-100 and MIL-101.* Langmuir, 2008. **24**(14): p. 7245-7250.
9. Finsy, V., et al., *Separation of CO_2/CH_4 mixtures with the MIL-53(Al) metal-organic framework.* Microporous and Mesoporous Materials, 2009. **120**(3): p. 221-227.
10. Yazaydin, A.O., et al., *Enhanced CO_2 Adsorption in Metal-Organic Frameworks via Occupation of Open-Metal Sites by Coordinated Water Molecules.* Chemistry of Materials, 2009. **21**(8): p. 1425-1430.
11. Banerjee, R., et al., *High-throughput synthesis of zeolitic imidazolate frameworks and application to CO_2 capture.* Science, 2008. **319**(5865): p. 939-943.
12. Liu, D.H., et al., *Understanding the Adsorption and Diffusion of Carbon Dioxide in Zeolitic Imidazolate Frameworks: A Molecular Simulation Study.* Journal of Physical Chemistry C, 2009. **113**(12): p. 5004-5009.
13. Ida, J. and Y.S. Lin, *Mechanism of high-temperature CO_2 sorption on lithium zirconate.* Environmental Science & Technology, 2003. **37**(9): p. 1999-2004.
14. Pfeiffer, H. and K.M. Knowles, *Reaction mechanisms and kinetics of the synthesis and decomposition of lithium metazirconate through solid-state reaction.* Journal Of The European Ceramic Society, 2004. **24**(8): p. 2433-2443.
15. Ida, J., R.T. Xiong, and Y.S. Lin, *Synthesis and CO_2 sorption properties of pure and modified lithium zirconate.* Separation And Purification Technology, 2004. **36**(1): p. 41-51.

16. Xiong, R.T., J. Ida, and Y.S. Lin, *Kinetics of carbon dioxide sorption on potassium-doped lithium zirconate.* Chemical Engineering Science, 2003. **58**(19): p. 4377-4385.
17. Zhao, T.J., et al., *Preparation and high-temperature CO_2 capture properties of nanocrystalline Na_2ZrO_3.* Chemistry Of Materials, 2007. **19**(13): p. 3294-3301.
18. Ochoa-Fernandez, E., et al., *Synthesis and CO_2 capture properties of nanocrystalline lithium zirconate.* Chemistry Of Materials, 2006. **18**(25): p. 6037-6046.
19. Han, C. and D.P. Harrison, *Simultaneous shift reaction and carbon dioxide separation for the direct production of hydrogen.* Chemical Engineering Science, 1994. **49**(24B): p. 5875-5883.
20. Martavaltzi, C.S. and A.A. Lemonidou, *Development of new CaO based sorbent materials for CO_2 removal at high temperature.* Microporous and Mesoporous Materials, 2008. **110**(1): p. 119.
21. Kuramoto, K., et al., *Repetitive carbonation-calcination reactions of Ca-based sorbents for efficient CO_2 sorption at elevated temperatures and pressures.* Industrial & Engineering Chemistry Research, 2003. **42**(5): p. 975-981.
22. Yong, Z., V. Mata, and A.E. Rodrigues, *Adsorption of carbon dioxide on basic alumina at high temperatures.* Journal Of Chemical And Engineering Data, 2000. **45**(6): p. 1093-1095.
23. Yong, Z., V.G. Mata, and A.E. Rodrigues, *Adsorption of carbon dioxide on chemically modified high surface area carbon-based adsorbents at high temperature.* Adsorption-Journal Of The International Adsorption Society, 2001. **7**(1): p. 41-50.
24. Kapoor, A., K.R. krishnamurthy, and A. Shirley, *Kinetic separation of carbon dioxide from hydrocarbons using carbon molecular sieve.* Gas Separation & Purification, 1993. **7**(4): p. 259-263.
25. Song, H.K. and K.H. Lee, *Adsorption of carbon dioxide on chemically modified carbon adsorbents*. Separation Science and Technology, 1998. **33**(13): p. 2039-2057.
26. Ding, Y. and E. Alpay, *Equilibria and kinetics of CO_2 adsorption on hydrotalcite adsorbent.* Chemical Engineering Science, 2000. **55**(17): p. 3461-3474.
27. Ding, Y. and E. Alpay, *Adsorption-enhanced steam-methane reforming.* Chemical Engineering Science, 2000. **55**(18): p. 3929-3940.

28. Ding, Y. and E. Alpay, *High temperature recovery of CO_2 from flue cases using hydrotalcite adsorbent.* Process Safety And Environmental Protection, 2001. **79**(B1): p. 45-51.
29. Nataraj, S., et al., *Materials selectivity adsorbing CO_2 from CO_2 containing streams* EP Patent No. 1006079A1, 2000.
30. Winter, F., et al., *A hydrotalcite-based catalyst system for the single-stage liquid-phase synthesis of MIBK.* Applied Catalysis A-General, 2006. **307**(2): p. 231-238.
31. Winter, F., A.J. van Dillen, and K.P. de Jong, *Supported hydrotalcites as highly active solid base catalysts.* Chemical Communications, 2005(31): p. 3977-3979.
32. Winter, F., et al., *Hydrotalcites supported on carbon nanofibers as solid base catalysts for the synthesis of MIBK.* Journal Of Catalysis, 2005. **236**(1): p. 91-100.
33. Angelescu, E., et al., *Solid base catalysts obtained from hydrotalcite precursors, for Knoevenagel synthesis of cinamic acid and coumarin derivatives.* Applied Catalysis A-General, 2006. **308**: p. 13-18.
34. Veldurthy, B., J.M. Clacens, and F. Figueras, *Magnesium-lanthanum mixed metal oxide: A strong solid base for the Michael addition reaction.* Advanced Synthesis & Catalysis, 2005. **347**(6): p. 767-771.
35. Bontchev, R.P., et al., *Synthesis, characterization, and ion exchange properties of hydrotalcite* $Mg_6Al_2(OH)_{16}(A)_x(A')_{2-x}\cdot 4H_2O$ (A, A' = Cl^-, Br^-, I^-, and NO_3^-, $2 \geq x \geq 0$) *derivatives.* Chemistry Of Materials, 2003. **15**(19): p. 3669-3675.
36. Costantino, U., et al., *Anion exchange of methyl orange into Zn-Al synthetic hydrotalcite and photophysical characterization of the intercalates obtained.* Langmuir, 1999. **15**(13): p. 4454-4460.
37. Mohanambe, L. and S. Vasudevan, *Anionic clays containing anti-inflammatory drug molecules: Comparison of molecular dynamics simulation and measurements.* Journal Of Physical Chemistry B, 2005. **109**(32): p. 15651-15658.
38. Roelofs, J., et al., *On the structure of activated hydrotalcites as solid base catalysts for liquid-phase aldol condensation.* Journal Of Catalysis, 2001. **203**(1): p. 184-191.
39. Ogawa, M. and H. Kaiho, *Homogeneous precipitation of uniform hydrotalcite particles.* Langmuir, 2002. **18**(11): p. 4240-4242.
40. van Dillen, A.J., et al., Proc. 6th Int. Congr. Catal. 2 1977: p. 677.

41. Toebes, M.L., et al., *The influence of oxidation on the texture and the number of oxygen-containing surface groups of carbon nanofibers.* Carbon, 2004. **42**(2): p. 307-315.

42. Winter, F., et al., *TEM and XPS studies to reveal the presence of cobalt and palladium particles in the inner core of carbon nanofibers.* Carbon, 2005. **43**(2): p. 327-332.

43. Cavani, F., F. Trifiro, and A. Vaccari, *Hydrotalcite-type anionic clays: Preparation, properties and applications.* Catalysis Today, 1991. **11**(2): p. 173.

44. Winter, F., *Hydrotalcite-Based Catalsts for the Synthesis of Methyl Isobutyl Ketone.* PhD Thesis, 2006: p. 125.

45. Costantino, U., et al., *New synthetic routes to hydrotalcite-like compounds - Characterisation and properties of the obtained materials.* European Journal Of Inorganic Chemistry, 1998(10): p. 1439-1446.

46. Kovanda, F., et al., *Crystallization of synthetic hydrotalcite under hydrothermal conditions.* Applied Clay Science, 2005. **28**(1-4): p. 101-109.

47. Kim, S.-N., et al., *CO_2 adsorption using amine-functionalized mesoporous silica prepared via anionic surfactant-mediated synthesis.* Microporous and Mesoporous Materials, 2008. **115**(3): p. 497-503.

48. Bailly, M.-L., et al., *A spectroscopy and catalysis study of the nature of active sites of MgO catalysts: Thermodynamic Brønsted basicity versus reactivity of basic sites.* Journal of Catalysis, 2005. **235**(2): p. 413-422.

49. Mario Chiesa, E.G., *Carbon Dioxide Activation by Surface Excess Electrons: An EPR Study of the CO_2^- Radical Ion Adsorbed on the Surface of MgO.* Chemistry - A European Journal, 2007. **13**(4): p. 1261-1267.

50. Fishel, C.T. and R.J. Davis, *Use of catalytic reactions to probe Mg-Al mixed oxide surfaces.* Catalysis Letters, 1994. **25**(1): p. 87-95.

51. Schneider, W.F., *Qualitative differences in the adsorption chemistry of acidic (CO_2, SO_x) and Amphiphilic (NO_x) species on the alkaline earth oxides.* Journal Of Physical Chemistry B, 2004. **108**(1): p. 273-282.

52. Florez, E., P. Fuentealba, and F. Mondragon, *Chemical reactivity of oxygen vacancies on the MgO surface: Reactions with CO_2, NO_2 and metals.* Catalysis Today, 2008. **133**: p. 216-222.

53. Pacchioni, G., *Physisorbed and Chemisorbed CO_2 at Surface and Step Sites of the Mgo(100) Surface.* Surface Science, 1993. **281**(1-2): p. 207-219.
54. Meixner, D.L., D.A. Arthur, and S.M. George, *Kinetics of desorption, adsorption, and surface diffusion of CO_2 on MgO(100).* Surface Science, 1992. **261**(1-3): p. 141-154.
55. Daub, C.D., et al., *Monte Carlo simulations of the adsorption of CO_2 on the MgO(100) surface.* Journal of Chemical Physics, 2006. **124**(11): p. 114706.
56. Preda, G., et al., *Formation of CO_2^-; Radical Anions from CO_2 Adsorption on an Electron-Rich MgO Surface: A Combined ab Initio and Pulse EPR Study.* The Journal of Physical Chemistry C, 2008. **112**(49): p. 19568-19576.
57. McKenzie, A.L., C.T. Fishel, and R.J. Davis, *Investigation Of The Surface-Structure And Basic Properties Of Calcined Hydrotalcites.* Journal Of Catalysis, 1992. **138**(2): p. 547-561.
58. Virnovskaia, A., et al., *Characterization of Pt,Sn/Mg(Al)O Catalysts for Light Alkane Dehydrogenation by FT-IR Spectroscopy and Catalytic Measurements.* The Journal of Physical Chemistry C, 2007. **111**(40): p. 14732-14742.
59. Karlsen, E.J., M.A. Nygren, and L.G.M. Pettersson, *Comparative study on structures and energetics of NO_x, SO_x, and CO_x adsorption on alkaline-earth-metal oxides.* Journal Of Physical Chemistry B, 2003. **107**(31): p. 7795-7802.
60. Jensen, M.B., et al., *CO_2 sorption on MgO and CaO surfaces: A comparative quantum chemical cluster study.* Journal Of Physical Chemistry B, 2005. **109**(35): p. 16774-16781.
61. Chimentao, R.J., et al., *Defect-induced strategies for the creation of highly active hydrotalcites in base-catalyzed reactions.* Journal Of Catalysis, 2007. **252**(2): p. 249-257.
62. Climent, M.J., et al., *Increasing the basicity and catalytic activity of hydrotalcites by different synthesis procedures.* Journal Of Catalysis, 2004. **225**(2): p. 316-326.

Chapter 3

On the influence and role of alkali metals on supported and unsupported activated hydrotalcites for CO_2 sorption

Abstract

The influence of alkali (K, Na) metal carbonate loading of activated supported and unsupported hydrotalcites (HT_{act}) on their CO_2 capture properties was investigated. The alkali-loaded supported hydrotalcites adsorb at 523 K, depending on the alkali metal (Na or K) and the preparation method, 1.7- 2.2 mmol $CO_2.g^{-1}_{HT}$ which exceeds the capacity of unloaded supported HT (1.3 mmol $CO_2.g^{-1}_{HT}$) and K-loaded unsupported HT (~0.3 $mmol.g^{-1}$). Key for the increase in capacity in alkali-loaded HT is a close contact at least at a mesoscopic level between HT and alkali metal carbonate. The alkali metal carbonate could be successfully introduced either by impregnation of a K_2CO_3 solution on as-synthesized HT or by leaving residual K (or Na), from the synthesis, in the final material. The latter method is advocated since it omits a washing step after precipitation. The increase in capture capacity for alkali loaded HTs points to a higher concentration of defects (low-coordination oxygen sites) on the surface of the activated alkali loaded HTs compared to the unloaded HT. We propose that the higher concentration of adsorption sites is caused by the presence of Na^+/K^+ on the surface of $Mg(Al)O_x$.

Introduction

Carbon Capture and Storage (CCS) may contribute to a decrease of the vast amounts of CO_2 (28 Gton in 2005 [1]) released into the atmosphere due to fossil fuel utilization [2]. When coupling CCS with the production of hydrogen, i.e. one of the possible energy carriers of the future, via the water-gas shift reaction (WGSR: $CO + H_2O \leftrightarrow CO_2 + H_2$) release of CO_2 into the atmosphere is prevented and the thermodynamic equilibrium of the reaction is shifted to the hydrogen side. This is called pre-combustion capture. Different materials such as lithium zirconates [3-6], sodium zirconates [7, 8], CaO [9-11], basic alumina [12] and carbon based adsorbents [13-15] have been described for pre-combustion capture. However none of these materials have all the required properties to operate in combination with the WGSR. The optimal sorbent should be selective towards CO_2, have a high adsorption capacity at high temperatures (>523 K), display adequate adsorption and desorption kinetics at operating conditions (facile regeneration), have long term stability upon cyclic use, have adequate mechanical strength and be of low cost.

Hydrotalcite, which belongs to the class of anionic clay minerals, meets most of these requirements and thus is a promising re-usable sorbent, although improvements are needed in the sorption capacity and desorption kinetics [16-23]. Several studies have been reported on the loading of alkali metal salts such as K_2CO_3 on HT, which significantly improved the CO_2 sorption capacity [16, 23-25]. Higher sorption capacities can also be achieved by small HT platelets deposited on a carbon nanofiber support [24]. Here we propose to combine both approaches, i.e. use a K-loaded supported HT, to arrive at a material with unprecedented CO_2-capture properties for HTs. The focus is on the preparation of the materials with emphasis on methods of alkali loading. A structure-performance relation for activated alkali-loaded and alkali-loaded supported HTs for CO_2 capture will be discussed.

2. Experimental

2.1 Preparation of K-loaded unsupported hydrotalcites

To an aqueous solution (150 mL) containing 0.7 mol NaOH and 0.09 mol Na_2CO_3 an aqueous solution (70 mL) of 0.1 mol $Mg(NO_3)_2 \cdot 6H_2O$ and 0.05 mol $Al(NO_3)_3 \cdot 9H_2O$ was

added drop wise. The resulting white suspension was aged at 298 K for 24 h under vigorous stirring. Subsequently, the suspension was filtered and washed extensively with demineralized water. After synthesis, the sample was dried for 24 h at 393 K. To increase the crystallite size of the HT, ageing was also performed at 333, 373 and 433 K. Ageing at higher temperatures, i.e. 373 and 433 K was performed in an autoclave. The synthesis mixture of NaOH, Na_2CO_3, $Mg(NO_3)_2 \cdot 6H_2O$ and $Al(NO_3)_3 \cdot 9H_2O$, as described above, was first stirred for 1 h at room temperature. Next, the precipitate was poured into a Teflon holder and placed into a stainless steel rotating autoclave followed by ageing for 16 h at the desired temperature. Subsequently, the suspension was filtered and washed extensively with demineralized water and dried for 24 h at 393 K. The HT samples (~2 g) were impregnated with 2 mL of an aqueous solution containing 1.6 mmol K_2CO_3 (K/Mg=0.2 (at/at), 11wt% K_2CO_3). After impregnation, the samples were dried for 24 h at 393 K. The samples are further denoted as $HT_{T\text{-}(x)}$ with T denoting the synthesis temperature of the HT in K and x denoting the K/Mg ratio.

Preparation of hydrotalcites with residual sodium or potassium

To an aqueous solution (150 mL) containing 0.7 mol NaOH and 0.09 mol Na_2CO_3 an aqueous solution (70 mL) of 0.1 mol $MgNO_3 \cdot 6H_2O$ and 0.05 mol $Al(NO_3)_3 \cdot 9H_2O$ was added drop wise. The resulting white suspension was aged at 333 K for 24 h under vigorous stirring. Subsequently, the suspension was filtered off and dried, without washing, for 24 h at 393 K. The sample, further denoted as HT_{Na}, was dried for 24h at 393 K. A second HT sample was prepared with 0.7 mol NaOH and 0.09 mol K_2CO_3 instead of Na_2CO_3. This sample will further be denoted as HT_K.

2.2 Preparation of alkali metal carbonate (K, Na) supported hydrotalcites

Carbon nanofibers

CNF were obtained from synthesis gas (H_2/CO), using a 20 wt% Ni/SiO_2 catalyst, at 823 K [25]. Removal of the growth catalyst and surface activation of the CNF were performed as reported in literature [27, 28] using subsequent treatments in aqueous 1 M KOH and concentrated HNO_3.

K-loaded CNF supported hydrotalcites

To prepare supported Mg-Al hydrotalcites (Mg/Al=2, (at/at)), 5.0 g CNF were impregnated in a 250 mL round-bottom flask with a solution containing 3.3 mL of $Mg(NO_3)_2$ (1.4 M) and $Al(NO_3)_3$ (0.7 M). After drying at 393 K, a solution of 3.0 mL NaOH (8.3 M) and Na_2CO_3 (0.56 M) was added. Ageing was performed in a water-saturated atmosphere, under a nitrogen flow (7 $mL.min^{-1}$), for 16 h at 333 K, followed by extensive washing with demineralized water and drying at 393 K for 24 h. After that, the sample was impregnated with an aqueous solution containing 0.4 mmol K_2CO_3 (K/Mg=0.2, 11 wt% K_2CO_3) and dried again for 24 h at 393 K. This sample is denoted as $HT_{(0.2)}$-CNF.

K_2CO_3 was also loaded on HT-CNF after heat treatment of the HT and removing surface oxygen groups from HT-CNF. HT-CNF, prepared as described above, was heated in N_2 (30 $mL.min^{-1}$) at 773 K (5 $K.min^{-1}$). Next, the sample was impregnated with an aqueous solution containing 0.4 mmol K_2CO_3 (K/Mg=0.2, 11 wt% K_2CO_3) and dried again for 24h at 393 K. This sample will be further denoted as $HT_{(0.2)}$-CNF_{ht} ($_{ht}$ = **h**eat **t**reatment).

CNF supported hydrotalcites with residual sodium or potassium

Preparation of supported Mg-Al hydrotalcite (Mg/Al=2) with residual sodium carbonate was similar to the method described above, with the following modification. After ageing in a water-saturated atmosphere under nitrogen at 333 K, the sample was dried without washing at 393 K for 24 h. This sample is denoted as HT_{Na}-CNF (Na/Mg=0.25, 11 wt%). A second sample was prepared with NaOH and K_2CO_3 instead of Na_2CO_3. This sample will further be denoted as HT_K-CNF (K/Mg=0.25, 15 wt%). General abbreviation of supported HT samples is denoted as HT_x-CNF.

Table 1 shows the abbreviations of sample names of unsupported and supported HT and their alkali carbonate content. Potassium carbonate loaded samples will be referred as ‘K-loaded’, sodium carbonate loaded samples will be referred as ‘Na-loaded’. In general, loaded (Na, K) samples will be referred as ‘alkali-loaded’. Activated samples (heat treated at 773 K) are denoted as $HT_{T\text{-}(x)\text{-}act}$, with T denoting the synthesis temperature of the HT in K and x denoting the K/Mg or Na/Mg atomic ratio, and 'act' refers to the activation step, i.e. heating to 773K. General supported samples will be referred to 'HT-CNF'.

Table 1. Abbreviations of sample names and their alkali carbonate loading.

Unsupported samples	K/Mg, Na/Mg (at/at)	Wt% alkali carbonate	Supported samples	K/Mg, Na/Mg (at/at)	Wt% alkali carbonate
HT	-	0	HT-CNF	-	0
$HT_{298\text{-}(0.1)}$	0.1	5.5			
$HT_{T\text{-}(0.2)}$*	0.2	11	$HT_{(0.2)}$-CNF_{ht}	0.2	11
			$HT_{(0.2)}$-CNF	0.2	11
$HT_{298\text{-}(0.4)}$	0.4	22			
HT_K	0.08, 0.25**	4, 15	HT_K-CNF	0.25	15
HT_{Na}	0.0, 0.4**	0, 20	HT_{Na}-CNF	0.25	12

*T = synthesis temperature at 298, 333, 373 and 433 K, ** ICP analysis, Na_2CO_3 + NaOH.

2.3 Characterization

Powder X-ray diffraction (XRD) patterns were measured using a Bruker-AXS D8 advance powder diffraction apparatus equipped with an automatic divergence slit (filtered Co-K_α radiation λ = 1.79026 Å). N_2-physisorption measurements were performed using a Micromeritics Tristar 3000 analyzer after drying the samples at 393 K in vacuum for at least 20 h prior to the measurements, pore volume at P/P_0 = 0.995. CO_2 loaded samples ($HT_{act\text{-}CO2}$) for nitrogen physisorption were cooled to RT after the adsorption step (vide infra). SEM micrographs were obtained using a Philips XL30FEG electron microscope equipped with an EDX detector for elemental analysis. TEM micrographs were obtained with an FEI Technai 20 FEG TEM operating at 200kV equipped with an EDX detector. TEM samples were dispersed on a holey carbon film supported on a copper grid.

2.4 CO_2 sorption measurements

Sorption measurements were performed in a plug-flow reactor with an inner diameter of 12 mm. The gas flows (N_2, CO_2) were passed down-flow through the reactor and controlled via mass flow controllers (Brooks 5850s). The total pressure in the setup was maintained at 1.10 bar, using a backpressure controller (Brooks 5866). A tubular oven was placed around the reactor to control the process temperature. The reactor was loaded with 2.0 g of unsupported HT sample (bed height 35 mm), using a sieve fraction with particle sizes of 212-500 µm. For HT_x-CNF the reactor was loaded with 5.0 g of sample (bed height 85 mm), which contained 0.5 g of alkali-loaded $HT_{T\text{-}x}$. All samples were activated by heating in N_2 (30 $mL.min^{-1}$) at 773 K (5 $K.min^{-1}$) for 1 h to remove CO_2 and water from the starting material

(HT_{act}, activation step). Please note, after activation the hydrotalcite material still retains its mesoscopic shape, i.e. the platelets are still present, but are showing broad $Mg(Al)O_x$ diffractions. After activation, adsorption measurements were carried out at 373, 523 and 673 K. All samples were subjected to at least two identical adsorption and desorption (773 K) cycles at all three temperatures to assess reproducibility.

Conditions for the adsorption and desorption steps are given in Table 2. The total flow throughout all experiments was 30 $mL.min^{-1}$. N_2 was humidified with CO_2-free water, using a saturator set at 331 K. All adsorption experiments were performed for 30 minutes in 5% CO_2. After adsorption, the system was flushed to achieve a CO_2 free environment in the setup. Desorption was performed by heat treatment in dry nitrogen (30 $mL.min^{-1}$) at 773 K (5 $K.min^{-1}$) for 1 h. Due to gasification of the CNF support material at higher temperatures in steam, only dry nitrogen was used during desorption to obtain comparable results between unsupported and supported HTs.

Blank measurements were performed either with a non-adsorbing material (SiC) or CNF, with the same particle size range and bed volume as the HT containing material. The effluent gas was analyzed by on-line FT-IR, using a Midac corporation 2000 M series. For each spectrum, 8 scans were accumulated with a resolution of 4 cm^{-1}; spectra were recorded every 13 seconds. The IR-cell, made of stainless steel, had a path length of 2 mm and contained CaF_2 windows. The sample compartment was continuously purged with a stream of dry N_2 to prevent interference of CO_2 present in the atmosphere. A background spectrum using an empty cell was acquired prior to a sorption measurement. The integrated area from 2280- 2390 cm^{-1} was used to quantify CO_2. A CO_2 concentration above 100 ppm is defined as breakthrough. From the breakthrough time and the flow and concentration, the amount of CO_2 was calculated.

Table 2. Experimental conditions for sorption measurements with 2g HT_{act} or 5g HT_{act}-CNF.

	Flow ($mL.min^{-1}$)	**Composition**	**Temp. (K)**
Activation	30	100% N_2	323 → 773 (5 $K.min^{-1}$, 1h)
Adsorption	30	83% N_2/ 12% H_2O/ 5% CO_2	523 (max. 30 min)
Desorption	30	100% N_2	523 → 773 (5 $K.min^{-1}$, 1h)

3. Results and discussion

3.1 Characterization of materials

The crystallinity of the HTs and presence of different alkali phases in the as-synthesized unsupported (Figure 1a) and supported (Figure 1b) samples were investigated by XRD. $HT_{as\text{-}298}$, i.e. unloaded unsupported HT showed diffraction lines at 2θ ≈13.5°, 27.6°, 40.5° correspond to the (003) (006) and (009/ 012) crystal planes of HT with carbonate in the interlayer. All unsupported alkali-loaded HT samples showed, in addition to the HT lines, diffraction lines which were representative for K_2CO_3 (*) or Na_2CO_3 (+).

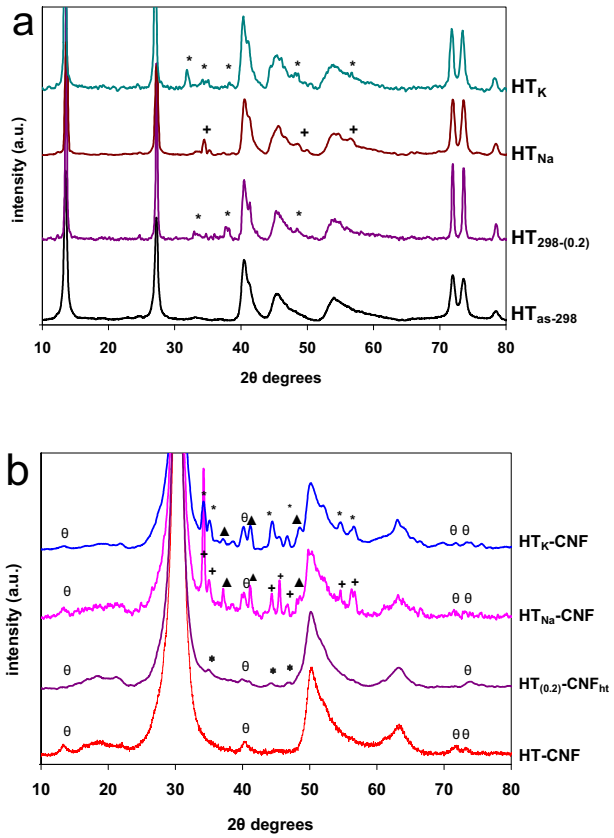

Figure 1. (a) XRD profiles of selected alkali-loaded unsupported HTs; (b) supported HTs; K_2CO_3 (*), Na_2CO_3 (+), NaOH (▲) and HT (θ).

The supported samples contained HT (θ) as inferred from diffractions at 2θ ≈13.5°, 40.5° and 73°. For alkali-loaded supported samples prepared via the residual alkali route K_2CO_3 (*) and Na_2CO_3 (+), diffraction lines were more pronounced compared to the impregnated sample ($HT_{(0.2)}$-CNF_{ht}). In addition, for these samples also peaks representative for NaOH were detected. Clearly, the HT signals from these samples were concealed by the signals from the alkali carbonates. Thus, all samples contained crystalline HT and could be successfully loaded with alkali metal-carbonate. To visualize the morphology of the HT and the location of the alkali-carbonates, an SEM and TEM study was performed.

Figure 2 shows selected SEM micrographs of as-synthesized HT_{333} (Figure 2A), K-loaded $HT_{333\text{-}(0.1)}$, $HT_{333\text{-}(0.2)}$, $HT_{333\text{-}(0.4)}$ (Figure 2B-D), HT with residual K (Figure 2E) and a HT in which potassium carbonate was added after activation (Figure 2D). The as-synthesized unloaded HT_{333} sample (Figure 2A) shows small crystalline HT platelets (average platelet size = 50 nm). By adding K_2CO_3 and increasing the K-loading, the materials became more dense, i.e. less space between the HTs platelets (Figure 2B- D). Leaving residual potassium carbonate or sodium carbonate in the HT (Figure 2E) resulted also in HTs with higher density (coverage with alkali metal) compared to the unloaded HT_{333}. Thus, the alkali metal of the loaded samples brought about more dense packing of HT platelets.

Potassium carbonate was never found separated from the HT when added on as-synthesized HTs or when using the residual alkali route. Only when K is loaded on the HT samples after activation, a fiber like phase (Figure 2F) is obtained which is most probably K_2CO_3 [26]. This is in agreement with reported data on activated HT, which also showed the presence of large K_2CO_3 domains [20]. Thus, alkali loading should be performed before activation to achieve a close contact between HT and alkali phase. Moreover, after activation, samples loaded with alkali carbonate before activation did not show any sign of K_2CO_3 segregation from the HT (data not shown).

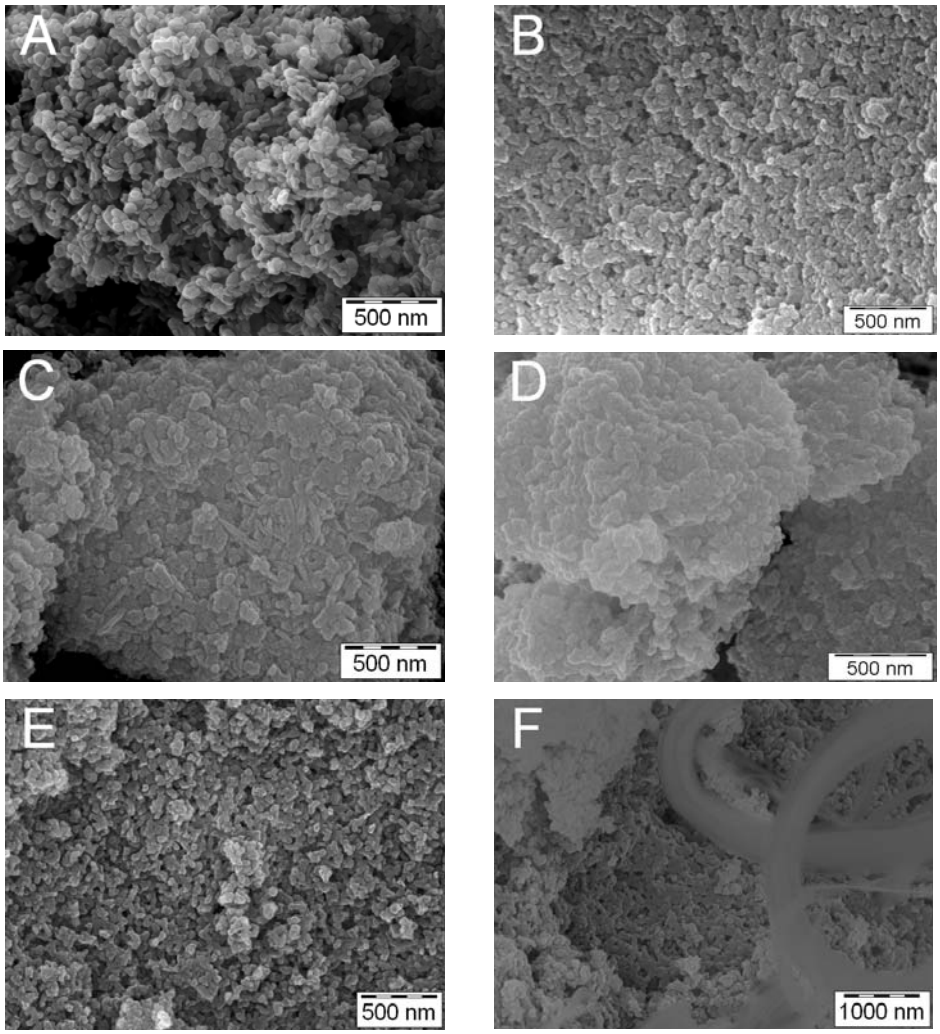

Figure 2. SEM images of as-synthesized unsupported HTs: (A) unloaded HT_{333}, (B) K-loaded $HT_{333\text{-}(0.1)}$, (C) K-loaded $HT_{333\text{-}(0.2)}$, (D) K-loaded $HT_{333\text{-}(0.4)}$, (E) HT_K , (F) K-loaded $HT_{333\text{-}(02.)\text{-}act}$, after heat treatment.

N_2 physisorption was used to investigate the influence of K-loading on the textural properties of unsupported as-synthesized HTs (Table 3). The surface area of unloaded HTs decreased with increasing ageing temperature, i.e. increasing platelet size, which is in good agreement with literature [33]. Micropores were not present in the samples. For HT prepared up to 333 K the surface area decreased with K_2CO_3 loading. For samples prepared at higher synthesis temperatures the K-loading did not affect the surface area or pore volume. Larger platelets (from higher synthesis temperatures) have less space between the individual platelets; more dense packing of platelets is not taking place upon K_2CO_3 addition. Increasing the K-loading on as-synthesized samples had no systematic effect on the surface area (21- 30 $m^2.g^{-1}$) and pore volume (0.16- 0.21 $ml.g^{-1}$) of the samples. The surface areas of the residual samples HT_{Na} and HT_K were comparable with the K-loaded ($HT_{T-(0.2)}$) samples. However, the pore volume was significantly larger. This indicates that only a small part between individual platelets was filled with alkali carbonate, which is supported by SEM pictures (Figure 2E).

Table 3. Physico-chemical properties of the various hydrotalcites.

HT_{as}			$HT_{as\text{-}K,\ Na}$		
Sample	S_{BET} $(m^2.g^{-1})$	V_{tot} $(cm^3.g^{-1})$	**Sample**	S_{BET} $(m^2.g^{-1})$	V_{tot} $(cm^3.g^{-1})$
HT_{298}	100	0.6	$HT_{298\text{-}(0.2)}$	21	0.16
HT_{333}	53	0.35	$HT_{333\text{-}(0.2)}$	30	0.25
HT_{373}	24	0.11	$HT_{373\text{-}(0.2)}$	23	0.13
HT_{433}	15	0.07	$HT_{433\text{-}(0.2)}$	20	0.11
			$HT_{333\text{-}(0.1)}$	25	0.21
			$HT_{333\text{-}(0.4)}$	21	0.16
			HT_{Na}	26	0.31
			HT_K	32	0.35

To investigate how the textural properties of the alkali-loaded HTs changed after CO_2 loading, nitrogen physisorption experiments were also performed on the activated CO_2 loaded samples (Figure 3). This figure shows that with increasing CO_2 sorption capacity, consequently with increasing potassium loading, the surface area of the CO_2 loaded samples decreased. This further points out that low K-loading already leads to a decrease of the surface area, while the uptake of CO_2 molecules by the activated HTs does not increase with increasing surface area [24].

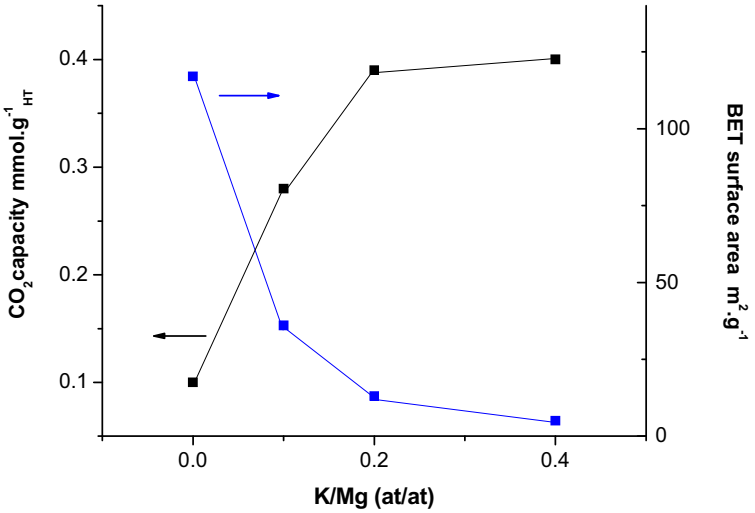

Figure 3. CO_2 capacity of activated HTs with different K_2CO_3 loadings *vs.* BET surface area (HTs loaded with CO_2 at 523 K).

Potassium loading of supported HTs can be performed either on HT-CNF, i.e. with oxygen containing functionalities still present on the carbon, or on HT-CNF after activation, i.e. after decomposing of HT and removal of the oxygen groups (HT-CNF_{ht}). To investigate the effectiveness of K_2CO_3-loading both approaches were pursued. The obtained materials were compared to those prepared via de residual K/Na route. For $HT_{(0.2)}$-CNF_{ht} and HT_{Na}-CNF small HT platelets were detected (Fig. 4A, C). EDX scans obtained with TEM revealed a higher percentage of potassium in proximity of the HT for sample $HT_{(0.2)}$-CNF_{ht} (Figure 4A) compared to sample $HT_{(0.2)}$-CNF (Figure 4B). Apparently, the presence of oxygen-containing groups on the carbon support of sample $HT_{(0.2)}$-CNF prevent the potassium carbonate to contact the HT. The needle shaped species (red circles) in Figure 4B, which is most probably segregated K_2CO_3, have only been observed on sample $HT_{(0.2)}$-CNF. Though, we could not perform EDX analysis, because the species vaporized under the electron beam and therefore it was not possible to verify this. Several TEM-EDX-analyses of the Na- and K-loaded supported samples revealed Na and K only in close contact with the HT. Representative images are shown in Figures 4C and D (squares).

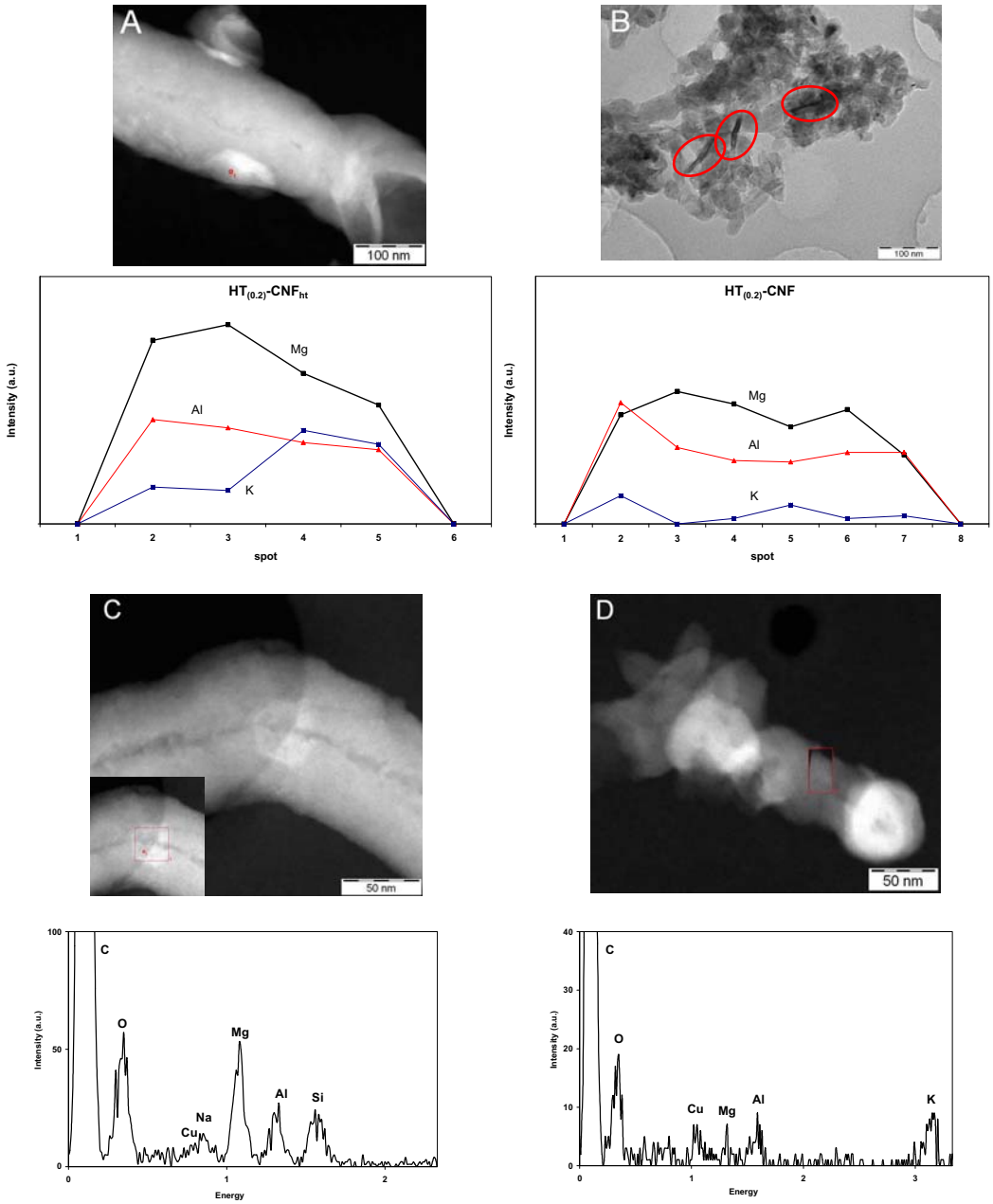

Figure 4. TEM micrographs and EDX spot analyses of $HT_{(0.2)}$-CNF_{ht} (A), $HT_{(0.2)}$-CNF (B), HT_{Na}-CNF (C) and HT_{k}-CNF (D). A, C and D in high angle angular dark field (HAADF).

N_2-physisorption was used to investigate the influence of the HT and the alkali carbonate loading on the textural properties of the as-synthesized supported HTs (Table 4). Deposition of HT and loading with alkali metal exhibited a surface area which is significantly lower than that of CNF, indicating partial filling and/ or blocking of the pores with HT and alkali carbonate. The relatively high average pore volumes of the alkali-loaded samples imply well accessible pore systems. The surface areas of HT_{Na}-CNF and HT_K-CNF were significantly lower than the supported K-loaded sample.

Table 4. Physico-chemical properties of various as-synthesized supported hydrotalcites.

Sample	S_{BET} ($m^2.g^{-1}$)	V_{tot} ($cm^3.g^{-1}$)
CNF	155	0.34
HT-CNF	97	0.19
$HT_{(0.2)}$-CNF_{ht}	99	0.30
HT_{Na}-CNF	56	0.21
HT_K-CNF	49	0.22

3.2 CO_2 adsorption and desorption kinetics

The results of representative CO_2-breakthrough experiments at 523 K for activated unsupported HTs have been compiled in Figure 5 and for activated supported HTs in Figure 6. For activated HT (dashed line, Figure 5) a breakthrough time of ~4 minutes, which corresponds to a capacity of ~0.1 $mmol.g^{-1}$, was observed. Breakthrough times of alkali-loaded HTs were significantly longer, irrespective of the method of alkali introduction and, within experimental error, similar for all these samples (0.27- 0.36 $mmol.g^{-1}$, Table 5). Capture capacities of activated supported HT and activated K-loaded supported HT exceeded that of their unsupported counter parts (1.3 $mmol.g^{-1}_{HT}$ for HT_{act}-CNF and 1.7 $mmol.g^{-1}_{HT}$ for $HT_{(0.2)\text{-}act}$-CNF_{ht}). These values were even further increased by leaving residual alkali carbonate on the supporting samples (2.2 $mmol.g^{-1}_{HT}$). Blank measurements with potassium carbonate supported on CNF showed that the maximum capacity was 0.07 $mmol.g^{-1}_{K2CO3}$ at 523 K. The capacity of supported HT increased with 0.4- 0.9 $mmol.g^{-1}_{HT}$, which showed the necessity of a good interaction between HT and K_2CO_3.

When K was introduced on the supported HT without heat treatment and with the presence of oxygen-containing groups on the surface ($HT_{(0.2)\text{-}act}$-CNF), the capture capacity was significantly lower (0.8 $mmol.g^{-1}_{HT}$) compared to the heat treated alkali-loaded supported

sample ($HT_{(0.2)\text{-}act}$-CNF_{ht}). This suggests that the oxygen groups on the CNF are nucleation sites for potassium carbonate and therefore the potassium carbonate does not migrate towards the HT. This results in a poor interaction between potassium carbonate and the HT (Figure 4B).

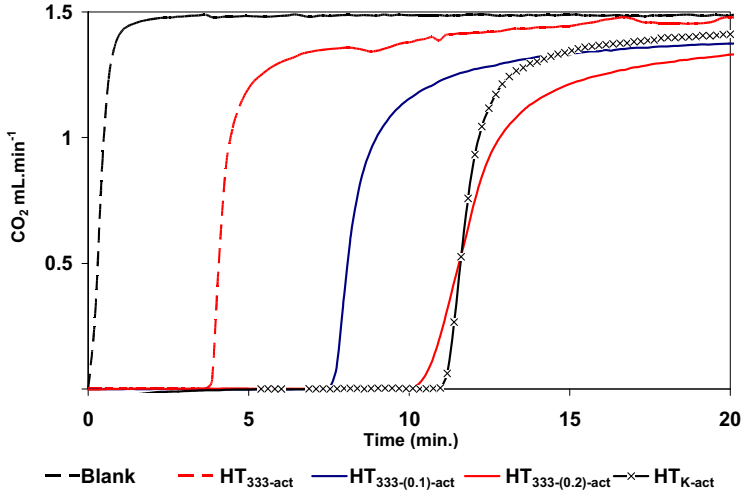

Figure 5. Representative breakthrough curves of (a) activated unsupported HTs (2g).

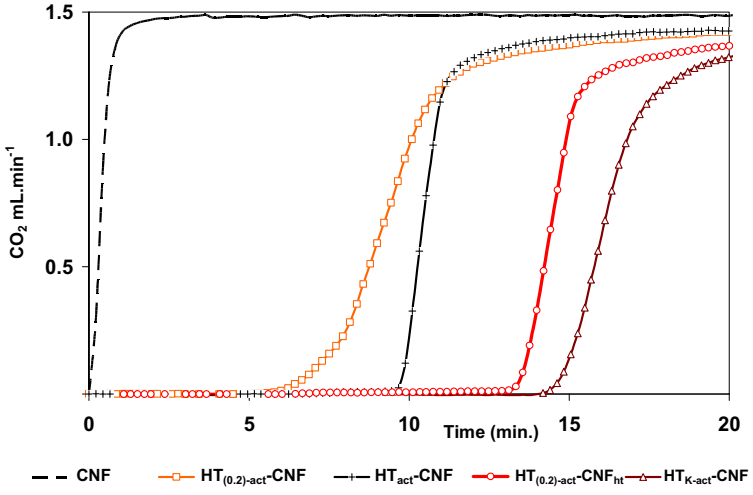

Figure 6. Activated supported HT (5g), flow 25 mL.min^{-1} N_2, 3.5 mL.min^{-1} H_2O, 1.5 mL.min^{-1} CO_2 s at 523 K.

Table 5. Adsorption capacity of unsupported and supported samples.

Unsupported HT	Adsorption capacity ($mmol.g^{-1}$) at 523 K	Supported HT	Adsorption capacity ($mmol.g^{-1}_{HT}$) at 523 K
$HT_{333\text{-act}}$	**0.13**	HT_{act}-CNF	**1.3**
$HT_{333\text{-}(0.1)\text{-act}}$	**0.32**	$HT_{(0.2)\text{-act}}$-CNF	**0.8**
$HT_{298\text{-}(0.2)\text{-act}}$	**0.34**	$HT_{(0.2)\text{-act}}$-CNF_{ht}	**1.7**
$HT_{333\text{-}(0.2)\text{-act}}$	**0.33**	$HT_{Na\text{-act}}$-CNF	**2.2**
$HT_{373\text{-}(0.2)\text{-act}}$	**0.31**	$HT_{K\text{-act}}$-CNF	**2.2**
$HT_{343\text{-}(0.2)\text{-act}}$	**0.28**		
$HT_{333\text{-}(0.4)\text{-act}}$	**0.34**	K_2CO_3-CNF	**0.07***
$HT_{Na\text{-act}}$	**0.27**		
$HT_{K\text{-act}}$	**0.36**		

* $mmol.g^{-1}_{K2CO3}$.

To evaluate the stability of alkali-loaded unsupported and alkali-loaded supported HTs, multiple adsorption-desorption cycles were performed (Figure 7). All activated unsupported and supported Na-loaded HTs showed stable behavior and no significant decrease in capacity was measured. The activated supported K-loaded samples ($HT_{(0.2)\text{-act}}$-CNF_{ht} (o) and $HT_{K\text{-act}}$-CNF (□)) showed a slight decrease in CO_2 capacity (0.2 $mmol.g^{-1}_{HT}$) within the first six cycles. Please note that the presence of steam during desorption will most likely negatively affect the cycle stability of the supported materials.

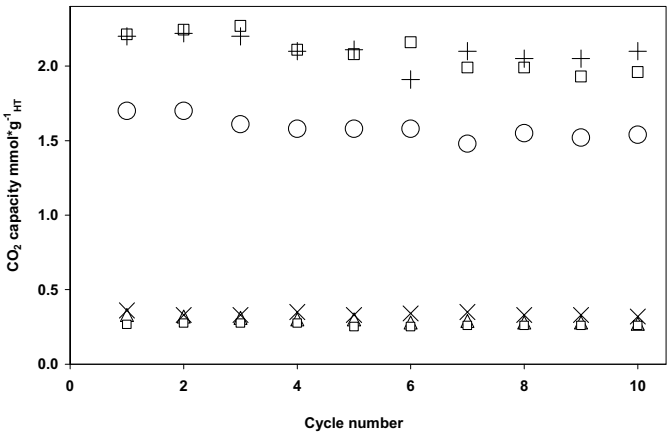

Figure 7. CO_2 capacity as function of adsorption-desorption cycles for selected samples; unsupported $HT_{333\text{-}(0.2)\text{-act}}$ (Δ), $HT_{Na\text{-act}}$ (□), $HT_{K\text{-act}}$ (×) and supported $HT_{(0.2)\text{-act}}$-CNF_{ht} (o), $HT_{Na\text{-act}}$-CNF (+) and $HT_{K\text{-act}}$-CNF (□).

It is of interest to measure the CO_2 sorption capacity at different temperatures to establish the maximum capacity of the sorbents. Figure 8 shows sorption capacities of activated unsupported (left) and supported (right) alkali-loaded HTs measured as function of temperature, i.e. 373, 523 and 673 K. The capacities of the unsupported alkali-loaded samples increased at all temperatures compared to the unloaded HT, regardless the method of alkali-loading (max 0.5 mmol.g^{-1} at 373 K). All alkali-loaded supported HTs exhibited higher capacities compared to the unsupported samples at all temperatures (except $HT_{(0.2)\text{-act}}$-CNF at 673 K). The supported samples with residual alkali metal obtained the highest capacities (3.2 mmol.g^{-1}_{HT} at 373 K).

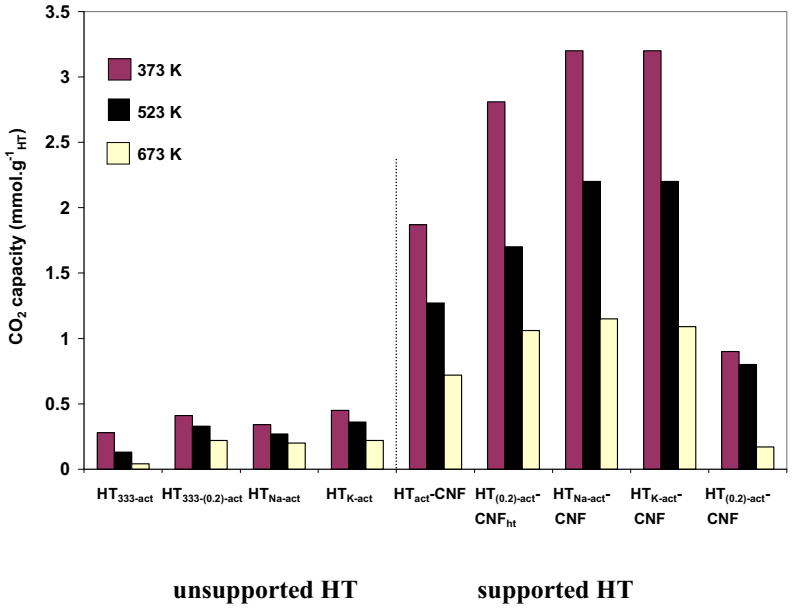

Figure 8. CO_2 capacity of a series of different activated HTs at three different temperatures.

3.3 Defect sites creation in activated alkali carbonate loaded HT.

Different explanations for the enhanced CO_2 capture properties of alkali loaded materials can be found in literature. Walspurger and co-workers claimed that aluminum oxide centers play a role in the destabilization of K_2CO_3, which might cause the increased CO_2 capacity [20]. Ebner and co-workers suggested that $Mg_6Al_2K_2O_x$ is formed, which enhanced

the CO_2 capture rate [27]. Fernandez and co-workers showed that doping $LiZrO_3$ with K_2CO_3 enhanced CO_2 absorption rates [28]. It was claimed that loading of potassium favors the diffusion of CO_2 through the $LiCO_3$ layer that is formed in the surface of the acceptor during the capture reaction. Our explanation for the increase in CO_2 capacity is based on the geometric rearrangement and defect surface structure of the various K-loaded HTs, and is discussed below.

In chapter 2 [24], we considered that defects play an important role for the enhanced CO_2 capture on supported HTs [29-37]. The active sites for CO_2 adsorption on activated HTs ($Mg(Al)O_x$) are associated with O^{2-}-Mg^{2+} surface sites ($MgO + CO_2 \leftrightarrow MgCO_3$). During sorption the acidic CO_2 reacts with basic O^{2-} sites depending on their coordination. Oxygen atoms located at edges and corners of the crystal planes have stronger basicity than oxygen atoms in terraces. In other words, the energy level of surface oxygen increases with decreasing coordination number. Consequently, the energy gap between O^{2-} and CO_2 is reduced on corners and edges and charge transfer from O^{2-} to CO_2 may occur. Pettersson *et al* [34, 35] calculated for MgO surfaces the energetically favorable interactions with CO_2. They concluded that on a regular unperturbed MgO(100) surface no CO_2 adsorption occurs. However, 3- and 4 coordinated O^{2-} edges and corners (O_{3c}, O_{4c}) showed a reduction in the energy gap. Consequently, adsorption with CO_2 on an edge or corner is more likely to occur. As a result of these findings, we propose that the activated, unsupported samples contain only few low-coordinated oxygen sites because the capacity of these samples is low (~0.1 $mmol.g^{-1}$). By depositing HT on a CNF support, we could increase the capacity by a factor of 10- 25, depending on the HT loading, which we attribute to a higher concentration in defects [24]. These results showed that deposition of the hydrotalcites on a support affects the nature of the activated hydrotalcite and the interaction with CO_2 which is reflected in the sorption capacity.

Loading the unsupported and supported HTs with alkali carbonate increased the capacity compared to unloaded HT and will now be considered in more detail. Loading the unsupported HT with alkali carbonate metal increased the capacity with 210- 280% at 523 K (Figure 8). On the other hand, the capacity of the supported HT, after loading with alkali metal carbonate, increased only 30- 70% at 523 K. This effect can be explained by the higher concentration of defects on the activated supported HT and the low amount of defects on activated unsupported HT. Thus, it is more likely that there is a higher increase in edges and

corners on an unsupported HT, after loading with alkali carbonate metal, than on an alkali carbonate supported HT (Figure 9). Defects (low-coordinated sites) can be formed by the partial substitution of Mg^{2+} by K^+ or Na^+ . However the ionic radius of Na^+ (r_{Na}^+ = 0.98 Å) and K^+ (r_K^+ = 1.33 Å) compared to that of Mg^{2+} (r_{Mg}^+ = 0.72 Å) and Al^{3+} (r_{Al}^+ = 0.53 Å) should be considered. The large size of the alkali metal ions may induce lattice strain in MgO, where ions than tend to coalesce and form clusters [38]. Because of the larger size of these alkali ions (K^+ or Na^+) it would be difficult to incorporate these ions extensively in an MgO lattice and incorporation in an activated HT would therefore be unlikely. It has been claimed, even with the smaller Li^+ ions, that oxygen defects prevail in the near-surface and not in the bulk phase [39-40]. We therefore propose that the K^+/Na^+ are located at the surface and not in the 'bulk' of the $MgAlO_x$. Our tentative mechanism is that K^+ plus substitutes an Mg^{2+} and additional oxygen vacancies at the surface are created. Possibly, more oxygen atoms in the vicinity of K^+ adsorb CO_2 (Figure 9).

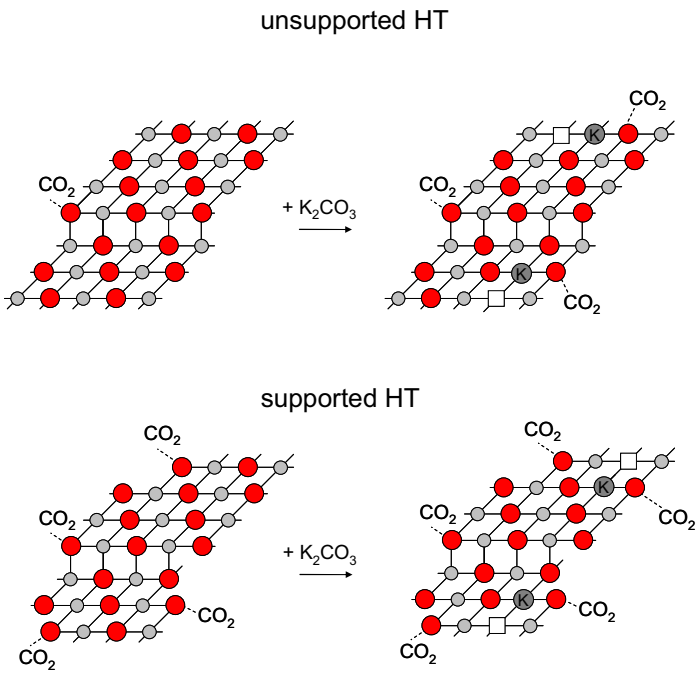

Figure 9. Schematic representation of addition of K_2CO_3. More low-coordinated sites (edges and corners), which are important for CO_2 adsorption, are formed. Light gray spheres are magnesium, red spheres are oxygen, dark gray spheres are potassium.

Conclusions

In this chapter the CO_2 capture properties of alkali-loaded unsupported and supported HTs were investigated. The CO_2 adsorption capacities of the activated alkali-loaded unsupported and supported hydrotalcites exceeded their unloaded counterparts at 523 K. We have presented a new facile synthesis for unsupported and supported HTs to load these with alkali metal by intentionally leaving K (or Na) in the HT. Crucial for increase in capacity is proximity between the alkali metal and the HT. The increase in capacity for alkali-loaded HT is attributed to a higher concentration of low-coordinated oxygen sites created by incorporation of alkali metal in the surface of activated HT.

Acknowledgements

This research has been carried out by Inorganic Chemistry and Catalysis, Debye Institute for Nanomaterials Science, Department of Chemistry in the CATO-project (Carbon Capture, Transport and Storage). Marjan Versluijs-Helder, Cor van der Spek, Hans Meeldijk and Ad Mens are thanked for SEM, TEM, and N_2-physisorption measurements. Valuable input from Ruud van den Brink, Paul Cobden, Daan Jansen and Rick Reijers (ECN, Petten the Netherlands) is acknowledged.

References

1. *Intergovernmental Panel on Climate Change.* IPCC, Climate Change 2007: The Physical Science Basis (Cambrigde Univ. Press, Cambridge, 2007).
2. http://CO_2-cato.nl/.
3. Ida, J. and Y.S. Lin, *Mechanism of high-temperature CO_2 sorption on lithium zirconate.* Environmental Science & Technology, 2003. **37**(9): p. 1999-2004.
4. Pfeiffer, H. and K.M. Knowles, *Reaction mechanisms and kinetics of the synthesis and decomposition of lithium metazirconate through solid-state reaction.* Journal Of The European Ceramic Society, 2004. **24**(8): p. 2433-2443.

5. Ida, J., R.T. Xiong, and Y.S. Lin, *Synthesis and CO_2 sorption properties of pure and modified lithium zirconate.* Separation And Purification Technology, 2004. **36**(1): p. 41-51.
6. Xiong, R.T., J. Ida, and Y.S. Lin, *Kinetics of carbon dioxide sorption on potassium-doped lithium zirconate.* Chemical Engineering Science, 2003. **58**(19): p. 4377-4385.
7. Zhao, T.J., et al., *Preparation and high-temperature CO_2 capture properties of nanocrystalline Na_2ZrO_3.* Chemistry Of Materials, 2007. **19**(13): p. 3294-3301.
8. Ochoa-Fernandez, E., et al., *Synthesis and CO_2 capture properties of nanocrystalline lithium zirconate.* Chemistry Of Materials, 2006. **18**(25): p. 6037-6046.
9. Han, C. and D.P. Harrison, *Simultaneous shift reaction and carbon dioxide separation for the direct production of hydrogen.* Chemical Engineering Science, 1994. **49**(24B): p. 5875-5883.
10. Martavaltzi, C.S. and A.A. Lemonidou, *Development of new CaO based sorbent materials for CO_2 removal at high temperature.* Microporous and Mesoporous Materials, 2008. **110**(1): p. 119.
11. Kuramoto, K., et al., *Repetitive carbonation-calcination reactions of Ca-based sorbents for efficient CO_2 sorption at elevated temperatures and pressures.* Industrial & Engineering Chemistry Research, 2003. **42**(5): p. 975-981.
12. Yong, Z., V. Mata, and A.E. Rodrigues, *Adsorption of carbon dioxide on basic alumina at high temperatures.* Journal Of Chemical And Engineering Data, 2000. **45**(6): p. 1093-1095.
13. Yong, Z., V.G. Mata, and A.E. Rodrigues, *Adsorption of carbon dioxide on chemically modified high surface area carbon-based adsorbents at high temperature.* Adsorption-Journal Of The International Adsorption Society, 2001. **7**(1): p. 41-50.
14. Kapoor, A., K.R. krishnamurthy, and A. Shirley, *Kinetic separation of carbon dioxide from hydrocarbons using carbon molecular sieve.* Gas Separation & Purification, 1993. **7**(4): p. 259-263.
15. Song, H.K. and K.H. Lee, *Adsorption of carbon dioxide on chemically modified carbon adsorbents*. Separation Science and Technology, 1998. **33**(13): p. 2039-2057.
16. Ding, Y. and E. Alpay, *Equilibria and kinetics of CO_2 adsorption on hydrotalcite adsorbent.* Chemical Engineering Science, 2000. **55**(17): p. 3461-3474.

17. Ding, Y. and E. Alpay, *Adsorption-enhanced steam-methane reforming.* Chemical Engineering Science, 2000. **55**(18): p. 3929-3940.
18. Ding, Y. and E. Alpay, *High temperature recovery of CO_2 from flue cases using hydrotalcite adsorbent.* Process Safety And Environmental Protection, 2001. **79**(B1): p. 45-51.
19. Nataraj, S., et al., *Materials selectivity adsorbing CO_2 from CO_2 containing streams* EP Patent No. 1006079A1, 2000.
20. Stéphane Walspurger, et al., *The Crucial Role of the K^+-Aluminium Oxide Interaction in K^+-Promoted Alumina- and Hydrotalcite-Based Materials for CO_2 Sorption at High Temperatures.* ChemSusChem, 2008. **1**(7): p. 643-650.
21. Cobden, P.D., et al., *Sorption-enhanced hydrogen production for pre-combustion CO_2 capture: Thermodynamic analysis and experimental results.* International Journal of Greenhouse Gas Control, 2007. **1**(2): p. 170
22. Reijers, H.T.J., et al., *Hydrotalcite as CO_2 sorbent for sorption-enhanced steam reforming of methane.* Industrial & Engineering Chemistry Research, 2006. **45**(8): p. 2522-2530.
23. Yong, Z. and A.E. Rodrigues, *Hydrotalcite-like compounds as adsorbents for carbon dioxide.* Energy Conversion And Management, 2002. **43**(14): p. 1865-1876.
24. Meis, N.N.A.H., J.H. Bitter, and K.P. de Jong, *Support and size effects of activated hydrotalcites for pre-combustion CO_2 capture.* Industrial & Engineering Chemistry Research, 2009, accepted for publication.
25. van Dillen, A.J., et al., Proc. 6th Int. Congr. Catal. 2 1977: p. 677.
26. Pabst, A., Am. Mineral., 1930. **15**: p. 69-73.
27. Ebner, A.D., S.P. Reynolds, and J.A. Ritter, *Understanding the adsorption and desorption behavior of CO_2 on a K-promoted hydrotalcite-like compound (HTlc) through nonequilibrium dynamic isotherms.* Industrial & Engineering Chemistry Research, 2006. **45**(18): p. 6387-6392.
28. Ochoa-Fernandez, E., et al., *Compositional Effects of Nanocrystalline Lithium Zirconate on Its CO_2 Capture Properties.* Industrial & Engineering Chemistry Research, 2008. **47**(2): p. 434-442.

29. Vidruk, R., et al., *Grain boundary control in nanocrystalline MgO as a novel means for significantly enhancing surface basicity and catalytic activity.* Journal of Catalysis, 2009. **263**(1): p. 196-204.

30. Chiesa, M. and E. Giamello, *Carbon dioxide activation by surface excess electrons: An EPR study of the CO_2^- radical ion adsorbed on the surface of MgO.* Chemistry-a European Journal, 2007. **13**(4): p. 1261-1267.

31. Pacchioni, G., *Physisorbed and Chemisorbed CO_2 at Surface and Step Sites of the Mgo(100) Surface.* Surface Science, 1993. **281**(1-2): p. 207-219.

32. Preda, G., et al., *Formation of CO_2^-; Radical Anions from CO_2 Adsorption on an Electron-Rich MgO Surface: A Combined ab Initio and Pulse EPR Study.* The Journal of Physical Chemistry C, 2008. **112**(49): p. 19568-19576.

33. Florez, E., P. Fuentealba, and F. Mondragon, *Chemical reactivity of oxygen vacancies on the MgO surface: Reactions with CO_2, NO_2 and metals.* Catalysis Today, 2008. **133**: p. 216-222.

34. Karlsen, E.J., M.A. Nygren, and L.G.M. Pettersson, *Comparative study on structures and energetics of NO_x, SO_x, and CO_x adsorption on alkaline-earth-metal oxides.* Journal Of Physical Chemistry B, 2003. **107**(31): p. 7795-7802.

35. Jensen, M.B., et al., *CO_2 sorption on MgO and CaO surfaces: A comparative quantum chemical cluster study.* Journal Of Physical Chemistry B, 2005. **109**(35): p. 16774-16781.

36. Schneider, W.F., *Qualitative differences in the adsorption chemistry of acidic (CO_2, SO_x) and Amphiphilic (NO_x) species on the alkaline earth oxides.* Journal Of Physical Chemistry B, 2004. **108**(1): p. 273-282.

37. Chimentao, R.J., et al., *Defect-induced strategies for the creation of highly active hydrotalcites in base-catalyzed reactions.* Journal Of Catalysis, 2007. **252**(2): p. 249-257.

38. Vouagner, D., C. Beleznai, and J.P. Girardeau-Montaut, *Characterization of the photoelectric effect on K^+-implanted W samples.* Applied Surface Science, 1999. **138-139**: p. 517-521.

39. Aritani H., *et al.*, *Characterization of Li-doped MgO catalysts for oxidative coupling of methane by means of Mg K-edge XANES*. The Journal of Physical Chemistry B, 2000. **104**: p. 10133-10134.

40. Hutchings G. J., *Promotion in heterogeneous catalysis: a topic requiring a new approach?* Catalysis Letters, 2001 **75**: p. 1-12.

Chapter 4

Absorption and desorption properties of potassium carbonate on carbon nanofibers for efficient post-combustion CO_2 capture

Abstract

This study focuses on developing a new easy regenerable sorbent for post-combustion CO_2 capture at low temperatures (373 K). Three different supports, Carbon Nanofibers (CNF), alumina (γ-Al_2O_3) and activated carbon (AC) loaded with K_2CO_3 were investigated. The K_2CO_3 loaded on CNF revealed excellent properties as CO_2 sorbent, displaying capacities of 1.2- 1.6 $mmol.g^{-1}_{sorbent}$ and fast desorption kinetics at low desorption temperatures (423- 523 K). These temperatures were too low to completely regenerate K_2CO_3-Al_2O_3 and K_2CO_3-AC and, consequently, these sorbents lost respectively 80 and 50% of their capacity after the first adsorption-desorption cycle. K_2CO_3-CNF could be regenerated to restore 80% of its capacity with a low energy input estimated at 2- 3 MJ/kg CO_2, which shows this sorbent's potential to become competitive to the currently used amines. The superior sorption properties of K_2CO_3-CNF were attributed to the good accessibility of the relatively small K_2CO_3 particles dispersed on the inert mesoporous carbon support.

Introduction

The ever increasing use of fossil energy brings about the emission of large amounts of carbon dioxide (CO_2) into the atmosphere. Carbon Capture and Storage (CCS) can mitigate CO_2 emissions released in the atmosphere [1]. CO_2 capture can be divided in two classes. Pre-combustion capture involves CO_2 trapped at high temperatures (523- 773 K) accompanied by the production of hydrogen, for example via the water-gas shift reaction ($CO + H_2O \leftrightarrow CO_2 + H_2$). Removal of CO_2 from flue gas streams, e.g. from power plants, at low temperatures (373-423 K) is referred to as post-combustion capture, and is the other class of CO_2 capture. For the latter, amine based scrubbers are currently the commercial option [2, 3]. The use of amines however, requires the use of special reactor materials due to their corrosive nature [2]. Other drawbacks of amines are their limited stability during operation, toxicity and need of a solvent (water) to prevent foaming and to keep the viscosity low [3]. The use of water as solvent makes the regeneration (desorption of CO_2) energy inefficient, since a considerable amount of energy is used for evaporating the water to release the entrapped CO_2.

Alternatives for amine scrubbers are solid regenerable adsorbents such as amines supported on SBA-15 [4-6] or MCM-41 [5, 6], MOFs [7-10], ZIFs [11, 12] and modified carbons [13, 14]. Though promising, these materials are expensive and prone to fouling and deterioration. Alternatively, alkali carbonate supported on carbon and refractory supports have been reported to be promising [14-21]. However, most of the reported K_2CO_3 based materials have low capacity [17, 20] or limited stability (e.g. K_2CO_3/MgO [17, 18]). In addition, regeneration properties are one of the most important factors to be considered and most materials require high temperatures for regeneration [17, 18, 22].

The process for CO_2 capture with K_2CO_3 consists of absorption (carbonation) (1) and regeneration (2), which in its most simplified equation form involves:

$$K_2CO_3 + H_2O + CO_2 \rightarrow 2HKCO_3 \qquad \Delta H^0 = -103\ KJ.mol^{-1} \quad \text{(absorption)} \quad (1)$$

$$2HKCO_3 \rightarrow K_2CO_3 + H_2O + CO_2 \qquad \Delta H^0 = +103\ KJ.mol^{-1} \quad \text{(regeneration)} \quad (2)$$

According to literature [20, 23, 24], in fact the absorption and regeneration proceeds via:

$$K_2CO_3 \bullet 1.5\ H_2O + CO_2 \rightarrow 2HKCO_3 + 0.5\ H_2O \qquad \Delta H^0 = -38\ KJ.mol^{-1}\ (absorption) \qquad (3)$$

$$2HKCO_3 + 0.5\ H_2O \rightarrow K_2CO_3 \bullet 1.5\ H_2O + CO_2 \qquad \Delta H^0 = +38\ KJ.mol^{-1}\ (regeneration) \qquad (4)$$

Please note that the heat effects involved in eq. (3- 4) are much more moderate than those in eq. (1- 2), and therefore are much more attractive for practical applications.

In this work the performance of three supported K_2CO_3 sorbents for CO_2 capture were investigated, i.e. Carbon Nanofibers (CNF), alumina (γ-Al_2O_3) and activated carbon (AC). The results from this work showed excellent absorption and regeneration properties for K_2CO_3-CNF as novel CO_2 sorbent, displaying low desorption temperatures, which makes this material competitive for the commercially used amines.

2. Experimental

2.1 Preparation of supported potassium carbonate

Carbon nanofibers

CNF were obtained from synthesis gas (H_2/CO) using a 20 wt% Ni/SiO_2 catalyst, at 823 K [25, 26]. Removal of the growth catalyst and oxidation of CNF was performed as reported in literature [27, 28] using subsequent treatments in aqueous 1 M KOH and concentrated HNO_3.

Preparation of CNF supported potassium carbonate

5.0 g of CNF were impregnated to incipient wetness in a 250 mL round-bottom flask with 4.0 mL of an aqueous 1.81 M K_2CO_3 solution. Next, the sample was dried at 393 K for 24 h in static air. This sample is denoted as K_{16}-CNF with the number 16 referring to the weight loading (%) of K_2CO_3. A second potassium carbonate sample was prepared with 4.0 mL of an aqueous 3.6 M K_2CO_3 solution. This sample will further be denoted as K_{29}-CNF.

Preparation of activated carbon R2030 (Norit) supported potassium carbonate

5.0 g of active carbon R2030 (Norit) was impregnated in a 250 mL round-bottom flask with 2.0 mL of an aqueous 3.6 M K_2CO_3 solution. Next, the sample was dried at 393 K for 24 h in static air. This sample is denoted as $K_{16\text{-}393}$-AC, with 393 referring to the drying temperature. A second sample was dried at 393 K for 2 h, where after the sample was dried for 48h at RT. This sample is denoted as $K_{16\text{-}293}$-AC.

Preparation of Al_2O_3 supported potassium carbonate

To prepare supported K_2CO_3, 5.0 g Al_2O_3 (Al 4193 E1/8", Engelhard) was impregnated in a 250 mL round-bottom flask with 4.0 mL of an aqueous 1.81 M K_2CO_3 solution. The sample was dried at 393 K for 24 h. This sample is denoted as K_{16}-Al_2O_3. A second potassium carbonate sample was prepared with 4.0 mL of an aqueous 3.6 M K_2CO_3 solution. This sample will further be denoted as K_{29}-Al_2O_3.

2.2 Characterization

Powder X-ray diffraction (XRD) patterns were measured using a Bruker-AXS D8 advance powder diffraction apparatus equipped with an automatic divergence slit (filtered Co-K_α radiation λ = 1.79026 Å). Diffractograms were recorded of the as-synthesized, calcined and *in-situ* CO_2 loaded materials. N_2-physisorption measurements were performed using a Micromeritics Tristar 3000 analyzer after drying the sorbents at 393 K in vacuum for at least 20 h prior to the measurements. SEM micrographs were obtained using a Philips XL30FEG electron microscope equipped with an EDX detector for elemental analysis. The calculations for the desorption energy requirements were performed with HSC chemistry for Windows.

2.3 CO_2 sorption measurements

Sorption measurements were performed in a quartz plug-flow reactor with an inner diameter of 12 mm. The gas flows (N_2, CO_2) were passed down-flow through the reactor and controlled via mass flow controllers (Brooks 5850s). The total pressure in the setup was maintained at 1.10 bar, using a backpressure controller (Brooks 5866). A tubular oven was placed around the reactor to control the process temperature. The reactor was loaded with 5 g of material containing K_2CO_3 (bed height 85 mm). All sorbents were activated by heating in

N_2 (30 mL.min^{-1}) at 773 K (5 K.min^{-1}) for 1 h to remove CO_2 and water from the starting material (activation step). Please note, to distinguish between as-synthesized samples and samples after heat treatment, the latter are called 'activated samples' (e.g. $K_{16\text{-}act}$-CNF).

Operating conditions for the adsorption at 373 K and the subsequent desorption steps are given in Table 1. The total gas flow used throughout all experiments was 30 mL.min^{-1}. N_2 was humidified with CO_2 free water using a saturator set at 331 K. All adsorption experiments were performed for at least 20 minutes after breakthrough (30- 300 minutes). After adsorption, the system was flushed with N_2. Desorption was performed in humid conditions (26.5 N_2/ 3.5 H_2O mL.min^{-1}) either at 423 or at 573 K (5 K.min^{-1}) for 1 h.

Blank measurements were performed either with SiC, CNF, Al_2O_3 or AC with the same bed volume as the K_2CO_3-sorbent containing material. CO_2 adsorption was nil with the SiC and CNF support, and both Al_2O_3 and AC support showed a capacity of 0.06 mmol.g^{-1} at 373 K, which is negligible considering the large capacity of the K_2CO_3-loaded sorbents (*vide infra*).

The effluent gas was analyzed by on-line FT-IR using a Midac corporation 2000 M series. For each spectrum, 8 scans were accumulated with a resolution of 4 cm^{-1}; spectra were recorded every 13 seconds. The IR-cell, made of stainless steel, had a path length of 2 mm and contained CaF_2 windows. The sample compartment was continuously purged with a stream of dry N_2 to prevent interference of CO_2 present in the atmosphere. A background spectrum using an empty cell was acquired prior to a sorption measurement. The integrated area from 2280- 2390 cm^{-1} was used to quantify the amount of CO_2 in the gas phase. A CO_2 concentration above 100 ppm is defined as breakthrough. From the breakthrough time and the flow and concentration the amount of CO_2 was calculated.

Table 1. Experimental conditions for sorption measurements at 373 K with 5 g activated supported sample.

	Flow (mL.min^{-1})	**Composition**	**Temp. (K)**
Activation	30	100% N_2	323→ 773 (5 K.min^{-1}, 1h)
Adsorption	30	83% N_2/ 12% H_2O/ 5% CO_2	373 (30- 300 min)
Desorption	30	88% N_2/ 12% H_2O	373→ 423/573 (5 K.min^{-1}, 1h)

3. Results and discussion

3.1 Characterization of materials

To study the morphology and location of K_2CO_3 on the support, an SEM study was performed. Figure 1 illustrates SEM images of samples K_{16}-CNF (A), K_{16}-Al_2O_3 (B), K_{29}-CNF (C), and K_{29}-Al_2O_3 (D). The white aggregates visible in Figure 1A (BSE-image) are K_2CO_3 particles as confirmed by EDX analysis. A detailed SEM image (inset) revealed that the potassium carbonate was predominantly in intimate contact with the CNF. K_2CO_3 was never observed separate from the CNF support. The K_2CO_3 aggregates on the alumina support were more difficult to distinguish (Figure 1-B). When increasing the K_2CO_3 loading to 29 wt% neither the support (CNF, Al_2O_3) nor discrete K_2CO_3 particles could be distinguished and a more uniform composition was observed (Figure 1-C and 1-D). Although a more dense packing was apparent for both samples, sample K_{29}-CNF still showed a porous structure dissimilar from the K_{29}-Al_2O_3, which indicates that a large part of potassium carbonate on the former support was accessible for carbonation.

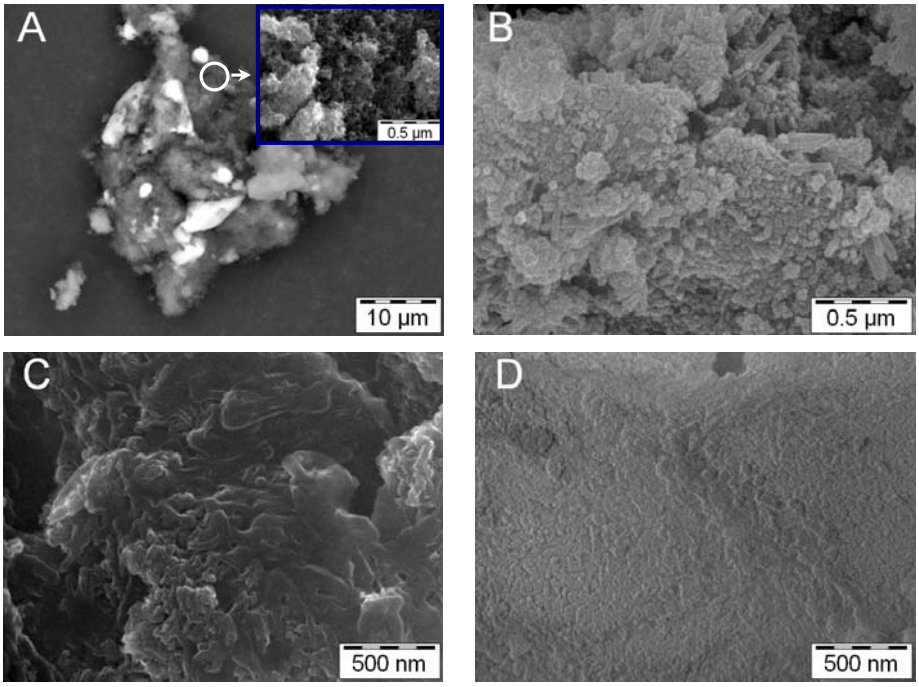

Figure 1. SEM images of: (A) K_{16}-CNF (BSE), (B) K_{16}-Al_2O_3, (C) K_{29}-CNF and (D) K_{29}-Al_2O_3.

The influence of K_2CO_3-loading on the surface area and pore volumes of the samples is presented in Table 2. A significant micropore volume was found for $K_{16\text{-}293}$-AC. In general, the surface areas and pore volume of all potassium loaded sorbents decreased compared to the unloaded samples, which indicated partial filling and/or blocking of the pores.

The large decrease in surface area for K_2CO_3-CNF samples compared to K_2CO_3-Al_2O_3 is tentatively explained. During surface-oxidation of the CNF using HNO_3, opening of the inner tubes of CNF occurs [27, 28]. Therefore, K_2CO_3 deposited on the CNF might have filled or closed the openings of the inner tubes, which could explain the large decrease in surface area.

Table 2. Physico-chemical properties of the various K_2CO_3 sorbents.

Sample	S_{BET} ($m^2.g^{-1}$)	V_{tot} ($cm^3.g^{-1}$)	Sample	S_{BET} ($m^2.g^{-1}$)	V_{tot} ($cm^3.g^{-1}$)	$V_{micropores}$ ($cm^3.g^{-1}$)
K_2CO_3	0	0				
CNF	150	0.37	K_{16}-CNF	61	0.27	0.00
			K_{29}-CNF	40	0.15	0.00
Al_2O_3	160	0.80	K_{16}-Al_2O_3	84	0.60	0.01
			K_{29}-Al_2O_3	79	0.45	0.01
AC	816	0.39	$K_{16\text{-}293}$-AC	551*	0.28	0.23

* mesopore surface area 79 $m^2.g^{-1}$

3.2 CO_2 adsorption and desorption

The above mentioned materials were studied for CO_2 sorption after activation at 773 K in N_2. Representative breakthrough curves for the first CO_2 adsorption cycle at 373 K are shown in Figure 2. Activated $K_{16\text{-}act}$-CNF and $K_{16\text{-}act}$-Al_2O_3 showed, for the first cycle, breakthrough times of ~105 and ~150 minutes, which corresponds to a capacity of 7.2 and 10.3 $mmol.g^{-1}_{K2CO3}$ respectively. The breakthrough time of $K_{29\text{-}act}$-CNF was 1.5 times longer compared to the $K_{16\text{-}act}$-CNF, which corresponds to a capacity of 5.5 $mmol.g^{-1}_{K2CO3}$.

Bulk K_2CO_3 showed a breakthrough at time zero, which corresponds to nil CO_2 uptake. However, after breakthrough a drop in gas phase CO_2 concentration was observed for this sample. This breakthrough curve showed that the sorption of CO_2 for bulk potassium carbonate was very slow, which after more than six hours, resulted in the carbonation to potassium bicarbonate, equation (1) or (3).

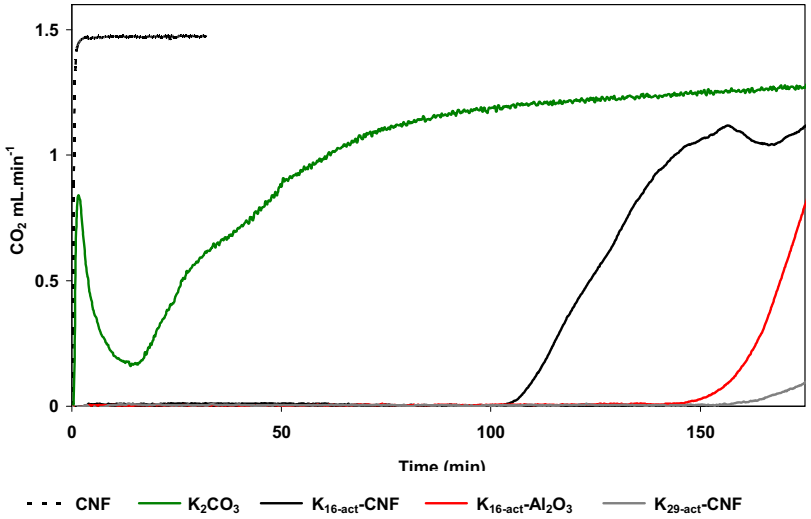

Figure 2. Breakthrough curves of CNF (blank experiment), bulk K_2CO_3 and activated supported K_2CO_3 (5g) for the first CO_2 uptake at 373 K, flow 25 mL.min^{-1} N_2, 3.5 mL.min^{-1} H_2O, 1.5 mL.min^{-1} CO_2.

The sorption capacities for all supported sorbents at 373 K varied from 1.5- 10.3 mmol.g$^{-1}_{K2CO3}$ (Table 3). Sorbent $K_{16\text{-}393\text{-}act}$-AC (dried 24 h at 393 K) displayed a low capacity of 1.5 mmol.g$^{-1}_{K2CO3}$. After modification of the synthesis procedure (drying for 2 h at 393, and thereafter at RT for 48 h) the capacity was increased up to 6.5 mmol.g$^{-1}_{K2CO3}$ ($K_{16\text{-}293\text{-}act}$-AC). These preparation details show the sensitivity of the AC support compared to the CNF support, which enabled a straightforward synthesis procedure and showed a higher capacity.

By increasing the weight loading of K_2CO_3, the sorption capacities per unit weight of K_2CO_3 decreased, which was more pronounced for the Al_2O_3 support (10.3 to 3.8 mmol. g$^{-1}_{K2CO3}$) than for the CNF samples (7.2 to 5.5 mmol.g$^{-1}_{K2CO3}$). The decrease in capacity with increasing K_2CO_3 loading might be explained by the more dense packing on the surface and thus a lower accessibility of K_2CO_3 at higher loading as indicated by figures 1C and D. Apparently, because of the more open structure of the CNF bodies compared to the Al_2O_3 support, the decrease for CNF-supported samples was smaller.

Table 3. Adsorption capacity of supported activated K_2CO_3 sorbents at 373 K for the first cycle at breakthrough.

Sample	Adsorption capacity ($mmol.g^{-1}_{K2CO3}$) at 373 K	Adsorption capacity ($mmol.g^{-1}_{sorbent}$) at 373 K
$K_{16\text{-act}}$-CNF	7.2	1.2
$K_{29\text{-act}}$-CNF	5.5	1.6
$K_{16\text{-act}}$-Al_2O_3	10.3	1.7
$K_{29\text{-act}}$-Al_2O_3	3.8	1.1
$K_{16\text{-393-act}}$-AC	1.5	0.2
$K_{16\text{-293-act}}$-AC	6.5	1.0
K_2CO_3		0
CNF		0
Al_2O_3		0.06
AC		0.06

To investigate the regeneration of the sorbents, which is a most important factor to be considered, temperature programmed desorption was performed up to 423 K (Figure 3a) or 573 K (Figure 3b), followed by an isothermal period of 1 h. Desorption at 423 K showed that $K_{16\text{-act}}$-CNF desorbed more than twice the amount of CO_2 then $K_{16\text{-act}}$-Al_2O_3 and $K_{16\text{-293-act}}$-AC, which showed the facile desorption characteristics of the CNF-based sample. A certain amount of CO_2 did not desorb from $K_{16\text{-act}}$-Al_2O_3 and $K_{16\text{-293-act}}$-AC and, consequently the capacity in the second cycle decreased (*vide infra*). The CO_2 desorption profiles of $K_{16\text{-act}}$-Al_2O_3 up to 523 K showed two peaks. This indicates that there are two kinds of structures within the sample, which was confirmed by XRD (Figure 5b).

The desorption peak at ~430 K for $K_{16\text{-act}}$-Al_2O_3 in figure 3b was consistent with those of $K_{16\text{-act}}$-CNF and $K_{16\text{-293-act}}$-AC, coined to the decomposition of $KHCO_3$. The second peak at 550 K was brought about by the decomposition of $KAl(OH)_2CO_3$ species [29]. These results show that a high temperature was needed to convert this structure into K_2CO_3-Al_2O_3. The second desorption maxima observed for $K_{16\text{-act}}$-CNF and $K_{16\text{-293-act}}$-AC at 450 and 475 K might be caused by different particle sizes of the potassium carbonate (Fig. 1A). Although we cannot exclude that deviation from linearity of the temperature program have played a role too.

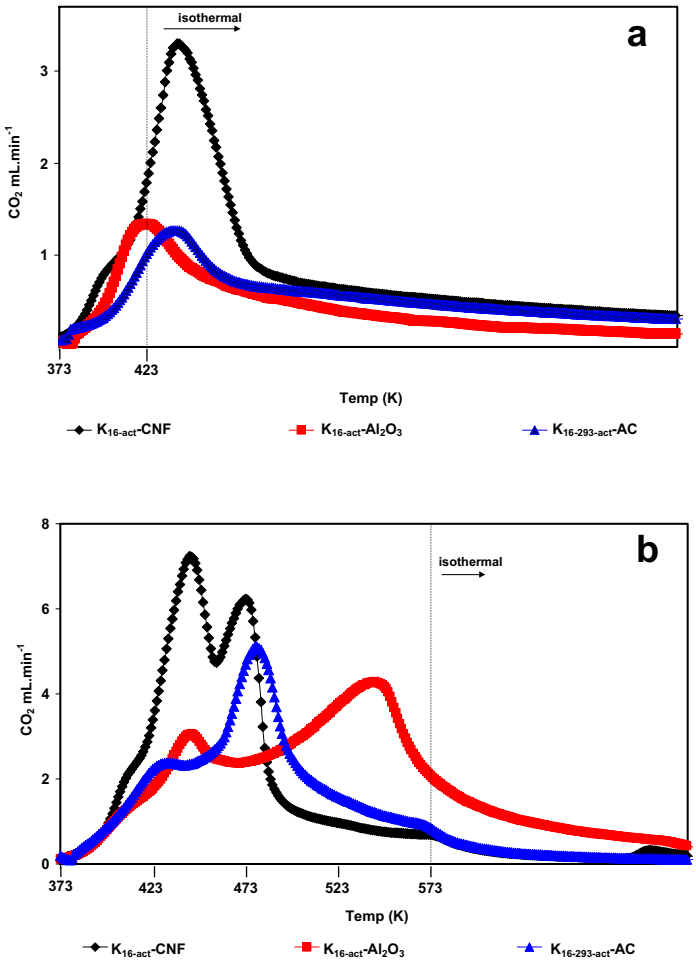

Figure 3. Representative desorption profiles of CO_2-loaded $K_{16\text{-act}}$-CNF, $K_{16\text{-act}}$-Al_2O_3 and $K_{16\text{-293-act}}$-AC at (a) 423 K, (b) 573 K; (5K.min^{-1}, 1 h), flow 26.5 mL.min^{-1} N_2, 3.5 mL.min^{-1} H_2O.

The CO_2 capacity of the activated sorbents was tested for multiple adsorption-desorption cycles while the desorption was performed at 423 or 573 K (Figure 4). The capacity for $K_{16\text{-act}}$-Al_2O_3 and $K_{16\text{-293-act}}$-AC sorbents decreased strongly after desorption at 423 K (Figure 4a), while sample $K_{16\text{-act}}$-CNF showed only a slight decrease after the first cycle, with an uptake of 80% from the original capacity in the second cycle. A temperature of 423 K was clearly too low to fully regenerate K_2CO_3-Al_2O_3 and K_2CO_3-AC which, as a

consequence, lost respectively 80% ($K_{16\text{-act}}$-Al_2O_3) and 50% ($K_{16\text{-293-act}}$-AC) of their capacity in the second cycle. The decrease in CO_2 capture capacity of $K_{16\text{-act}}$-Al_2O_3, after regeneration at these lower temperatures was attributed to the irreversible formation of $KAl(OH)_2CO_3$.

After desorption at higher temperature (573 K, Figure 4b), all samples showed only a slight decrease in capacity. Sample $K_{16\text{-293-act}}$-AC displayed a continuous decrease in capacity, even after seven cycles, while $K_{16\text{-act}}$-CNF was stable after four cycles. Comparison of the desorption profiles showed that $K_{16\text{-act}}$-CNF had most favorable facile desorption kinetics and stability.

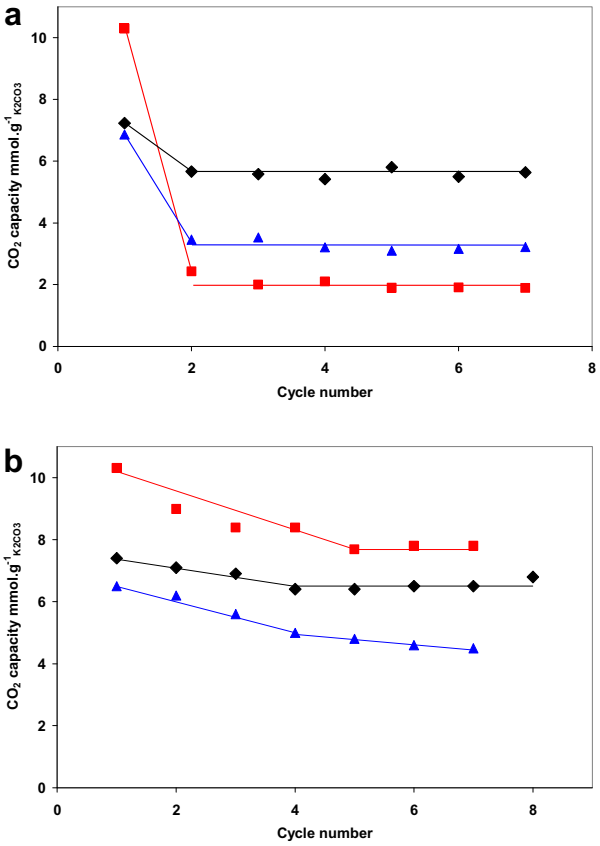

Figure 4. CO_2 capacity as function of adsorption-desorption cycles for selected sorbents at 373 K, (a) desorption at 423 K; (b) after desorption at 573 K; (5K.min^{-1}, 1 h), flow 26.5 mL.min^{-1} N_2, 3.5 mL.min^{-1} H_2O; $K_{16\text{-act}}$-CNF (♦), $K_{16\text{-act}}$-Al_2O_3 (■),$K_{16\text{-293-act}}$-AC (▲).

The presence of alkali phases in the as-synthesized sorbents and the structural changes in morphology after CO_2 loading was investigated by XRD (Figure 5). Figure 5a and b show the XRD patterns of K_{16}-CNF and K_{16}-Al_2O_3, as-synthesized, activated and after CO_2 loading at 373 K. Figure 5c shows an XRD pattern of bulk potassium carbonate (bottom) and the XRD pattern after six hours of CO_2 loading in the presence of steam. Next to the support, K_2CO_3 was the main phase detected on both the activated sorbents (Figure 5a and b). After loading with CO_2, sample $K_{16\text{-act-}CO2}$-CNF showed only the presence of $KHCO_3$, indicating that all K_2CO_3 has been converted to $KHCO_3$. For the Al_2O_3-supported sample on the other hand, two different phases were observed after adsorption at 373 K, $KHCO_3$ (•) and $KAl(OH)_2CO_3$ (▲). The formation of $KAl(OH)_2CO_3$, which is too stable to release CO_2 at 423 K, has been observed before [22] and could explain the lower capacity of this sample in the second cycle after desorption at low temperature.

The major differences in the specific surface areas (Table 2) suggests that the differences in sorption behavior of the supported potassium carbonate sorbents and bulk potassium carbonate can be attributed to structural characteristics. The reaction between bulk K_2CO_3 and CO_2 is probably mass-transfer limited due to the hampered diffusion through a $KHCO_3$ layer. For comparison, the maximum layer thickness of $CaCO_3$ was estimated at around 50 nm for a fast CO_2 uptake by CaO sorbents [30]. Apparently, the facile CO_2 uptake by K_2CO_3 requires nanoparticles on a support combined with a good accessibility of these particles. The combination of the porous structure of the CNF support and small K_2CO_3 particles leads to a highly efficient and stable sorbent.

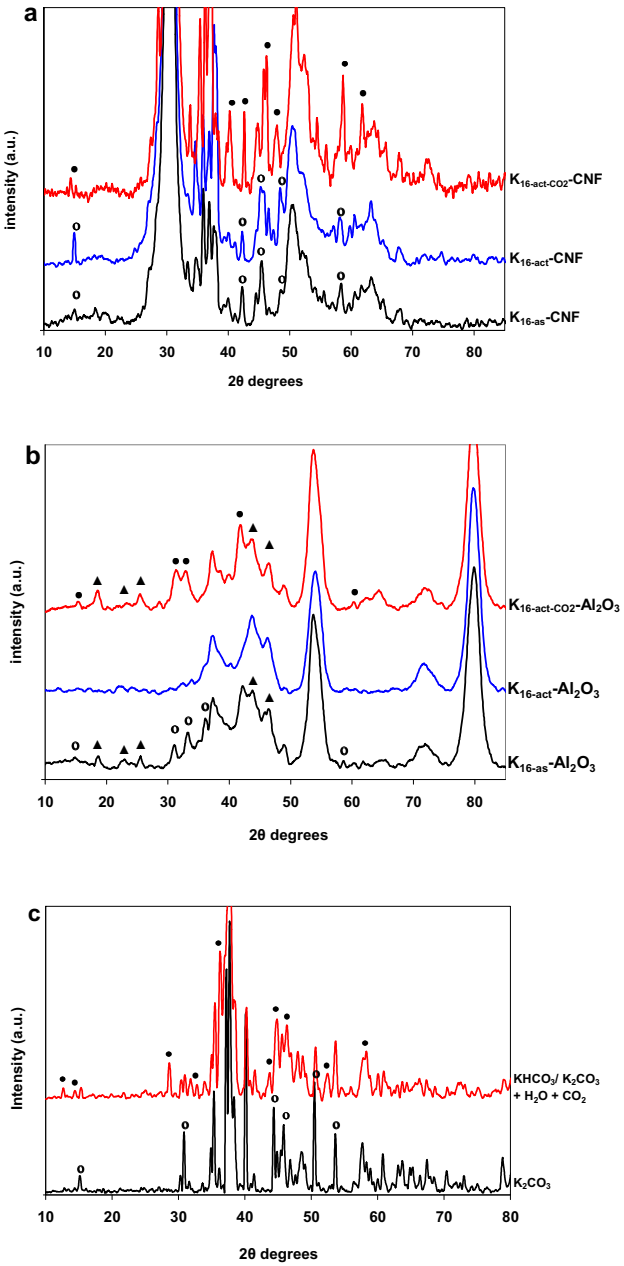

Figure 5. (a) XRD profiles of K_{16}-CNF as-synthesized, after activation and after CO_2 loading for 2 hours; (b) XRD profiles of K_{16}-Al_2O_3 as-synthesized, after activation and after CO_2 loading for 3 hours; (c) XRD profiles of bulk K_2CO_3 (bottom) and after CO_2 loading for 6 hours; (o) K_2CO_3, (•) $KHCO_3$ (▲) $KAl(OH)_2CO_3$.

3.3 Energy requirements and sorbent capacity

The energy needed for desorption, i.e. heating the support and desorbing the CO_2, is a crucial consideration for practical applications, such as for power plants. Therefore we have calculated the total heat consumption for desorption. Table 4 compares the sensible heat needed for the temperature rise and the chemical heat to desorb carbon dioxide. For comparison, the total heat consumption for an amine based systems from literature is included in Table 4. The activated carbon and alumina sorbents required higher temperatures to desorb all carbon dioxide, and therefore necessitated additional heat. Clearly, the CNF supported samples compare favorably with the amine based system, and thus showing potential to be regenerated more efficiently. Moreover, in commercial power plants, a certain amount of heat involved in this process can be recovered, which may reduce the total energy consumption by ~25%. The actual value of heat of desorption is critical for these potassium carbonate sorbents.

Table 4. Comparison of heat requirements for CO_2 desorption.

Sample	Heating sorbents (MJ/ kg CO_2)	Chemical heat (MJ/ kg CO_2)*	Total heat consumption (MJ/ kg CO_2)
K_{16}-CNF	1	1- 2	2- 3
K_{29}-CNF	1	1- 2	2- 3
$K_{16\text{-}293}$-AC	2	1- 2	3- 4
K_{16}-Al_2O_3	2	1- 2	3- 4
K_{29}-Al_2O_3	3	1- 2	4- 5
MEA**			4 ([24])
K_2CO_3-AC			2 ([24])

* ΔH^0 = 40- 100 kJ.mol^{-1}, input 2 kmol of $KHCO_3$ at 1 bar pressure.
** monoethanolamine
Specific heat capacity (C_p): 0.91 kJ.kg^{-1}.K^{-1} (Al_2O_3), 0.92 kJ.kg^{-1}.K^{-1} (CNF, AC) at 373 K.

The initial CO_2 capture capacities per gram sorbent of $K_{16\text{-}act}$-CNF (1.2 mmol.g^{-1}) and $K_{29\text{-}act}$-CNF (1.6 mmol.g^{-1}) were compared with post-combustion materials from literature (Figure 6). The capacities of the K_2CO_3-loaded CNF sorbents were on a par with those of the MCM-41-amine [5, 6], SBA-15-amine [4-6] and commercially used absorbents amines [24] (~2 mmol.g^{-1}). However, the continuous usage of dissolved amines has the disadvantage of the toxicity and corrosive nature of the amine.

The K_2CO_3 samples loaded on CNF displayed facile regeneration properties and were stable during multiple cycles (Figure 4). These results point toward the potential utility of these samples in separation and sequestration using post-combustion capture. For practical applications, natural gas fired power stations are preferred, since potassium carbonate will be negatively affected by formation of sulfates from SO_2 and SO_3 in coal-based power stations.

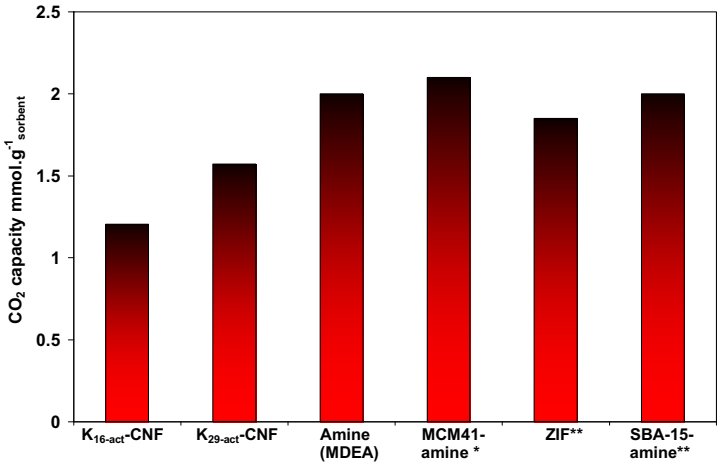

Figure 6. Comparison of the CO_2 sorption capacities on different sorbent materials for post-combustion at 373 K. * measured at 273 K, ** measured at 298- 348 K.

Conclusions

The CO_2 capture properties of three different supports (carbon nanofibers, γ-Al_2O_3, activated carbon) loaded with potassium carbonate were investigated. The novel sorbent K_2CO_3 supported on carbon nanofibers showed a high sorption capacity and excellent regeneration properties for post-combustion capture. The accessible structure and the chemical inertness of CNF and relatively small K_2CO_3 particles are considered key to the favorable properties. In addition, K_2CO_3-CNF could be regenerated with a low energy input, estimated at 2- 3 MJ/kg CO_2, which shows this sorbent's potential to become competitive to the currently used amines. To conclude, heat of desorption is critical for these potassium carbonate sorbents.

Acknowledgements

This research has been carried out by Inorganic Chemistry and Catalysis, Debye Institute for Nanomaterials Science, Department of Chemistry in the CATO-project (Carbon Capture, Transport and Storage). Marjan Versluijs-Helder, and Ad Mens are thanked for SEM and N_2-physisorption measurements.

References

1. *Intergovernmental Panel on Climate Change.* IPCC, Climate Change 2007: The Physical Science Basis (Cambrigde Univ. Press, Cambridge, 2007).
2. Fauth, D.J., et al., *Eutectic salt promoted lithium zirconate: Novel high temperature sorbent for CO_2 capture.* Fuel Processing Technology, 2005. **86**(14-15): p. 1503-1521.
3. Rinker, E.B., S.S. Ashour, and O.C. Sandall, *Absorption of Carbon Dioxide into Aqueous Blends of Diethanolamine and Methyldiethanolamine.* Industrial & Engineering Chemistry Research, 2000. **39**(11): p. 4346-4356.
4. Wang, X., et al., *Infrared Study of CO_2 Sorption over "Molecular Basket" Sorbent Consisting of Polyethylenimine-Modified Mesoporous Molecular Sieve.* The Journal of Physical Chemistry C, 2009. **113**(17): p. 7260-7268.
5. Hicks, J.C., et al., *Designing Adsorbents for CO_2 Capture from Flue Gas-Hyperbranched Aminosilicas Capable of Capturing CO_2 Reversibly.* Journal of the American Chemical Society, 2008. **130**(10): p. 2902-2903.
6. Yue, M.B., et al., *Efficient CO_2 capturer derived from as-synthesized MCM-41 modified with amine.* Chemistry-a European Journal, 2008. **14**(11): p. 3442-3451.
7. Yazaydın, A.Ö., et al., *Enhanced CO_2 Adsorption in Metal-Organic Frameworks via Occupation of Open-Metal Sites by Coordinated Water Molecules.* Chemistry of Materials, 2009. **21**(8): p. 1425-1430.
8. Finsy, V., et al., *Separation of CO_2/CH_4 mixtures with the MIL-53(Al) metal-organic framework.* Microporous and Mesoporous Materials, 2009. **120**(3): p. 221-227.
9. Llewellyn, P.L., et al., *High uptakes of CO_2 and CH_4 in mesoporous metal-organic frameworks MIL-100 and MIL-101.* Langmuir, 2008. **24**(14): p. 7245-7250.

10. Babarao, R. and J.W. Jiang, *Molecular screening of metal-organic frameworks for CO_2 storage.* Langmuir, 2008. **24**(12): p. 6270-6278.
11. Liu, D.H., et al., *Understanding the Adsorption and Diffusion of Carbon Dioxide in Zeolitic Imidazolate Frameworks: A Molecular Simulation Study.* Journal of Physical Chemistry C, 2009. **113**(12): p. 5004-5009.
12. Banerjee, R., et al., *High-throughput synthesis of zeolitic imidazolate frameworks and application to CO_2 capture.* Science, 2008. **319**(5865): p. 939-943.
13. Yong, Z., V.G. Mata, and A.E. Rodrigues, *Adsorption of carbon dioxide on chemically modified high surface area carbon-based adsorbents at high temperature.* Adsorption-Journal Of The International Adsorption Society, 2001. **7**(1): p. 41-50.
14. Song, H.K. and K.H. Lee, *Adsorption of carbon dioxide on chemically modified carbon adsorbents*
    Separation Science and Technology, 1998. **33**(13): p. 2039-2057.
15. Okunev, A.G., et al., *Sorption of Carbon Dioxide from Wet Gases by K_2CO_3-in-Porous Matrix: Influence of the Matrix Nature.* Reaction Kinetics and Catalysis Letters, 2000. **71**(2): p. 355-362.
16. Lee, S.C. and J.C. Kim, *Dry potassium-based sorbents for CO_2 capture.* Catalysis Surveys from Asia, 2007. **11**(4): p. 171-185.
17. Lee, S.C., et al., *CO_2 absorption and regeneration of alkali metal-based solid sorbents.* Catalysis Today, 2006. **111**(3-4): p. 385-390.
18. Lee, S.C., et al., *Development of regenerable MgO-based sorbent promoted with K_2CO_3 for CO_2 capture at low temperatures.* Environmental Science & Technology, 2008. **42**(8): p. 2736-2741.
19. Hayashi, H., et al., *Efficient recovery of carbon dioxide from flue gases of coal-fired power plants by cyclic fixed-bed operations over K_2CO_3-on-carbon.* Industrial & Engineering Chemistry Research, 1998. **37**(1): p. 185-191.
20. Hirano, S., et al., *Cyclic Fixed-Bed Operations over K_2CO_3-on-Carbon for the Recovery of Carbon-Dioxide under Moist Conditions.* Bulletin of the Chemical Society of Japan, 1995. **68**(3): p. 1030-1035.

21. Okunev, A.G., et al., *Sorption of carbon dioxide by the composite sorbent of potassium carbonate in porous matrix.* Russian Chemical Bulletin, 2003. **52**(2): p. 359-363.

22. Wang, Y., J.H. Zhu, and W.Y. Huang, *Synthesis and characterization of potassium-modified alumina superbases.* Physical Chemistry Chemical Physics, 2001. **3**(12): p. 2537-2543.

23. Lee, S., et al., *The effect of water on the activation and the CO_2 capture capacities of alkali metal-based sorbents.* Korean Journal of Chemical Engineering, 2006. **23**(3): p. 374-379.

24. Shigemoto, N., et al., *Material Balance and Energy Consumption for CO_2 Recovery from Moist Flue Gas Employing K_2CO_3-on-Activated Carbon and Its Evaluation for Practical Adaptation.* Energy & Fuels, 2006. **20**(2): p. 721-726.

25. Meis, N.N.A.H., J.H. Bitter, and K.P. de Jong, *Support and Size Effects of Activated Hydrotalcites for Pre-combustion CO_2 Capture.* Industrial & Engineering Chemistry Research, 2009.

26. Meis, N.N.A.H., J.H. Bitter, and K.P. de Jong, *On the influence and role of alkali metals on supported and unsupported activated hydrotalcites for CO_2 sorption.* Industrial & Engineering Chemistry Research, 2010, manuscript submitted**.**

27. Winter, F., et al., *TEM and XPS studies to reveal the presence of cobalt and palladium particles in the inner core of carbon nanofibers.* Carbon, 2005. **43**(2): p. 327-332.

28. Toebes, M.L., et al., *The influence of oxidation on the texture and the number of oxygen-containing surface groups of carbon nanofibers.* Carbon, 2004. **42**(2): p. 307-315.

29. Lee, S.C., et al., *Novel regenerable potassium-based dry sorbents for CO_2 capture at low temperatures.* Journal of Molecular Catalysis B-Enzymatic, 2009. **56**(2-3): p. 179-184.

30. Alvarez, D. and J.C. Abanades, *Determination of the Critical Product Layer Thickness in the Reaction of CaO with CO_2.* Industrial & Engineering Chemistry Research, 2005. **44**(15): p. 5608.

Chapter 5[a]

Summary and concluding remarks

The average concentration of CO_2 in the atmosphere has been increasing since the start of the industrial revolution in the 18th century from 280 ppm to 380 ppm nowadays, and continues to increase because of the enormous human usage of fossil fuels (oil, gas, coal). This can strongly affect the climate, causing the Earth's surface to warm up, the so called 'amplified greenhouse effect' or 'anthropogenic global warming' (AGW). Studies showed that the increase in carbon dioxide, and the consequent increase in temperature, have already caused acidification of oceans, decrease of tropical forests, release of methane from permafrost, vanishing of arctic summer ice and decline of glaciers.

There are three options to decrease the CO_2 emissions. The first is to reduce the usage of energy, e.g. through the use of hybrid cars and led-lamps. Secondly, alternative energy sources based on renewables which emit little or no CO_2 can be used. Examples are wind, solar, water, and geothermal energy, biomass and biofuel. The last option is to capture and permanently store the CO_2 released during the usage of fossil fuels (CCS: Carbon Capture and Storage). CCS can be divided in three main routes, i.e. oxy-fuel combustion, post-combustion capture and pre-combustion capture. Oxy-fuel combustion uses pure oxygen for the combustion instead of air and the flue gas has therefore a much lower volume and a high concentration of CO_2. Drawback of this method is the cost of pure oxygen and therefore the technology is not yet used. In post-combustion capture, diluted CO_2 is captured and separated from flue gases produced by the combustion of fossil fuels. In pre-combustion capture the fossil fuel is converted to hydrogen (H_2) and carbon monoxide (CO), followed by the conversion of carbon monoxide by the water-gas shift reaction to carbon dioxide and more hydrogen. The formed CO_2 is then captured and the hydrogen can either be burned in turbines or used in fuel cells, where only water vapor is released.

In both cases (pre- and post-combustion), the captured CO_2 is released, either by temperature or pressure swing, to regenerate the sorbent whereby a pure stream of CO_2 is released. This is, within the CCS chain, the most important and most energy intensive step. The stream is further compressed and transported to a location where it is injected into empty oil or gas fields or into deep geological formations (aquifers) for permanent storage. Storage of CO_2 can provide an interim solution towards a worldwide economy based on sustainable energy usage.

In recent years, a great deal of interest has been shown for using solid sorbents for CO_2 capture as alternatives for amine-scrubbers. None of these materials have all the required properties to operate for CO_2 capture. The ideal solid sorbent should be selective towards CO_2, have a high adsorption capacity, display adequate adsorption and desorption kinetics at

operating conditions (facile regeneration), have long term stability upon cyclic use, adequate mechanical strength and low costs of the material.

The research described in this thesis concerns the development of solid basic sorbents for CO_2 capture. An anionic clay, hydrotalcite, was chosen as sorbent, which was shown to be a promising material for CO_2 capture at high temperatures, i.e. under pre-combustion conditions. The as-synthesized hydrotalcite (HT), usually with carbonate in the interlayer, displays no activity for CO_2 capture. The method to acquire an active sorbent from the precursor involves an activation step (HT_{act}). After activation, i.e. a heat treatment at 773 K which destroyed the layered structured and removed the carbonate, a mixed oxide ($Mg(Al)O_x$) was formed which could capture CO_2. Numerous investigations reported in literature on activated (and rehydrated) hydrotalcites, showed that large differences in (catalytic) properties may be observed, depending on the preparation of the precursor or the activation procedure. However, up to now, no systematic study on the relation between the physico-chemical properties of hydrotalcites and their CO_2 capture properties has been performed and is reported here.

Chapter 2 describes the influence of lateral platelet size (of the HT before activation) and the use of a support on the CO_2 capture properties of HT. A series of hydrotalcites with differences in lateral platelets sizes (~40 nm- 2 μm) was prepared. In addition, small HT platelets (~20 nm) were deposited on carbon nanofiber (CNF). CNF supported HT was prepared with three different loadings (5, 10, 18 wt%). The use of this support material is attractive because of its favorable physico-chemical properties, i.e. high mechanical strength, high surface area, tunable surface properties and the absence of micropores. However, the use of a support can decrease the weight or volume based sorption capacity of a material.

The size and physical properties of the various supported and unsupported HTs were evaluated with X-ray diffraction (XRD), electron microscopy (SEM, TEM) and N_2-physisorption. CO_2-sorption of the hydrotalcites was determined with infrared spectroscopy (FT-IR) by analysis of the effluent gas from a fixed bed reactor at 523 K. There was no significant difference in the CO_2 sorption capacities at 523 K for all unsupported HTs, regardless of the platelet size of the HT precursor (~0.1 $mmol.g^{-1}$).

The capacities of the activated supported HT at 523 K were significantly increased compared to the activated unsupported HT (1.3- 2.5 $mmol.g^{-1}{}_{HT}$). We propose that the increase in capacity for the activated, supported HTs is the result of a higher amount of defects on the small immobilized $Mg(Al)O_x$ crystals. The amount of low-coordinated oxygen in activated, unsupported samples is identical on a weight-basis for all samples. After

activation, the samples lose their original crystalline platelet structure (although the platelets shape of the HTs remain). Apparently, larger $Mg(Al)O_x$ particles contain more surface defects per unit surface area and, consequently, higher coverage of CO_2.

In **Chapter 3** the influence of the addition of alkali metal carbonate (K_2CO_3 en Na_2CO_3) to unsupported and CNF supported HTs on their CO_2 capture properties is discussed. The alkali metal carbonate can be introduced either by impregnation of a K_2CO_3 solution on as-synthesized HT or by leaving residual potassium or sodium carbonate, from the synthesis, in the final material. The latter method is advocated, since it omits a washing step after precipitation. The physical properties and alkali metal carbonate loadings on the unsupported and supported HTs were evaluated with XRD, SEM, TEM and N_2-physisorption.

To achieve a close contact between the HT and the alkali carbonate, it was shown that alkali carbonate metal loading should be performed before activation of the HT. Electron microscopy and N_2-physisorption revealed that only then the alkali metal carbonate is in close contact with the HT and well accessible at at least a mesoscopic level. The alkali-loaded unsupported HT showed a much higher capacity (~0.3 $mmol.g^{-1}$) at 523 K compared to the unloaded HTs. The alkali-loaded supported hydrotalcites adsorbed 1.7 -2.2 $mmol.g_{HT}^{-1}$, depending on the preparation method, which exceeds slightly the capacity of supported unpromoted HT. The increase in capacity for alkali-loaded HTs point to a higher concentration of defects (low-coordination oxygen sites) on the surface of the activated alkali-loaded HTs compared to the unloaded HT. The higher concentration of adsorption might be caused by the presence of Na^+/K^+ on the surface of $Mg(Al)O_x$. Due to the larger size of these alkali ions it would be difficult to incorporate these ions extensively in an MgO lattice, and incorporation in an activated HT would therefore be unlikely. As a result, we propose that the K^+/Na^+ are located at the surface and not in the 'bulk' of the $MgAlO_x$. Our tentative mechanism is that K^+ plus substitutes an Mg^{2+} and additional oxygen vacancies at the surface are created.

The relative increase in capacity supported HT after alkali carbonate addition was smaller as for the unsupported HT. This is explained by the fact that supported the HT already possessed a higher number of adsorption sites (defects) and thus the influence of K/Na is less significant for these samples.

The research described in **Chapter 4** focuses on post-combustion capture at low temperatures (373 K). A new developed sorbent for CO_2 capture, i.e. potassium carbonate (K_2CO_3) deposited on carbon nanofibers (CNF) was compared with potassium carbonate (16% or 29 wt%) deposited on activated coal (AC) and alumina (Al_2O_3). The physical

properties of the potassium carbonate loaded sorbents were evaluated using XRD, SEM and N_2-physisorption. K_2CO_3 loaded on the CNF support revealed excellent properties as CO_2 sorbent compared to the K_2CO_3-AC and K_2CO_3-Al_2O_3 sorbents, having the highest capacity and fast desorption kinetics at low desorption temperatures (423- 523 K).

These temperatures were too low to regenerate K_2CO_3-AC and K_2CO_3-Al_2O_3 which, as a consequence, lost 50 and 80% of their capacity after the first adsorption-desorption cycle. The favorable properties of K_2CO_3-CNF are considered to originate from relatively small K_2CO_3 particles combined with a good accessibility of these particles surrounded by the CNF. In addition, calculations for the total heat consumption for desorption of the sorbent were made. The K_2CO_3-CNF could be regenerated with a low energy input estimated at 2- 3 MJ/kg CO_2, far below the energy needed for the currently used amine-scrubbers, which shows this sorbent's potential to become competitive with established post-combustion sorbents.

Currently, (new) processes for CO_2 capture are demonstrated nationally and internationally on pilot scale. For CO_2 capture, however, the overall processes are typically 20% less efficient. Thus, as an example, when using CO_2 capture in power plants, five power plants are needed, in stead of four, where the energy of the fifth power plant is used to capture and store the CO_2. This is obviously still not efficient enough, therefore further investigation of sorbent materials described in this dissertation for pre- and post-combustion capture is needed. These investigations might contribute to a lower energy demand and higher energy efficiency. Further research should focus on the development of (new) sorbents for CO_2 capture with high capacities, stability and low energy demands for regeneration. This includes different types of modified metal oxides as magnesium and calcium oxide, with the combination of a suitable support.

Chapter 5[b]

Samenvatting en conclusies

Sinds het begin van de industriële revolutie (1750) zijn grote hoeveelheden koolstofdioxide (CO_2) in de atmosfeer terechtgekomen. Het enorme gebruik van fossiele brandstoffen (olie, gas, kolen) heeft geresulteerd in een concentratiestijging van 280 ppm naar 380 ppm CO_2. Deze stijging kan van invloed zijn op het klimaat en resulteren in opwarming van de aarde. Dit proces wordt ook wel het 'versterkt broeikaseffect' (‘global warming’) genoemd. De CO_2-concentratiestijging heeft nu al een negatief effect op het milieu, zoals verzuring van oceanen en opwarming van de aarde. Dit laatste heeft weer als gevolg dat gletsjers en permafrost smelten.

Er zijn drie mogelijkheden om de uitstoot van koolstofdioxide te verminderen en om de negatieve effecten hiervan op het milieu tegen te gaan. De eerste optie is het efficiënter omgaan met energie, onder andere door het gebruik van hybride auto’s en led-lampen. Een andere mogelijkheid is het gebruik van schone/hernieuwbare energiebronnen zoals windenergie, zonne-energie, waterenergie en biomassa. Als laatste optie kan de CO_2, die door het gebruik van fossiele brandstoffen gevormd wordt, worden afgevangen en opgeslagen. Deze optie wordt vaak beschouwd als een tussenoplossing in de transitie naar schone brandstoffen. Door CO_2 af te vangen en daarna permanent onder de grond op te slaan kan de uitstoot van CO_2 in de atmosfeer worden vermeden. Dit proces wordt CCS (Carbon Capture and Storage) genoemd. Er zijn drie basistechnologieën mogelijk voor CO_2-afvang, te weten ‘oxy-fuel combustion’, ‘post-combustion capture’ en ‘pre-combustion capture’. Oxy-fuel combustion gebruikt zuivere zuurstof voor de verbranding in plaats van lucht. Hierdoor kan het CO_2 in een laag volume en hoge concentratie worden afgevangen. Nadeel van deze methode zijn de hoge kosten van zuivere zuurstof, waardoor oxy-fuel combustion nog niet op grote schaal wordt toegepast. In post-combustion capture wordt het CO_2 na verbranding van koolwaterstoffen afgevangen en geconcentreerd in een sorbent. Bij pre-combustion capture, zoals de water-gas-shift-reactie, wordt het CO_2 tijdens de waterstofproductie uit koolwaterstoffen afgevangen. Waterstof kan hierna worden verbrand in een turbine of kan worden gebruikt in een brandstofcel waarbij alleen nog waterdamp vrij komt. In beide gevallen (pre- en post-combustion) wordt, na een desorptiestap, het geconcentreerde CO_2 uit het sorbent gehaald en permanent opgeslagen in bijvoorbeeld lege olie- en gasvelden of diepe zoute zeelagen (aquifers). Het sorbent kan dan opnieuw worden gebruikt. De belangrijkste stap in het hele proces voor CO_2-opslag, die ook het meeste energie kost, is de

concentratie/scheidingsstap van het CO_2 door middel van een sorbent. Opslag van CO_2 kan een tussenoplossing zijn op weg naar een economie die gebaseerd is op alternatieve brandstoffen.

Als sorbent zijn verschillende vaste basische materialen beschreven in de literatuur, als alternatief voor amine oplossingen. Tot op heden is er echter geen materiaal gevonden dat alle eigenschappen bezit voor een perfect sorbent, zoals alleen selectiviteit voor CO_2, hoge capaciteit, langdurige stabiliteit, mechanische sterkte en adequate desorptiekinetiek. Ook moet een CO_2-sorbent makkelijk te synthetiseren en goedkoop te produceren zijn.

Het onderzoek beschreven in deze dissertatie heeft tot doel gehad het ontwikkelen van een vast basisch sorbent dat geschikt is voor CO_2-afvang. Er is gekozen voor hydrotalciet (HT), een anionische klei, waarmee initieel al veelbelovende resultaten zijn geboekt in het afvangen van CO_2 bij hoge temperaturen (relevant voor pre-combustion).

Hydrotalciet (HT) wordt meestal gesynthetiseerd met carbonaat in de tussenlaag. Om een actief hydrotalciet geschikt voor CO_2-adsorptie te verkrijgen moet het HT geactiveerd (HT_{act}) worden door verhitting tot ~773 K, waarbij HT ontleedt en een gemengd oxide wordt gevormd ($Mg(Al)O_x$). Uit de vele studies naar de eigenschappen van deze geactiveerde hydrotalcieten is gebleken dat grote verschillen in (katalytische) eigenschappen kunnen optreden, afhankelijk van de bereidingswijze en activeringsprocedure. Een studie naar de relatie tussen fysisch-chemische eigenschappen van hydrotalcieten en de CO_2-capaciteit was echter tot op heden niet uitgevoerd.

Hoofdstuk 2 beschrijft de invloed van de plaatgrootte (voor activatie) en het gebruik van het dragermateriaal op de CO_2-eigenschappen van hydrotalcieten. Twee verschillende soorten hydrotalcietmaterialen zijn bestudeerd, te weten ongedragen HTs met verschillende laterale plaatgrootte (~40 nm- 2 μm) en met zeer kleine laterale afmeting (~20 nm) koolstofnanovezels gedragen HTs (HT-CNF). De koolstofnanovezels gedragen HTs werden met drie verschillende beladingen gesynthetiseerd (5, 10, 18 wt%). Koolstofnanovezels zijn zeer attractief als dragermateriaal vanwege de mechanische sterkte, het grote oppervlak en de bewerkbaarheid van de nanovezels. Echter, toepassing van een dragermateriaal kan de CO_2-capaciteit van het materiaal op volumebasis verminderen.

De grootte en de fysische eigenschappen van de verschillende gedragen en ongedragen hydrotalcieten werden geëvalueerd met behulp van röntgendiffractie (XRD),

elektronenmicroscopie (TEM, SEM) en N_2-physisorptiemetingen. Met behulp van infrarood spectroscopische (FT-IR) metingen van de gasfase werd de CO_2-adsorptie gemeten in een fixed-bed reactor bij 523 K.

Ondanks het grote verschil in laterale dimensie van de hydrotalciet precursor bleek er geen significant verschil in de adsorptiecapaciteit van de ongedragen HTs (~0.1 mmol.g^{-1}). Na activatie van de HT-materialen verschilden de gemeten capaciteiten bij 523 K van de gedragen en ongedragen HTs echter wel significant. De gedragen HTs vertoonden een onovertroffen activiteit die 10- 25 keer hoger was vergeleken met ongedragen HTs (1.3- 2.5 mmol.g^{-1}_{HT}).

De hogere capaciteit van de gedragen HTs komt door een hogere wanorde (defecten) op de verankerde kleine $Mg(Al)O_x$ kristallieten. Terwijl de hoeveelheid laag gecoördineerd zuurstof in geactiveerd, ongedragen HT identiek is op gewichtsbasis voor alle HTs. Na activatie verliezen de HTs hun originele plaatstructuur, maar de vorm van de HT-plaatjes blijft bestaan. Grotere $Mg(Al)O_x$ deeltjes hebben blijkbaar meer defecten per oppervlakte-eenheid en derhalve een hogere bedekkingsgraad van CO_2.

In **hoofdstuk 3** wordt de invloed van toevoeging van alkalicarbonaat (K_2CO_3 en Na_2CO_3) op ongedragen en gedragen hydrotalcieten op koolstofnanovezels op de CO_2 capaciteit bij hoge temperatuur (523 K) behandeld. Het bleek mogelijk om via verschillende syntheseroutes het alkalicarbonaat op het HT aan te brengen. Dit kon door middel van een directe impregnatie van het alkalicarbonaat in het HT. Een tweede mogelijkheid is om HT na synthese niet te zuiveren, waarbij het alkalicarbonaat geïncorporeerd blijft in het HT. De laatste methode heeft de voorkeur omdat hierdoor de zuiveringstappen achterwege gelaten kunnen worden. De fysische eigenschappen en beladingen van het alkalicarbonaat op de ongedragen en gedragen HTs werden geëvalueerd met XRD, SEM, TEM en N_2-physisorptie.

Hier werd aangetoond dat het alkalicarbonaat goed was gedispergeerd over het HT, mits het ongedragen HT was beladen voor activatie. De toegankelijkheid van het K_2CO_3 wordt toegeschreven aan een goede interactie tussen het HT en het alkalicarbonaat. De met alkalicarbonaat beladen ongedragen hydrotalcieten lieten bij 523 K een factor 3 verhoging van de capaciteit zien (~0.3 mmol.g^{-1}), vergeleken met niet gepromoteerde HTs. Ook de koolstofnanovezels gedragen alkalicarbonaat hydrotalcieten gaven, afhankelijk van de

bereidingsmethode, een verbeterde capaciteit van 1.7- 2.2 $mmol.g^{-1}_{HT}$, vergeleken met de gedragen HTs en de ongedragen alkalicarbonaat geladen HTs.

De verhoogde capaciteit voor de met alkalicarbonaat geladen hydrotalcieten wordt toegeschreven aan een hogere concentratie van defecten (laaggecoördineerde zuurstofplaatsen) ontstaan door impregnatie van alkalicarbonaat. De hogere concentratie wordt vermoedelijk veroorzaakt door de aanwezigheid van Na^+/K^+ op het oppervlak van $Mg(Al)O_x$. Deze alkali-ionen zijn relatief groot en incorporatie van grote hoeveelheden in een MgO rooster is daarom onwaarschijnlijk. Daarom wordt verondersteld dat de Na^+/K^+ zich op het oppervlak van het $Mg(Al)O_x$ bevindt en niet in de bulk. Het voorgestelde mechanisme substitueert een Na^+/K^+ op een Mg^{2+} en derhalve ontstaat een zuurstofvacature op het oppervlak. De capaciteit van de alkalicarbonaat gedragen HTs was relatief minder toegenomen vergeleken met de ongedragen alkalicarbonaat HTs. Dit komt mede doordat op gedragen hydrotalcieten een hogere concentratie van adsorptieplaatsen (defecten) aanwezig is, waardoor de invloed van alkalicarbonaat minder is voor deze materialen.

Het onderzoek gepresenteerd in **hoofdstuk 4** concentreert zich op 'post-combustion capture' bij lage temperaturen (373 K). Een nieuw absorptiemateriaal voor CO_2-afvang, kaliumcarbonaat (K_2CO_3) gedispergeerd op koolstofnanovezels (CNF), werd vergeleken met kaliumcarbonaat (16% of 29%) gedispergeerd op geactiveerde kool (AC) en alumina (Al_2O_3). De fysische eigenschappen van het kaliumcarbonaat op de verschillende dragers werden geëvalueerd met behulp van XRD, SEM en N_2-physisorptie.

De eigenschappen voor CO_2-absorptie van het K_2CO_3-CNF sorbent waren superieur ten overstaande van de sorbents K_2CO_3-AC en K_2CO_3-Al_2O_3. Bij een lage temperatuur (423 K) was het mogelijk om K_2CO_3-CNF bijna geheel te desorberen. Van de oorspronkelijke capaciteit kon 80% worden gerecupereerd, terwijl K_2CO_3-AC en K_2CO_3-Al_2O_3 respectievelijk 50% en 80% van de oorspronkelijke capaciteit verloren. De open structuur en relatief kleine kaliumcarbonaatdeeltjes, omringd door het CNF, geven een hoge contactefficiëntie en toegankelijkheid voor het CO_2. Vooral de combinatie van deze eigenschappen van de koolstofnanovezels resulteerde in de superieure kwaliteiten van dit materiaal, zoals een makkelijke regeneratie en een hoge capaciteit.

Verder is een berekening gemaakt voor de totale energiebehoefte die nodig is voor desorptie van de sorbents. Het K_2CO_3-CNF had een lage totale energiebehoefte die werd geschat op

2- 3 MJ/kg CO_2. Deze behoefte ligt ver beneden die van de nu toegepaste amine-scrubbers, wat de potentie laat zien van dit nieuwe sorbent.

Momenteel vindt in binnen- en buitenland opschaling plaats van vernieuwde processen voor CO_2-afvang met bijbehorende sorbents. Demonstratieopstellingen laten zien dat de geïntegreerde processen met CO_2-afvang ongeveer 20% minder efficiënt zijn. Hierdoor zou er nu voor elke vier elektriciteitscentrales, een vijfde nodig zijn om de energie te produceren die nodig is om CO_2 af te vangen en op te slaan. Daarom is verder onderzoek nodig naar de beschreven materialen in deze dissertatie voor pre- en post-combustion capture. Dit kan bijdragen aan een lagere energiebehoefte en een hogere efficiëntie voor CO_2-afvang. Het vervolg dient bij voorkeur gericht te zijn op het verder ontwikkelen van (nieuwe) materialen voor CO_2-afvang met hogere capaciteiten, verbeterde stabiliteit en lagere energiebehoeftes voor regeneratie, waarbij gedacht kan worden aan modificatie van magnesium- en calciumoxides in combinatie met geschikte dragermaterialen.

List of publications and presentations

Publications

N.N.A.H. Meis, J.H. Bitter, K.P. de Jong, *Support and size effects of activated hydrotalcites for pre-combustion CO_2 capture*, Industrial & Engineering Chemistry Research, 2009 (accepted).

N.N.A.H. Meis, J.H. Bitter, K.P. de Jong, *On the influence and role of alkali metals on supported and unsupported activated hydrotalcites for CO_2 sorption*, Industrial & Engineering Chemistry Research (submitted).

N.N.A.H. Meis, J.H. Bitter, K.P. de Jong, *Absorption and desorption properties of potassium carbonate on carbon nanofibers for efficient post-combustion CO_2 capture* (in preparation).

Oral Presentations

N.N.A.H. Meis, J.H. Bitter, K.P. de Jong, *Promoted and supported hydrotalcites for enhanced CO_2 capture*, 10th Netherlands' Catalysis and Chemistry Conference, Noordwijkerhout, the Netherlands, March 2009

N.N.A.H. Meis, J.H. Bitter, K.P. de Jong, *Carbon nanofiber supported hydrotalcites for enhanced CO_2 capture*, 3th International Symposium on Carbon for Catalysis, Berlin, Germany, November 2009.

J.H. Bitter, N.N.A.H. Meis, K.P. de Jong**,** *Supported hydrotalcites for CO_2 capture: - Towards a structure-activity relation*, 4th CATO-day, Petten, the Netherlands, June 2008.

J.H. Bitter, N.N.A.H. Meis, K.P. de Jong**,** *carbon nanofiber supported hydrotalcites for enhanced CO_2 capture*, ABC-6, Genova, Italy, May 2008

N.N.A.H. Meis, J.H. Bitter, K.P. de Jong, *Supported hydrotalcites as a novel sorbent for CO_2 capture*, 9th Netherlands' Catalysis and Chemistry Conference, Noordwijkerhout, the Netherlands, March 2008.

J.H. Bitter, N.N.A.H. Meis, K.P. de Jong**,** *Hydrotalcites for CO_2 capture - current status and perspectives*, 2nd CATO-day, Utrecht, the Netherlands, June 2006.

Poster Presentations

N.N.A.H. Meis, J.H. Bitter, K.P. de Jong, *Towards a quantitative structure activity relationship for CO_2 capture by hydrotalcites,* E-MRS Fall Meeting, Warsaw, Poland, September 2008, best poster award.

N.N.A.H. Meis, J.H. Bitter, K.P. de Jong, *Towards a quantitative structure activity relationship for CO_2 capture by hydrotalcites*, 14th International Congress on Catalysis, Seoul, Korea, July 2008.

N.N.A.H. Meis, J.H. Bitter, K.P. de Jong, *Structure activity relation of well defined hydrotalcites for CO_2 adsorption*, 8th Netherlands' Catalysis and Chemistry Conference, Noordwijkerhout, the Netherlands, March 2008.

N.N.A.H. Meis, J.H. Bitter, K.P. de Jong, *Preparation and in situ characterization of well defined hydrotalcites for CO_2 adsorption*, 11th Roermond Conference on Catalysis, June 2006.

Dankwoord

Het dankwoord, een van de laatste stukken die je schrijft, en het stuk dat het meest gelezen wordt. Of zelfs alleen gelezen wordt, terwijl de rest van het werk, ‘waar veel bloed zweet en tranen inzit,’ wordt overgeslagen. Naast het bedanken van mensen voor hun bijdrage aan dit boekje, heb ik berekend dat ik tijdens mijn promotieonderzoek, de afgelopen 4 jaar, tussen de 20 en 25 ton CO_2 heb uitgestoten. Dit is alleen de uitstoot van mijn auto (Vught - Utrecht, 65 km enkele reis, na 4 jaar ~120.000 km). Het CO_2-verbruik voor experimentele doeleinden tijdens mijn onderzoek was ongeveer 70 kg. Conclusie: je kunt beter onderzoek doen dan auto rijden.

Mijn promotor Krijn wil ik bedanken voor de vier jaar dat hij mij heeft begeleid. Elke keer wist je weer nieuwe wetenschappelijke inzichten te creëren waardoor mijn onderzoek weer verder kon. Ook van je kritische vragen heb ik veel geleerd en deze lieten mij het onderzoek weer van een ander perspectief bekijken. Jos, mijn 'te vroeg verlaten' co-promotor wil ik bedanken voor het wegwijs maken in de anorganische chemie aan het begin van mijn promotieonderzoek. Het was maar een erg korte tijd waarin je mij hebt begeleid en ik vond het jammer dat je zo vroeg al met pensioen bent gegaan. Gelukkig heb ik er een goede vervangende co-promotor voor in de plaats gekregen. Harry, mijn co-promotor, ondanks dat het onderwerp hydrotalcieten relatief nieuw was en je al na een halfjaar het stokje van Jos kreeg overgedragen, had je altijd weer nieuwe ideeën en inzichten. Het was ook erg prettig dat je deur altijd openstond voor een wetenschappelijk of niet-wetenschappelijk (auto’s) praatje.

Mijn dank gaat ook uit naar alle mensen buiten de Universiteit Utrecht waarmee ik de afgelopen 4 jaar heb samengewerkt. Paul Cobden, Rick Reijers, Ruud van den Brink en Daan Jansen van ECN wil ik bedanken voor alle goede discussies. Iedereen binnen het ‘CATO-team’ wil ik bedanken voor alle leuke CATO-dagen en alle gedachtewisselingen. In het bijzonder wil ik hiervoor Eric Lysen, Sander van Egmond en Mirjam van Deutekom bedanken. Earl Goedheer van TNO wil ik bedanken voor alle moeite voor het, helaas niet gelukte, patent. Arno Kentgens, Ernst van Eck en Andreas Brinkmann wil ik bedanken voor de NMR-metingen. Ondanks dat er een ‘klein foutje’ in de eerste metingen zat, zijn de nieuwe resultaten toch weer veelbelovend.

Binnen de Universiteit Utrecht wil ik verder nog de studenten die voor mij onderzoek hebben gedaan naar hydrotalcieten en CO_2-afvang bedanken. Parcival, ondanks dat je resultaten niet konden worden verwerkt in dit boekje, heb je toch een stukje bijgedragen aan het tot stand komen van hoofdstuk 2. Sander, altijd vrolijk en daarom erg leuk om te begeleiden. Een deel van jouw onderzoek staat beschreven in hoofdstuk 3. Eva, je hebt hydrotalcieten gemaakt met verschillende aluminium beladingen, dit heeft een duidelijk inzicht gegeven hoe hydrotalcieten zich daaronder gedragen. Ik wens jullie allen nog veel succes met afstuderen en carrières.

Mijn kamergenoten, van wie er ondertussen een aantal zijn geweest, wil ik bedanken voor alle gezelligheid, zinnige en onzinnige discussies. Stan en Cristina zijn alweer een tijdje uit N219 vertrokken, het was erg gezellig met jullie, het gaat jullie goed. Emiel, metal!, bedankt voor alle computer break downs die je voor mij hebt opgelost en voor alle inderdaad leuke zinnige en onzinnige discussies. Ik verwacht binnen een aantal jaar toch meer dan alleen dr. de Smi(d)t voor je naam. Anna I., zo'n spontane Spaanse kom ik waarschijnlijk niet snel meer tegen. Veel plezier met je werk in Spanje, zoals je graag wilde, wat dichter bij je familie. Clare, bedankt dat je me 's ochtends wakker hield met al je leuke verhalen. Succes verder met je AiO-schap. Anne M.F., je hebt deels het stokje in hydrotalcieten/basische materialen van me overgenomen, zonder CO_2-opslag, heel veel succes hiermee. Misschien komt de CO_2 er vanzelf wel in. Ik vond het erg leuk om met je te discussiëren over allerlei (wetenschappelijke) onderwerpen, in het Nederlands, ga zo door!

Nadia, je bent een bijzondere collega geweest en zal dat altijd blijven. Wat als we twee jaar geleden onze ideeën hadden doorgezet… Adri, het is toch knap dat wij 25 jaar op nog geen kilometer van elkaar hebben gewoond in het Brabantse Vught, op dezelfde school hebben gezeten (Maurick college) en elkaar pas voor het eerst hebben leren kennen tijdens onze AiO-periode. Als dat niet bijzonder is. Mariska, het is je toch gelukt om ook mij een stukje van jouw onderzoek te laten meesnuiven, heerlijk (ha). Alle drie heel veel succes met de laatste loodjes en bedankt voor de gezellige tijd de afgelopen jaren. Verder wil ik nog mijn (oud-)collega's, Johan, Inge, Tamara, Leticia, Marianne, Bart (metal!), Annelie, Arjan, Daphne, Xander, en Bas bedanken voor de sfeervolle lunches, borrels, LIIT's etc.

Marjan bedankt voor de hulp met XRD-metingen en alle SEM-plaatjes (hoeveel?...heel veel!) die je hebt gemaakt. Verder wil ik Hans Meeldijk en Cor van der Spek

bedanken voor de TEM-metingen, Ad^{M} voor alle N_2-fysisorptie metingen, Fouad en Tom voor hulp met IR-metingen. De glasblazers wil ik bedanken voor het eindeloos maken van mijn reactor, zonder jullie snelheid van reparatie, was ik nu nog bezig met mijn onderzoek.

Dymph en Monique, dank je wel voor alle hulp bij administratieve zaken en alle andere ondersteuning. Monique, in het bijzonder, veel geluk met je familieaanwinst, Kian.

Anneke Joosten-Gosma heel erg bedankt voor het 'finale corrigeren' van mijn proefschrift. Wat ook heel plezierig was de afgelopen jaren was met zijn vieren op vrijdagavond gezellig tot rust komen bij ons of bij jullie thuis. Dat blijven we doen. Maarten, maatje, zaterdag blijft 'onze' avond, in weer en wind. Christ, je bent nu gesetteld met Esther, join the club again…

Pap en Mam, Ivo, Diane, Danique en ??, Olaf, Anoek en Marijke (mijn 'voor altijd' 2^{e} vriendinnetje uit Geertrui en omstreken) bedankt voor alles, ook voor het aanhoren van mijn (on)begrijpelijk onderzoek. In het bijzonder wil ik nog een keer mijn twee broertjes Ivo en Olaf noemen, die de extra zware taak op zich nemen om met carnaval mijn paranimfen te zijn.

Mieke en Wil, 'schoon' pa en ma, Antoine, Saskia, Chantal, John, ook jullie bedankt voor de steun en voor het aanhoren van mijn (on)begrijpelijk onderzoek. Saskia, je bent de volgende in de familie, heel veel succes met de laatste loodjes van je onderzoek.

Irene, mijn alweer bijna zeven jaar vriendin, je hebt me door de afgelopen 4-5 jaren gesteund en me naar het eindresultaat (dit boekje) gesleept in moeilijke tijden, als het onderzoek 'even' niet meezat. Ook heb je eindeloos mijn hydrotalcietverhalen, verhalen over CO_2-afvang, opslag enz. aangehoord, niet begrepen, begrepen en uiteindelijk ook mee gediscussieerd over al deze onderwerpen. Je hebt zelfs af en toe voor eindredacteur gespeeld, wat je erg goed afgaat. Nu dit voorbij is gaan we op naar een grotere dimensie, ons nieuwe huis, met tuin! Waar we samen nog lang van gaan genieten.

Als je hier nu niet bent genoemd en je vond toch dat je hier bij had moeten staan, sorry, bij deze. Volgende keer beter!...? Ik ga het dankwoord eindigen met een Maori uitspraak:

Toitu he kainga: whatungarongaro he tangata.
Long after people have disappeared the land will remain.

Niels

Curriculum Vitae

Niels Meis werd geboren op 30 november 1978 te Vught. In 1997 behaalde hij het HAVO diploma aan het Maurick College te Vught en in hetzelfde jaar begon hij aan zijn studie organische chemie aan de Hogeschool van Utrecht. In 1998 behaalde hij zijn propedeuse. Na een stage bij N.V. Organon te Oss werd in het jaar 2001 het HLO diploma verkregen. In september van dat jaar werd begonnen met de verkorte studie scheikunde aan de Universiteit Utrecht, waarvan het hoofdvak werd voltooid bij sectie Organische Synthese (prof. dr. G. Van Koten) in april 2004. Van januari 2005 tot april 2009 was hij werkzaam als Assistent in Opleiding (AiO) in de sectie Anorganische Chemie & Katalyse onder begeleiding van dr. J.H. Bitter en prof. Dr. Ir. K.P. de Jong. Een deel van de verkregen onderzoeksresultaten staat beschreven in dit proefschrift.